

DISSERTATION

SYNTHESIS AND ELECTRICAL PROPERTY MEASUREMENTS OF  
INDIVIDUAL LAYERED TRANSITION METAL DICHALCOGENIDE  
NANOTUBES AND NANOWIRES

Submitted By

David B. Seley

Department of Chemistry

In partial fulfillment of the requirements

For the Degree of Doctor of Philosophy

Colorado State University

Fort Collins, Colorado

Spring 2008

UMI Number: 3321313

### INFORMATION TO USERS

The quality of this reproduction is dependent upon the quality of the copy submitted. Broken or indistinct print, colored or poor quality illustrations and photographs, print bleed-through, substandard margins, and improper alignment can adversely affect reproduction.

In the unlikely event that the author did not send a complete manuscript and there are missing pages, these will be noted. Also, if unauthorized copyright material had to be removed, a note will indicate the deletion.

**UMI**<sup>®</sup>

---

UMI Microform 3321313

Copyright 2008 by ProQuest LLC.

All rights reserved. This microform edition is protected against unauthorized copying under Title 17, United States Code.

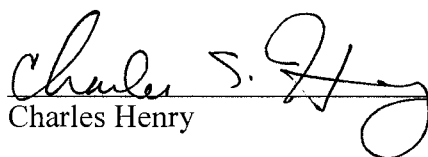
ProQuest LLC  
789 E. Eisenhower Parkway  
PO Box 1346  
Ann Arbor, MI 48106-1346

COLORADO STATE UNIVERSITY

January 4, 2008

WE HEREBY RECOMMEND THAT THE DISSERTATION PREPARED UNDER OUR SUPERVISION BY DAVID B. SELEY ENTITLED SYNTHESIS AND ELECTRICAL PROPERTY MEASUREMENTS OF INDIVIDUAL LAYERED TRANSITION METAL DICHALCOGENIDE NANOTUBES AND NANOWIRES BE ACCEPTED AS FULFILLING IN PART REQUIREMENTS FOR THE DEGREE OF DOCTOR OF PHILOSOPHY.

Committee on Graduate Work

  
\_\_\_\_\_

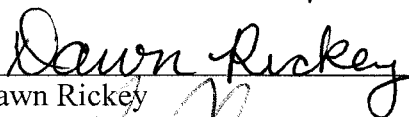
Charles Henry

  
\_\_\_\_\_

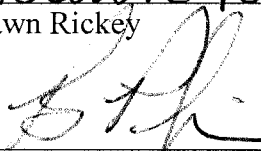
Branka Ladanyi

  
\_\_\_\_\_

Venkatesan Manivannan

  
\_\_\_\_\_

Dawn Rickey

  
\_\_\_\_\_

Adviser – Bruce Parkinson

  
\_\_\_\_\_

Department Head

## ABSTRACT OF DISSERTATION

### SYNTHESIS AND ELECTRICAL PROPERTY MEASUREMENTS OF INDIVIDUAL LAYERED TRANSITION METAL DICHALCOGENIDE NANOTUBES AND NANOWIRES

Nanotubes of the layered transition metal dichalcogenides (LTMDs) including  $\text{MoS}_2$ ,  $\text{WS}_2$ ,  $\text{ReS}_2$ , and  $\text{ReSe}_2$  have been synthesized. Additionally, nanowires of  $\text{WS}_2$  have been synthesized. All of the 1-dimensional structures synthesized used some form of a template to structurally direct 1-dimensional growth. The synthesis of the nanotubes of  $\text{MoS}_2$ ,  $\text{WS}_2$ , and  $\text{ReS}_2$  utilized the pores of anodic aluminum oxide membranes to direct nanotube growth.  $\text{WS}_2$  nanowires were grown with the assistance of the surfactant cetyltrimethylammonium bromide.  $\text{ReSe}_2$  nanotubes were synthesized by using Se nanotubes as a sacrificial template.

The nanotubes and nanowires were characterized by scanning electron microscopy (SEM), transmission electron microscopy (TEM), energy dispersive spectroscopy (EDS), and X-ray diffraction (XRD). Information about the shape, identity, and nanostructure was gained utilizing these techniques.

Electron beam lithography was used to make electrical contacts to the nanowires. Once the contacts were made, two point room temperature current voltage curves were recorded for  $\text{MoS}_2$ ,  $\text{ReS}_2$ , and  $\text{ReSe}_2$  nanotubes. The current voltage characteristics displayed I-V curves that were nearly linear, nearly symmetric, and nearly rectifying for these systems. The currents passed through these nanotubes ranged from nanoamperes to

microamperes. Additional experiments on  $\text{ReSe}_2$  nanotubes indicated a change in resistance with exposure to ammonia and photocurrent generation when exposed to light.

David B. Seley  
Department of Chemistry  
Colorado State University  
Fort Collins, CO 80523  
Spring 2008

## **Acknowledgments**

I would first like to thank my entire family for the support and encouragement they have provided throughout this endeavor: my mother Jackie, my brother Jeff and his family, and my sister Lesli and her family. All of them have given words of encouragement during challenging times. I would also like to thank Leslie Shoblo for her understanding, patience, and humor during the final push.

My adviser, Bruce Parkinson, has been of great help and support during the course of this project. Manashi Nath has been a wonderful resource in many conversations regarding syntheses and overall science. The Parkinson group members, past and present, are acknowledged for their helpful discussions and well-timed motivational speeches.

Lastly, I would like to thank three people that have influenced who I am and what motivates me. Ed Engler, Richard Krinsky, and Paul Vorndam have inspired me and driven me to strive harder in different aspects of my life. These lessons have carried over into my time in graduate school and I continue to be indebted to them.

## **Dedication**

This dissertation is dedicated to the memory of my father, Larry, who passed away the year before I came to graduate school. I learned a great deal from him, and his wisdom has been a guiding force throughout my life. I will always remember and cherish our lengthy conversations concerning all aspects of life. He challenged me to better myself in terms of both education and compassion. I will always be grateful for that.

## Table of Contents

<b>Chapter 1: Background on Nanotubes.....</b>	<b>1</b>
1.1 Carbon Nanotubes	1
1.2 Oxide Nanotubes	6
1.3 Chalcogenide Nanotubes	11
<b>Chapter 2: Surfactant-Assisted Synthesis of WS<sub>2</sub> Nanowires.....</b>	<b>30</b>
<b>Chapter 3: Synthesis and Characterization of MoS<sub>2</sub> and WS<sub>2</sub> Nanotubes...</b>	<b>42</b>
<b>Chapter 4: Template Synthesis of ReS<sub>2</sub> Nanotubes and Electrical Property Measurements.....</b>	<b>62</b>
<b>Chapter 5: ReSe<sub>2</sub> Nanotubes Synthesized From Sacrificial Templates.....</b>	<b>78</b>
5.1 Introduction	79
5.2 Experimental Methods	81
5.3 Results and Discussion	82
5.4 Conclusions	87
<b>Chapter 6: Electrical Property Measurements of Individual ReSe<sub>2</sub> Nanotubes.....</b>	<b>91</b>
<b>Chapter 7: Concluding Remarks and Future Work.....</b>	<b>109</b>
<b>Appendix A: Electron Beam Lithography.....</b>	<b>115</b>
A.1 Introduction	116
A.2 NPGS Software	120
A.3 Initial Writing Step	124
A.4 Defining Nanowire Position	125
A.5 Drawing Contacts to Nanotubes	127

A.6 Run File Editor for Contacting Nanotubes	130
A.7 Electron Beam Writing	134
<b>Appendix B: Study of Thermoelectric Properties of 1-Dimensional Nanowire Arrays.....</b>	<b>139</b>

## Index of Figures

Fig. 1.1: Folding of carbon nanotubes.....	2
Fig. 1.2: Current voltage characteristics of carbon nanotube transistor.....	4
Fig. 1.3: Resistance change in CNT as a function of gas.....	5
Fig. 1.4: SEM of TiO <sub>2</sub> nanotubes.....	7
Fig. 1.5: TEM of Al <sub>2</sub> O <sub>3</sub> nanotube.....	9
Fig. 1.6: SEM of Fe <sub>2</sub> O <sub>3</sub> nanotubes.....	10
Fig. 1.7: TEM of WS <sub>2</sub> nanotube.....	11
Fig. 1.8: Current voltage curve of WS <sub>2</sub> nanotube.....	14
Fig 1.9: TEM of single-walled MoS <sub>2</sub> nanotubes.....	15
Fig 1.10: SEM of CdS nanotubes.....	20
Fig 1.11: TEM of CdS nanotubes.....	20
Fig 2.1: XRD pattern of (CTA) <sub>2</sub> WS <sub>4</sub> precursor.....	32
Fig 2.2: SEM images of WS <sub>2</sub> nanowires.....	34
Fig 2.3: SEM of sea urchin structures of WS <sub>2</sub> nanowires.....	35
Fig. 2.4: WS <sub>2</sub> nanowires at different temperatures.....	36
Fig. 2.5: TEM of WS <sub>2</sub> nanowires.....	38
Fig. 3.1: SEM and TEM of WS <sub>2</sub> nanotubes.....	45
Fig. 3.2: SEM and TEM of MoS <sub>2</sub> nanotubes.....	46
Fig. 3.3: TEM of high temperature synthesis of MoS <sub>2</sub> nanotube.....	49
Fig. 3.4: Images of interdigitated array fabricated in clean room.....	50
Fig. 3.5: MoS <sub>2</sub> nanotube on interdigitated array.....	51
Fig. 3.6: SEM of Au electroplated on MoS <sub>2</sub> nanotubes.....	52

Fig. 3.7: Current voltage curves for MoS <sub>2</sub> nanotubes.....	55
Fig. 4.1: TEM of ReS <sub>2</sub> nanotubes.....	65
Fig. 4.2: TEM of ReS <sub>2</sub> nanowires.....	67
Fig. 4.3: Current voltage curves for ReS <sub>2</sub> nanotubes.....	69
Fig. 4.4: Current voltage curves for ReS <sub>2</sub> nanotubes with 4 contacts.....	71
Fig. 5.1: Layered structure of ReSe <sub>2</sub> .....	80
Fig. 5.2: SEM of Se and ReSe <sub>2</sub> nanotubes with XRD pattern.....	84
Fig. 5.3: TEM of ReSe <sub>2</sub> nanotubes.....	86
Fig. 6.1: SEM of ReSe <sub>2</sub> nanotubes.....	94
Fig. 6.2: Rectifying current voltage curves of ReSe <sub>2</sub> nanotubes.....	95
Fig. 6.3: Linear current voltage curves of ReSe <sub>2</sub> nanotubes.....	97
Fig. 6.4: Nearly symmetric current voltage curve of ReSe <sub>2</sub> nanotube.....	98
Fig. 6.5: Initial photorcurrent response of ReSe <sub>2</sub> nanotube.....	100
Fig. 6.6: Effect of light on resistance of ReSe <sub>2</sub> nanotubes.....	101
Fig. 6.7: Effect of ammonia on resistance of ReSe <sub>2</sub> nanotubes.....	103
Fig. 6.8: SEM of ReSe <sub>2</sub> nanotubes before and after measurements.....	104
Fig. A.1: Run file for Sample 3.....	122
Fig. A.2: CAD pattern for Sample 3.....	123
Fig. A.3: CAD pattern for reference grid.....	124
Fig. A.4: CAD pattern for JEOL Starter file.....	127
Fig. A.5: Completed CAD pattern for contacted nanowires.....	129
Fig. A.6: CAD pattern for VO2Align file.....	132

Fig A.7: Run file containing alignment entities.....	133
Fig. B.1: Illustration of nanoimprint lithography.....	143
Fig. B.2: Diagram of graphite susceptor.....	145
Fig. B.3: Illustration of device for measuring thermoelectric properties.....	146

## Index of Tables

Table 2.1: Summary of synthesis parameters for WS <sub>2</sub> nanowires.....	37
Table 3.1: Summary of synthesis conditions for MoS <sub>2</sub> and WS <sub>2</sub> nanotubes...	47
Table 3.2: Summary of I-V measurements on MoS <sub>2</sub> nanotubes.....	58
Table 4.1: Summary of I-V measurements on ReS <sub>2</sub> nanotubes.....	73

## **Chapter 1: Nanotube Background**

Over the past 22 years, the advent of nanotechnology and nanomaterials has created immense excitement in the scientific community. Research in the area of nanomaterials is ubiquitous. Perusing virtually any of the major scientific journals will likely yield several related articles. Much of this interest is due to the modified electronic properties of these extremely small materials due to what is referred to as the quantum size effect. The range of applications for these materials spans the gamut from molecular wires to solid lubricants. This introduction is arranged to cover the three largest classes of nanotubes: carbon nanotubes, oxide nanotubes, and chalcogenide nanotubes.

### **1.1 Carbon Nanotubes**

The discovery of carbonaceous nanomaterials ushered in a new era of research in nanotechnology. The discovery of  $C_{60}$ , buckminsterfullerene, inspired a great deal of research in nanomaterials, particularly carbon containing materials.<sup>1</sup> Iijima's subsequent discovery of carbon nanotubes produced from layered graphite, provided additional novel structures to investigate.<sup>2</sup>

Carbon nanotubes are cylinders of graphene typically closed at either end. They exhibit extremely interesting physical and electronic properties and are the prototypes for nanotube research. They can be multiple or single walled and are very resistant to mechanical deformation. It is generally accepted that the reason for the formation of

carbon nanotubes is their propensity to fold due to the presence of dangling bonds at the edges of the graphene sheet. Figure 1.1 depicts a sheet of graphene and the parameters that determine whether the nanotube will be zigzag, armchair, or chiral when this sheet is rolled into a tube. The chiral vector  $C_h$  is defined by the equation  $C_h = na_1 + ma_2$ , where  $a_1$  and  $a_2$  are unit vectors and  $n$  and  $m$  are integers. When  $n = m$  and the chiral angle  $\theta$  is  $30^\circ$ , armchair nanotubes result. When either  $n$  or  $m$  is 0, and the chiral angle is 0, zigzag nanotubes result. All other nanotubes with chiral angles between 0 and  $30^\circ$  are chiral nanotubes. Nanotubes for which  $n - m = 3i$ , where  $i$  is an integer, are metallic. All other nanotubes are semiconducting.<sup>3</sup>

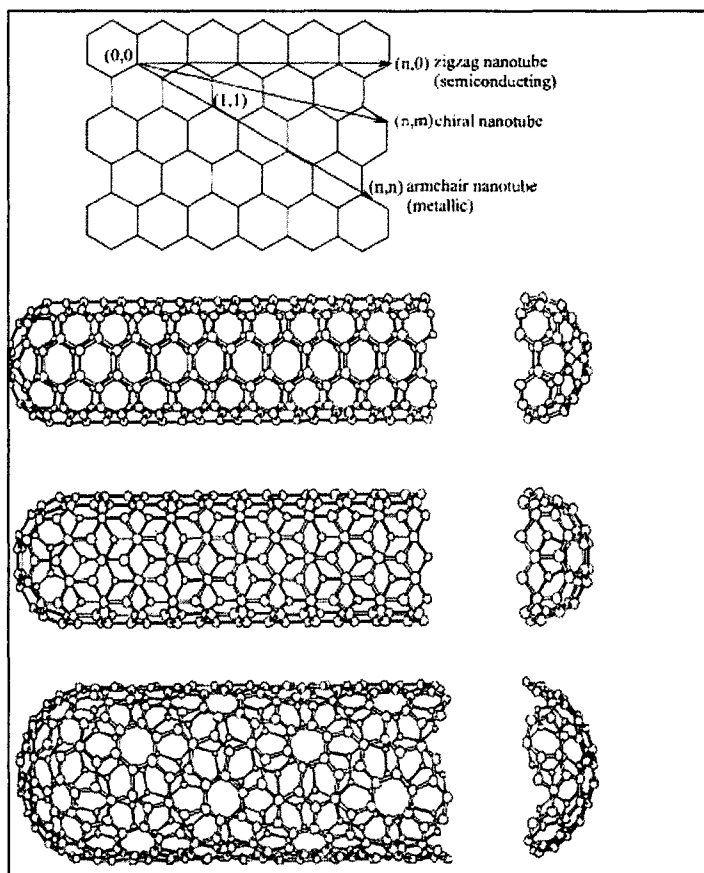


**Figure 1.1** The folding of carbon nanotubes results in zigzag, armchair, or chiral nanotubes.<sup>3</sup>

In the years that followed their discovery much research has been done in the area of carbon nanotubes. Early studies focused on obtaining higher synthetic yields and physical and electrical property determination. The most desirable carbon nanotubes are the single wall carbon nanotubes (SWCNT) that contain only one layer of graphene. This removes some of the uncertainty in subsequent electrical property and gas sensing measurements. As expected, the SWCNTs are also on average smaller in diameter than multiwalled carbon nanotubes (MWCNTs). One of the early synthetic strategies to obtain SWCNTs was that of Thess and co-workers that produced a 70% yield.<sup>4</sup> This synthesis has since been improved upon and now is accepted as the best way to obtain SWCNT.<sup>5</sup>

One of the ongoing interests is to exploit the unique electrical properties of carbon nanotubes. Early measurements of the electrical properties of individual multiwalled carbon nanotubes were made by Dai and coworkers.<sup>6</sup> They used an atomic force microscope with a conducting tip to measure the resistance of individual nanotubes along different lengths of the nanotubes. Important studies by Tans demonstrated the utility of carbon nanotubes as molecular wires and when incorporated into a field-effect transistors (FET).<sup>7,8</sup> Figure 1.2 represent a current voltage curve for the nanotube FET fabricated by Tans and coworkers.

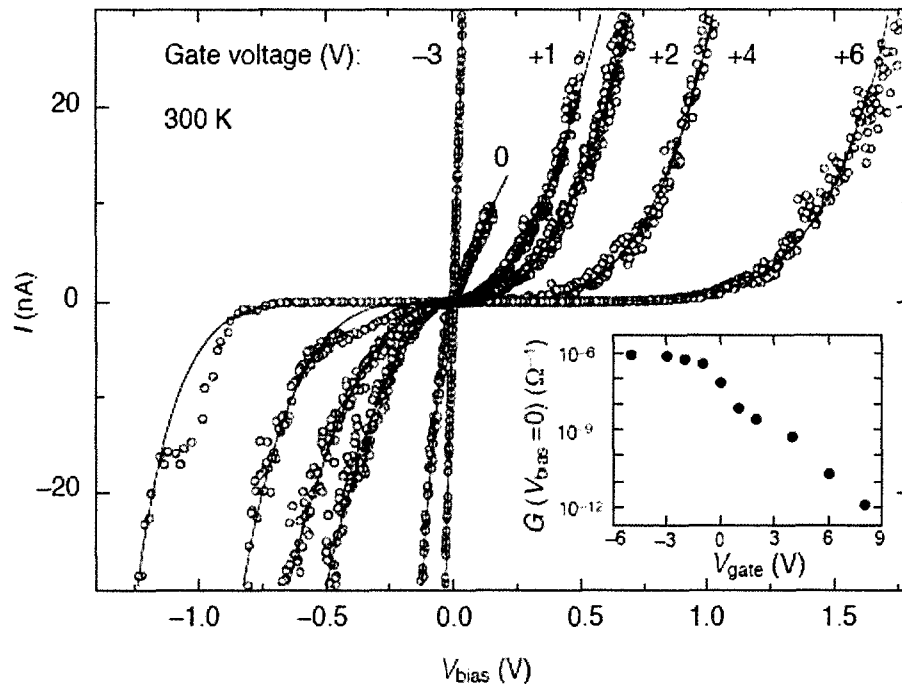


**Figure 1.2.** Current voltage characteristics of an individual carbon nanotube in a 3 terminal transistor device.<sup>7</sup>

As seen in the inset of the figure, the SWCNT is a p-type semiconductor. At negative gate voltages, the current increases dramatically and then saturates. At positive gate voltages, the resistance of the nanotube increases. Following this seminal work, Kong and then Collins demonstrated the use of carbon nanotubes as chemical sensors.<sup>9,10</sup> The current voltage characteristics of the SWCNTs changed with the introduction of different gases. Kong exposed  $\text{NH}_3$  and  $\text{NO}_2$  to individual SWCNTs. The  $\text{NH}_3$  gas had the effect of decreasing the conductance of the nanotube, while the  $\text{NO}_2$  gas had the reverse effect. Figure 1.3 shows the current voltage characteristics representative of these two experiments.

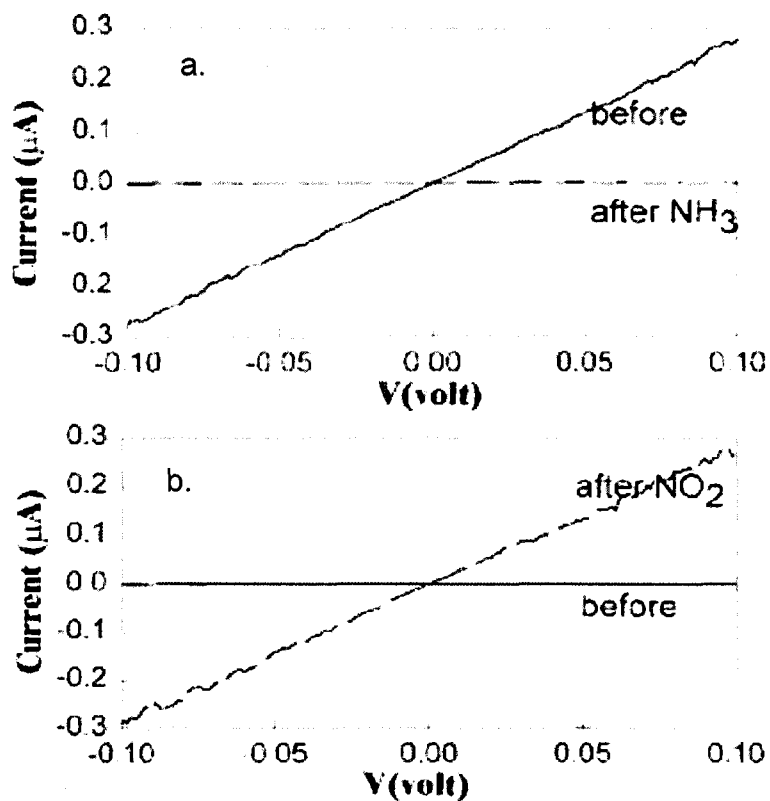


**Figure 1.3.** Current voltage characteristics of a SWCNT; a.) shows IV curve before and after exposure to  $\text{NH}_3$  gas at a gate voltage of 0V; b.) shows the IV curves before and after exposure to  $\text{NO}_2$  gas at a gate voltage of 4V.<sup>9</sup>

The fact that every atom within a SWCNT is a surface atom provides an excellent opportunity to measure changes in the electrical properties or dielectric constant of the nanotubes as a function of surface adsorption of analytes.<sup>11,12</sup> The surfaces of carbon nanotubes have also been functionalized to act as chemical sensors for specific analytes.<sup>13,14</sup>

In addition to the interesting electrical properties of carbon nanotubes, a very recent experiment demonstrated yet another amazing aspect of these materials. A great deal of work on SWCNTs has been done by researchers at IBM. In 2001, they demonstrated that SWCNTs could be ambipolar; that is, conduct electrons and holes equally well.<sup>15</sup> This was accomplished by the formation of TiC bonds at the contacts after annealing the metallized nanotube. All previous studies indicated that SWCNTs were p-type. With this new effect, the same researchers were able to inject an electron on one end of a SWCNT and a hole on the other end and have them combine inside the SWCNT to yield an IR photon.<sup>16</sup> This opened another door for the application of SWCNTs as photonic devices. Clearly, carbon nanotubes have received the most research attention. Without this large body of work on carbon nanotubes, the field of nanotube research would be stalled.

## **1.2 Oxide Nanotubes**

Nanotubes of many other different materials have also been synthesized. Oxidic nanotubes and nanowires have gained considerable attention due to their applications as catalysts and sensors. Vanadium oxide nanotubes have been made using carbon nanotubes as a template.<sup>17</sup> The  $V_2O_5$  acted to either fill the hollow space inside the CNTs or to coat the outside of the CNTs. More recently,  $VO_x$  nanotubes have been synthesized using an aliphatic structural directing amine in combination with hydrothermal synthesis.<sup>18</sup>

A large body of research has been dedicated to  $\text{TiO}_2$  nanotubes due to the photocatalytic properties of this material. The first example of  $\text{TiO}_2$  nanotubes in the literature was the use of a polymer mold that had been incorporated into an anodic aluminum oxide membrane as a template for the formation of these tubes.<sup>19</sup> Subsequent to this work, Lakshmi and co-workers described a more facile route to  $\text{TiO}_2$  nanotubes using a sol-gel technique and the pores of an anodic aluminum oxide membrane.<sup>20</sup> A sol-gel route followed by hydrothermal synthesis has also been described to make  $\text{TiO}_2$  nanotubes with very small ( $\sim 8$  nm) diameters.<sup>21</sup>

An important contribution to the formation of  $\text{TiO}_2$  nanotubes came from Grimes and co-workers, who demonstrated that anodizing Ti sheets resulted in the formation of  $\text{TiO}_2$  nanotubes.<sup>22</sup> These same researchers have continued to improve the anodizing conditions to make very long nanotubes of  $\text{TiO}_2$ .<sup>23</sup> Figure 1.4 shows an SEM image of these high aspect ratio  $\text{TiO}_2$  nanotubes.

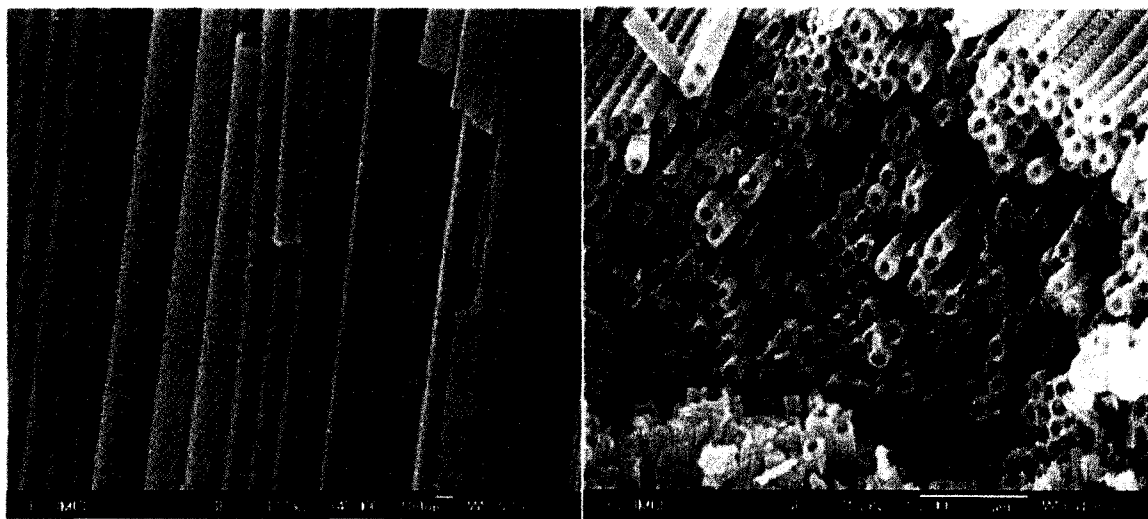


**Figure 1.4.** SEM micrographs of  $\text{TiO}_2$  nanotubes made from the anodization of Ti: a) cross section of tubes, b) top surface of tubes.<sup>23</sup>

TiO<sub>2</sub> nanotubes have been used to fabricate dye-sensitized solar cells (DSSCs). One of the initial reports of this application included the synthesis of TiO<sub>2</sub> nanotubes via a solvothermal route.<sup>24</sup> Adachi and co-workers spread a 4 μm thick layer of TiO<sub>2</sub> nanotubes on conducting glass and exposed the nanotubes to a ruthenium dye. The efficiency of the cell was close to 5%. More recently, a transparent array of TiO<sub>2</sub> nanotubes was perpendicularly grown via anodization of Ti on conducting glass.<sup>25</sup> This work further demonstrates the potential applications of TiO<sub>2</sub> nanotubes for photocatalytic applications.

Alumina nanotubes have been synthesized using several techniques. The first report of Al<sub>2</sub>O<sub>3</sub> nanotubes was in 1997 by Rao and co-workers.<sup>26</sup> Using a solution of aluminum isopropoxide mixed with carbon nanotubes followed by heating, Al<sub>2</sub>O<sub>3</sub> coated CNTs were formed. Al<sub>2</sub>O<sub>3</sub> nanotubes have been synthesized without the use of CNTs via the stepwise anodization of Al thin films.<sup>27</sup> An interesting application of alumina nanotubes uses the Al<sub>2</sub>O<sub>3</sub> nanotube as a top gate for a MWCNT field effect transistor.<sup>28</sup> The process consists of suspending MWCNTs in an ethanolic solution of aluminum nitrate. Upon addition of CO<sub>2</sub> under pressure, a mixed supercritical fluid is made allowing the aluminum nitrate to dissolve. The resultant products are MWCNTs discontinuously coated with Al<sub>2</sub>O<sub>3</sub>. This sporadic sheathing is taken advantage of for the

creation of a top gate via a focused ion beam (FIB) deposition of Pt leads. Alumina nanotubes have also been made through the simple dissolution of anodic aluminum oxide membranes by a solution of NaOH.<sup>29</sup> Using a very similar method, unusual looking perforated Al<sub>2</sub>O<sub>3</sub> nanotubes have been made.<sup>30</sup> Figure 1.5 shows an example of this exotic looking nanotube.

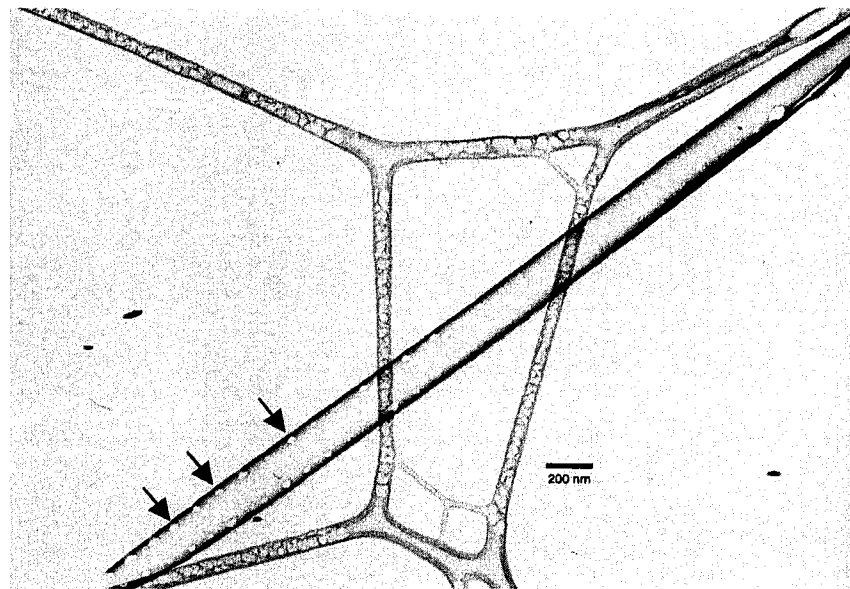


**Figure 1.5.** TEM image of a perforated Al<sub>2</sub>O<sub>3</sub> nanotube. The arrows indicate the periodic spacing of holes along the walls of the nanotube.<sup>30</sup>

$\alpha$ -Fe<sub>2</sub>O<sub>3</sub> is of interest due to its catalytic and gas sensing properties.<sup>31,32</sup> Recently, nanotubes of  $\alpha$ -Fe<sub>2</sub>O<sub>3</sub> have been synthesized in the pores of AAO.<sup>33</sup> Interest quickly grew in the nanotubular form of  $\alpha$ -Fe<sub>2</sub>O<sub>3</sub>. In addition to the AAO template method, carbon nanotubes were also used as a template to form nanotubes of  $\alpha$ -Fe<sub>2</sub>O<sub>3</sub>.<sup>34</sup> In 2005, single crystalline  $\alpha$ -Fe<sub>2</sub>O<sub>3</sub> nanotubes were synthesized via a hydrothermal method.<sup>35</sup> The method involved the reaction of FeCl<sub>3</sub> and NH<sub>4</sub>H<sub>2</sub>PO<sub>4</sub> at a temperature of 220 °C for 48

hours. The nanotubes were about 250 to 400 nm long and about 95 to 110 nm in diameter as shown in Figure 1.6. The as synthesized nanotubes were  $\alpha$ -Fe<sub>2</sub>O<sub>3</sub>, hematite, but could be converted into the  $\gamma$ -Fe<sub>2</sub>O<sub>3</sub>, maghemite via a reduction and oxidation process. The fact that the nanotubes are single-crystalline provides an advantage over previous synthetic routes as well as potential for photocatalytic applications.



**Figure 1.6.** SEM images of the single crystalline Fe<sub>2</sub>O<sub>3</sub> nanotubes formed by hydrothermal synthesis.<sup>35</sup>

SiO<sub>2</sub> nanotubes have been synthesized by several techniques. A sol-gel technique was used to synthesize amorphous SiO<sub>2</sub> nanotubes in 1995.<sup>36</sup> Following this work, Rao and coworkers used CNTs as templates for the formation of SiO<sub>2</sub> nanotubes.<sup>26</sup> In the years following, SiO<sub>2</sub> nanotubes were formed via surfactant-assisted synthesis, and organogel synthesis.<sup>37</sup> Recently, Ta<sub>2</sub>O<sub>5</sub> nanotubes were synthesized using SiO<sub>2</sub> nanorods as templates.<sup>38</sup> Nb<sub>2</sub>O<sub>5</sub> and Ta<sub>2</sub>O<sub>5</sub> nanotubes have been obtained using a nanoscroll to nanotube thermal transformation.<sup>39</sup> Fluorescent RuO<sub>2</sub> nanotubes derived from a

$\text{Ru}_3(\text{CO})_{12}$  precursor have been achieved in the pores of an AAO membrane.<sup>40</sup> The interest in both the synthesis and applications of oxide nanotubes has continued for several years and is still growing rapidly.

### 1.3 Chalcogenide Nanotubes

The first group of materials found to form nanotubular structures after carbon were the layered transition metal dichalcogenides. These materials have a structure with a metal sandwiched between two chalcogen atoms to comprise one layer. The layers are separated by a van der Waals gap analogous to the graphite structure. These materials exhibit a wide range of physical and electronic properties and are highly anisotropic. Tenne and co-workers found that  $\text{WS}_2$  closed structures and nanotubes could be formed by exposing a thin film of W to  $\text{H}_2\text{S}$  at  $1000\text{ }^\circ\text{C}$ .<sup>41</sup> Figure 1.7 shows a TEM image of a  $\text{WS}_2$  nanotube formed in this process.

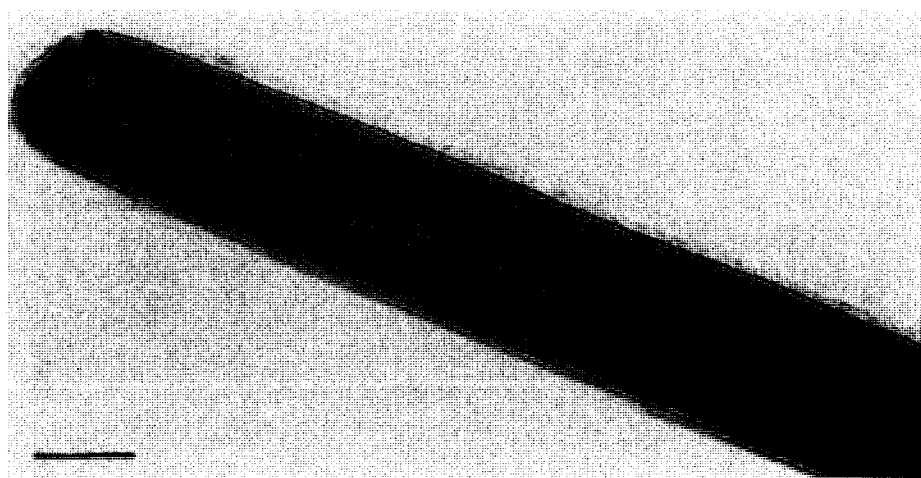


**Figure 1.7.** Closed end nanotube of  $\text{WS}_2$  formed by heating a thin film of tungsten in the presence of  $\text{H}_2\text{S}$ . Scale bar is  $10\text{ nm}$ .<sup>41</sup>

Soon thereafter, the same researcher discovered that another transition metal dichalcogenide (TMD), MoS<sub>2</sub>, also formed closed fullerene-like structures and nanotubes.<sup>42</sup> These discoveries created a flurry of interest in the field of inorganic nanotubes. A great deal of research has been done on these two TMD materials including searching for better synthetic routes, studying their physical properties, and determining their electronic properties. The following sections will review the research dedicated to these TMD nanotubes.

The interest in WS<sub>2</sub> nanotubes has led many researchers to seek alternative synthetic routes. Chemical vapor transport reactions are common in solid-state syntheses. Remskar used such a reaction to make tubes of WS<sub>2</sub> in 1998.<sup>43</sup> Many of these tubular structures of WS<sub>2</sub> exhibited diameters on the order of microns and were hence referred to as microtubes. However, nanotubes with diameters less than 100 nm were also formed. Nath and co-workers used a simple decomposition reaction of the ammonium tetrathiotungstate salt to yield WS<sub>2</sub> nanotubes.<sup>44</sup> Carbon nanotubes have been used as a template to create WS<sub>2</sub> nanotubes.<sup>45</sup> Tenne used a fluidized bed reactor to form very long and crystalline nanotubes of WS<sub>2</sub>.<sup>46</sup> These multiwalled nanotubes could be as long as hundreds of microns. Mackie and co-worker subjected WS<sub>2</sub> powder to acid treatment and heating to form WS<sub>2</sub> nanotubes and closed shell structures.<sup>47</sup>

Notwithstanding the many efforts that require extreme reaction conditions, there have been some reports of the synthesis of WS<sub>2</sub> nanotubes via a soft chemical approach.

In 2004, Li and co-workers were able to make WS<sub>2</sub> nanotubes by reacting the surfactant cetyltrimethylammonium bromide (CTAB), thioacetamide, and tungsten oxide hydrothermally.<sup>48</sup> Not long after this work, Therese and co-workers also used a similar approach to make nanotubes of WS<sub>2</sub>.<sup>49</sup> This researcher synthesized WO<sub>3</sub> nanorods hydrothermally, followed by exposure to H<sub>2</sub>S gas at 840 ° C for 30 minutes.

WS<sub>2</sub> nanotubes have found applications as solid lubricants. Tenne demonstrated that WS<sub>2</sub> nanotubes could survive pressures of up to 21 GPa, a strength superior to that of even carbon nanotubes.<sup>50</sup> The shear modulus of WS<sub>2</sub> nanotubes was subsequently calculated for nanotubes of varying diameter.<sup>51</sup> WS<sub>2</sub> nanotubes have also been used as probe tips in atomic force microscopy (AFM).<sup>52</sup> Several other applications of WS<sub>2</sub> nanotubes have been investigated. WS<sub>2</sub> nanotubes have been functionalized and incorporated into a polymer matrix of polystyrene and polymethylmethacrylate.<sup>53</sup> There has also been interest in WS<sub>2</sub> nanotubes as electrode materials in lithium ion batteries.<sup>54</sup>

Bulk WS<sub>2</sub> is an indirect band gap semiconductor with a band gap of 1.35 eV.<sup>55</sup> Seifert and co-workers have investigated the electronic structure of WS<sub>2</sub> nanotubes theoretically.<sup>56</sup> The band gap has been predicted to increase with tube diameter. Scanning probe microscopy was performed on WS<sub>2</sub> nanotubes and current voltage characteristics were determined.<sup>57</sup> Figure 1.8 shows a room temperature current voltage curve. The current voltage curve shows the nanotube exhibiting semiconducting behavior. Curiously, a current voltage curve on a nanotube with a larger diameter shows

essentially the same magnitude of current under identical experimental conditions. This indicates that the current is limited by junction properties rather than nanotube properties. There does appear to be a trend indicating an increase in band gap as a function of tube diameter.

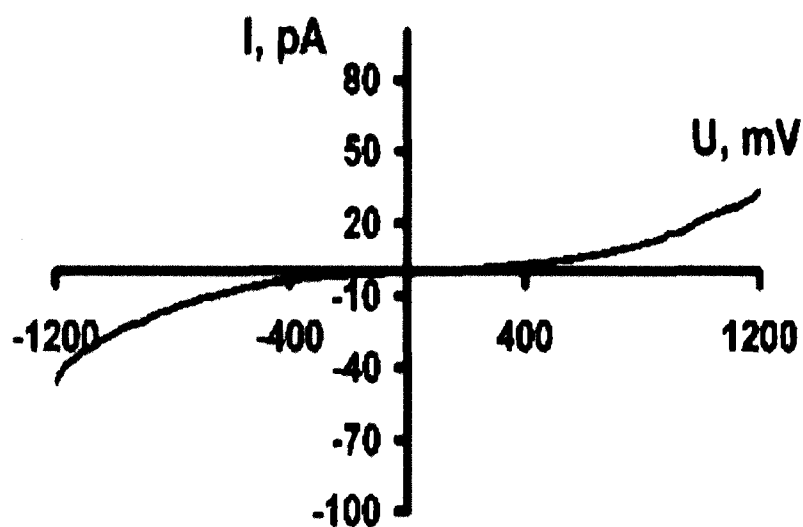


**Figure 1.8.** Room temperature current voltage curve of a single  $WS_2$  nanotube via scanning tunneling microscopy.<sup>57</sup>

$MoS_2$  nanotubes have also received considerable attention in the last several years. Following the discovery of these nanotubes, Feldman and co-workers devised a high rate gas flow route to prepare these materials resulting in milligram quantities.<sup>58</sup> They started with the molybdenum sub-oxide powder as a precursor, which sometimes results in incomplete sulfidation with the exposure to  $H_2S$  gas. In an effort to avoid the incomplete sulfidization of the nanotubes, Hsu and co-workers devised a different

experimental set up to achieve MoS<sub>2</sub> nanotubes.<sup>59</sup> They started with MoS<sub>2</sub> powder dispersed on a flat Mo electrode covered with a sheet of Mo foil. Subsequent sulfidization of the MoS<sub>2</sub> powder, in combination with resistively heating the Mo foil at temperatures of 600 – 800 °C for 30 minutes, resulted in oxide free MoS<sub>2</sub> nanotubes. As with WS<sub>2</sub> nanotubes, MoS<sub>2</sub> nanotubes can be formed by the decomposition of the ammonium tetrathiomallate precursor.<sup>44,60</sup>

In an extremely interesting experiment, single-walled MoS<sub>2</sub> nanotubes were formed by the chemical vapor transport method by Remskar in 2001.<sup>61</sup> C<sub>60</sub> fullerenes were used as a growth promoter in the evacuated silica ampoule with MoS<sub>2</sub> carried out at 1010 K for 22 days with a temperature gradient of 6 K/cm. Iodine was used as the transport reagent. The tubes contain interstitial iodine left over from the transport process. The diameters of the tubes are close to 1 nm based on TEM images. Figure 1.9 shows a high-resolution TEM image of a bundle of these single-walled nanotubes.

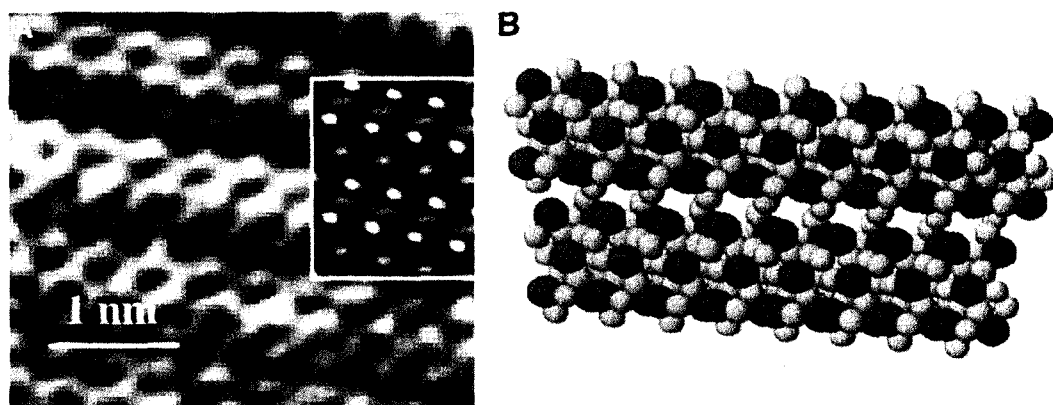


**Figure 1.9.** Single-wall MoS<sub>2</sub> nanotubes; A) HR-TEM image of bundle of MoS<sub>2</sub> nanotubes. Inset is image simulation of parallel stacking; B) model of structure.<sup>61</sup>

The single-walled MoS<sub>2</sub> nanotubes were later studied by STM and revealed metallic behavior.<sup>62</sup> This agrees with theoretical predictions suggesting that all MoS<sub>2</sub> nanotubes with a diameter of greater than 2 nm are semiconducting.<sup>63</sup> The important aspect of this work is that, unlike any other nanotube preparation either carbon or inorganic, every nanotube should have an identical structure.

There is still interest in new synthetic strategies for preparing MoS<sub>2</sub> nanotubes. In 2006, Loh and co-workers used a single-source precursor, tetrakis(diethylaminodithiocarbomato)molybdate(IV), decomposed thermally within the pores of an AAO template.<sup>64</sup> These used MoO<sub>3</sub> nanorods followed by sulfidization to obtain MoS<sub>2</sub> nanotubes.<sup>65</sup> Nanotubes and nanocoils of MoS<sub>2</sub> intercalated with hexadecylamine were formed via a solvothermal route.<sup>66</sup>

MoS<sub>2</sub> nanotubes have been investigated for several applications. MoS<sub>2</sub> has been used as a solid lubricant and its nanostructures have also been investigated for their tribological properties.<sup>67</sup> The H<sub>2</sub> storage properties of MoS<sub>2</sub> nanotubes have been investigated by Chen and co-workers.<sup>68</sup> MoS<sub>2</sub> nanotubes have also been studied for their catalytic properties. In 2002, MoS<sub>2</sub> nanotubes were studied as a catalyst for the methanation of CO with H<sub>2</sub>.<sup>69</sup> Subsequently, MoS<sub>2</sub>-Ni nanocomposites were used as hydrodesulfurization catalysts.<sup>70</sup> Nickel particles were coated onto the surface of the MoS<sub>2</sub> nanotubes via a solution route and then exposed to sulfur containing gases. The MoS<sub>2</sub>-Ni nanocomposite showed a higher level of catalytic activity for removing the

sulfur containing gases than do MoS<sub>2</sub> nanoparticles without the nickel. Finally, single-walled MoS<sub>2</sub> nanotubes have been used as Li ion storage materials for rechargeable lithium batteries.<sup>71</sup>

Given the large amount of research dedicated to MoS<sub>2</sub> and WS<sub>2</sub> nanotubes, it is not surprising that other LTMDs have been the focus of research into the formation of nanotube materials. NbS<sub>2</sub> nanotubes were among the first LTMDs other than MoS<sub>2</sub> and WS<sub>2</sub> to be formed. In 2001, Nath and Rao were able to make nanotubes of NbS<sub>2</sub> and TaS<sub>2</sub> via the decomposition of the respective trisulfides under reducing conditions and high temperatures.<sup>72</sup> That same year, NbS<sub>2</sub> nanotubes were made by Zhu using carbon nanotubes as a template.<sup>73</sup> Silver alloyed NbS<sub>2</sub> nanotubes were prepared by electron beam irradiation or microwave treatment of (NbS<sub>4</sub>)<sub>x</sub>I crystals.<sup>74</sup> The group IV disulfides of HfS<sub>2</sub> and ZrS<sub>2</sub> have also been formed by the decomposition of their trisulfide precursors.<sup>75</sup>

NbSe<sub>2</sub> is of interest owing to its superconducting nature. Nanotubes of this material were formed by exposing bulk NbSe<sub>2</sub> to high doses of electron beam irradiation.<sup>76</sup> A chemical approach has also been used to make these nanotubular structures. Nath and co-workers have prepared NbSe<sub>2</sub> nanotubes by the decomposition of the NbSe<sub>3</sub> precursor under Ar flow at temperatures of about 700 °C for 30 minutes.<sup>77</sup> Subsequent to nanotube formation, the superconducting transition of the nanotubes was confirmed. The selenide nanotubes analogous to MoS<sub>2</sub> and WS<sub>2</sub> have been formed by the

decomposition of the respective triselenides and also the decomposition of ammonium tetraselenate precursors.<sup>78</sup>

MoTe<sub>2</sub> nanotubes have been synthesized using various techniques including the first reported in 2001 where bulk MoTe<sub>2</sub> was exposed to a high dose of electron irradiation.<sup>79</sup> Following this discovery, another synthetic route to MoTe<sub>2</sub> nanotubes was described.<sup>80</sup> In this approach, Te powder was ultrasonically treated with Mo(CO)<sub>6</sub> in decalin. Following ultrasonic treatment, the amorphous precipitate was calcined at 650 °C under N<sub>2</sub> flow for 4-10 hours. The resultant product contained multiwalled MoTe<sub>2</sub> nanotubes. A recent theoretical paper has suggested that single-walled MoTe<sub>2</sub> nanotubes are stable, but this is unverified as yet.<sup>81</sup>

ReS<sub>2</sub> has a lower symmetry structure due to the existence of Re-Re metal-metal bonds within the layers of the triclinic structure.<sup>55</sup> It has been studied as an electrode material and as a hydrodesulfurization catalyst.<sup>82</sup> ReS<sub>2</sub> nanotubes have been formed through the sulfidization of RuO<sub>2</sub> in 2001.<sup>83</sup> The majority of the products were inorganic fullerene-like structures, however, some nanotubes were formed. A more rational synthesis was described in the same year involving the use of carbon nanotubes as a template.<sup>84</sup>

There have been reports of TiS<sub>2</sub> nanotubes in the literature. Nath and Rao were the first researchers to make TiS<sub>2</sub> nanotubes.<sup>75</sup> This was accomplished by the decomposition of a trisulfide precursor of Ti. More recently, Chen and co-workers were

able to obtain  $\text{TiS}_2$  nanotubes from reacting  $\text{TiCl}_4$  in a mixture of  $\text{H}_2$  gas with  $\text{H}_2\text{S}$  gas at  $450\text{ }^\circ\text{C}$  for 30 minutes.<sup>85</sup> These same researchers used a different route for the synthesis of  $\text{TiS}_2$  nanotubes that involved a chemical vapor transport reaction using  $\text{I}_2$  as the transport agent.<sup>86</sup> After the synthesis, these nanotubes were studied for their application as  $\text{H}_2$  storage materials. The nanotubes reversibly stored 2.5 weight % of  $\text{H}_2$ .

A few other TMD nanotubes have been reported in the literature.  $\text{TiSe}_2$  nanotubes were synthesized by heating a pellet of ball-milled Ti and Se in an atmosphere of Ar at  $650\text{ }^\circ\text{C}$  for 8 hours.<sup>87</sup>  $\text{VS}_2$  nanotubes were reported in 2004.<sup>88</sup> This synthesis is especially noteworthy, considering that bulk  $\text{VS}_2$  exists only as  $\text{A}_x\text{VS}_2$ , where A is an alkali metal or copper. The authors used  $\text{VO}_x$  nanotubes as a starting material, where x is 2.3. The  $\text{VO}_x$  nanotubes were placed in a furnace at  $225\text{ }^\circ\text{C}$  for 22 hours and exposed to  $\text{H}_2\text{S}$  gas.

Several other chalcogenide nanotubes have been synthesized via various chemical routes. CdS has long been of interest as a direct band gap semiconductor. CdS nanotubes were first prepared using a surfactant-assisted synthesis.<sup>89</sup> CdSe nanotubes were also prepared in the same report using similar experimental conditions. Both nanotubes of CdS and CdSe exhibited photoluminescent properties. CdS nanotubes have since been made using different surfactant-assisted approaches. Using  $\text{Cd}(\text{OH})\text{Cl}$  as a sacrificial template followed by a gelatin soft template, CdS nanotubes were synthesized by Miao and co-workers.<sup>90</sup> Following the lead of these researchers, Li and co-workers

circumvented the soft template and directly converted  $\text{Cd}(\text{OH})_2$  nanowires into nanotubes of  $\text{CdS}$ .<sup>91</sup> It is notable that in both synthetic routes using a sacrificial template, the nanotubes that resulted exhibited rough surfaces comprised of polycrystalline  $\text{CdS}$ . However, this does not diminish the fact that nanotubes of this material were in fact made. Figures 1.10 and 1.11 show representative examples of these unique looking  $\text{CdS}$  tubes.

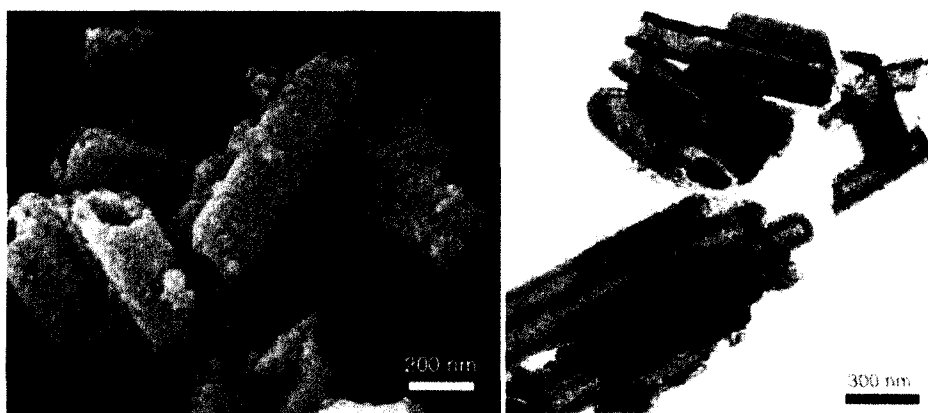


**Figure 1.10.** SEM and TEM of  $\text{CdS}$  nanotubes formed using a sacrificial and a soft template.<sup>90</sup>

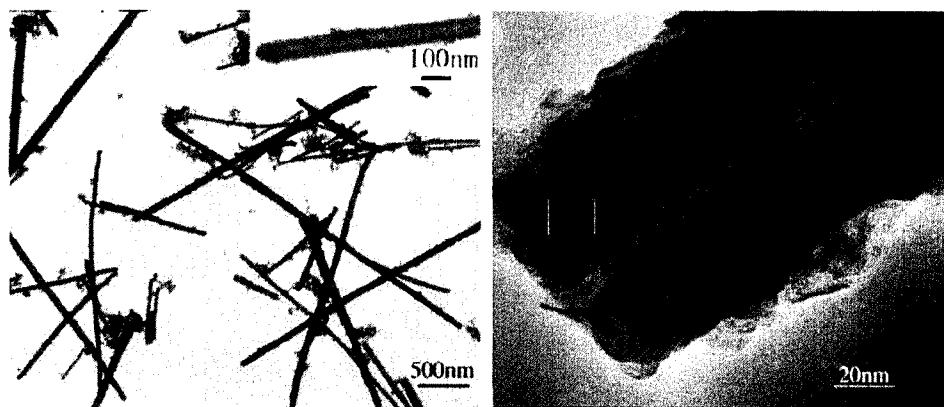


**Figure 1.11.**  $\text{CdS}$  nanotubes formed using the sacrificial template of  $\text{Cd}(\text{OH})_2$ .<sup>91</sup>

Various other nanotubular sulfides have also been synthesized. ZnS nanotubes were formed using ZnO nanobelts as a precursor.<sup>92</sup> The ZnO nanobelts were dispersed in ethanol and treated ultrasonically. A saturated H<sub>2</sub>S solution was then added at room temperature and the reaction vessel was sealed for 24 hours. The solution was subsequently dried at 90 °C, resulting in ZnS nanotubes. Bi<sub>2</sub>S<sub>3</sub> nanotubes have been synthesized using very fine powder of Bi<sub>2</sub>S<sub>3</sub> heated with S in a flow through furnace at 640 °C under Ar for 2 hours.<sup>93</sup> Very recently, Sb<sub>2</sub>S<sub>3</sub> nanotubes have been produced using a wet chemical approach. SbCl<sub>3</sub> was dissolved in oleylamine and combined with a solution of S dissolved in oleylamine followed by heating at 175 °C for 90 minutes.<sup>94</sup>

CdSe nanotubes have been formed using a surfactant-assisted approach and also by using 1-D t-Se nanorods as sacrificial templates.<sup>89,95</sup> The use of Se nanowires as sacrificial templates is an interesting synthetic approach, in that many selenide nanotubular systems may be formed from this route. In the experiment, t-Se nanowires were mixed with either CdCl<sub>2</sub> or Cd(NO<sub>3</sub>)<sub>2</sub> in an aqueous solution and heated at 100 °C for 8 hours. To obtain nanotubes of CdSe, the products, consisting of a core of Se nanowires and a shell of CdSe, were heated at 230 °C, effectively subliming the residual Se and leaving CdSe nanotubes. Another selenide nanotube was synthesized by the same researcher using t-Se nanowires as sacrificial templates.<sup>96</sup> RuSe<sub>2</sub> nanotubes were formed by reacting Ru(acac)<sub>3</sub> with Se nanowires dispersed in ethanol and heated to 80 °C for 3 days. ZnSe nanotubes have been synthesized through thermal evaporation of a mixture of ZnSe, SnO, and SnO<sub>2</sub>.<sup>97</sup> The resulting products consisted of ZnSe nanotubes filled

with Sn nanorods. Lastly, cadmium thioglycolic acid nanowires were used as sacrificial templates to make CdTe nanotubes with tunable diameters.<sup>98</sup>

Despite the large body of work relating to the synthesis of TMD nanotubes, many opportunities exist for the discovery of new materials. In addition, it is clear from the literature that very little work has been done measuring the electrical properties of most of the TMD nanotube systems. Given the vast amount of research on the electrical property measurements of carbon nanotubes, a solid paradigm exists for measuring the electrical properties of other nanotubular materials.

## References:

1. Kroto, H. W.; *Nature*, **1985**, 318, 162-163.
2. Iijima, S.; *Nature*, **1991**, 354, 56-68.
3. Rao, C. N. R.; Satishkumar, B. C.; Govindaraj, A.; Nath, M.; *ChemPhysChem*, **2001**, 2, 78-105.
4. Thess, A.; Lee, R.; Nikolaev, P.; Dai, H.; Petit, P.; Robert, J.; Xu, C.; Lee, Y. H.; Kim, S. G.; Rinzler, A. G.; Colbert, D. T.; Scuseria, G. E.; Tomanek, D.; Fischer, J. E.; Smalley, R. E.; *Science*, **1996**, 273, 483-487.
5. Nikolaev, P.; Bronikowski, M. J.; Bradley, R. K.; Rohmund, F.; Colbert, D. T.; Smith, K. A.; Smalley, R. E.; *Chemical Physics Letters*, **1999**, 313, 91-97.
6. Dai, H.; Wong, E. W.; Lieber, C. M.; *Science*, **1996**, 272, 523-526.
7. Tans, S. J.; *Nature*, **1997**, 386, 474-477.
8. Tans, S. J.; *Nature*, **1998**, 393, 49-52.
9. Kong, J.; Franklin, N. R.; Zhou, C. W.; Chapline, M. G.; Peng, S.; Cho, K. J.; Dai, H. J.; *Science*, **2000**, 287, 622-625.
10. Collins, P. G.; Bradley, K.; Ishigami, M.; Zettl, A.; *Science*, **2000**, 287, 1801-1804.
11. Li, J.; Lu, Y. J.; Ye, Q.; Cinke, M.; Han, J.; Meyyappan, M.; *Nano Letters*, **2003**, 3, 929-933.
12. Chopra, S.; McGuire, K.; Gothard, N.; Rao, A. M.; Pham, A.; *Applied Physics Letters*, **2003**, 83, 2280-2282.
13. Lin, Y. H.; Lu, F.; Tu, Y.; Ren, Z. F.; *Nano Letters*, **2004**, 4, 191-195.
14. Pengfei, Q. F.; Vermesh, O.; Grecu, M.; Javey, A.; Wang, O.; Dai, H. J.; Peng, S.; Cho, K. J.; *Nano Letters*, **2003**, 3, 347-351.
15. Martel, R.; Derycke, V.; Lavoie, C.; Appenzeller, J.; Chan, K. K.; Tersoff, J.; Avouris, Ph.; *Physical Review Letters*, **2001**, 87, 26805-1 – 26805-4.
16. Misewich, J. A.; Martel, R.; Avouris, Ph.; Tsang, J. C.; Heinze, S.; Tersoff, J.; *Science*, **2003**, 783-786.
17. Ajayan, P. M.; Stephan, O.; Redlich, Ph; Colliex, C.; *Nature*, **1995**, 375, 564-567.

18. Spahr, M. E.; Bitterli, P.; Nesper, R.; Muller, M.; Krumeich, F.; Nissen, H. U.; *Ang. Chem. Intl. Edn.*, **1998**, *37*, 1263-1265.
19. Hoyer, P.; *Langmuir*, **1996**, *12*, 1411-1413.
20. Lakshmi, B.; Dorhout, P. K.; Martin, C. R.; *Chemistry of Materials*, **1997**, *9*, 857-862.
21. Kasuga, T.; Hiramatsu, M.; Hoson, A.; Sekino, T.; Niihara, K.; *Langmuir*, **1998**, *14*, 3160-3163.
22. Gong, D.; Grimes, C. A.; Varghese, O. K.; Hu, W.; Singh, R. S.; Chen, Z.; Dickey, E. C.; *Journal of Materials Research*, **2001**, *16*, 3331-3334.
23. Paulose, M.; Shankar, K.; Yoriya, S.; Prakasam, H. E.; Varghese, O. K.; Mor, G. K.; Latempa, T. A.; Fitzgerald, A.; Grimes, C. A.; *Journal of Physical Chemistry B*, **2006**, *110*, 16179-16184.
24. Adachi, M.; Murata, Y.; Okada, I.; Yoshikawa, S.; *Journal of the Electrochemical Society*, **2003**, *150*, G488-G493.
25. Mor, G. K.; Shankar, K.; Paulose, M.; Varghese, O. K.; Grimes, C. A.; *Nano Letters*, **2006**, *6*, 215-218.
26. Satishkumar, B. C.; Govindaraj, A.; Vogl, E. M.; Basumallick, L.; Rao, C. N. R.; *Journal of Materials Research*, **1997**, *12*, 604-606.
27. Pu, L.; Bao, X.; Zou, J.; Feng, D.; *Angewandte Chemie International Edition*, **2001**, *40*, 1490-1493.
28. Fu, L.; Liu, Y.; Liu, Z.; Han, B.; Cao, L.; Wei, D.; Yu, G.; Zhu, D.; *Advanced Materials*, **2006**, *18*, 181-185.
29. Xiao, Z. L.; Han, C. Y.; Welp, U.; Wang, H. H.; Kwok, W. K.; Willing, G. A.; Hiller, J. M.; Cook, R. E.; Miller, D. J.; Crabtree, G. W.; *Nano Letters*, **2002**, *2*, 1293-1297.
30. Seley, D. B.; Parkinson, B. A.; unpublished results.
31. Brown, A. S. C.; Hargreaves, J. S. J.; Rijniersce, B.; *Catalysis Letters*, **1998**, *53*, 7-13.
32. Huo, L.; Li, W.; Lu, L.; Cui, H.; Xi, S.; Wang, J.; Zhao, B.; Shen, Y.; Lu, Z.; *Chemistry of Materials*, **2000**, *12*, 790-794.

33. Shen, X.; Liu, H.; Chen, K.; Hong, J.; Xu, Z.; *Chemistry Letters*, **2004**, 33, 1128-1129.
34. Sun, Z.; Yuan, H.; Liu, Z.; Han, B.; Zhang, X.; *Advanced Materials*, **2005**, 17, 2993-2997.
35. Jia, C.; Sun, L.; Yan, Z.; You, L.; Luo, F.; Han, X.; Pang, Y.; Zhang, Z.; Yan, C.; *Angewandte Chemie International Edition*, **2005**, 44, 4328-4333.
36. Nakamura, H.; Matsui, Y.; *Journal of the American Chemical Society*, **1995**, 117, 2651-2652.
37. a.) Ono, Y.; Nakashima, K.; Sano, M.; Kanekiyo, Y.; Inoue, K.; Hojo, J.; Shinkai, S.; *Chemical Communications*, **1998**, 1477-1478. b.) Jung, J. H.; Ono, Y.; Shinkai, S.; *Langmuir*, **2000**, 16, 1643-1649. c.) Lin, H.; Mou, C.; Liu, S.; *Advanced Materials*, **2000**, 12, 103-106.
38. Chueh, Y.; Chou, L.; Wang, Z.; *Angewandte Chemie International Edition*, **2006**, 45, 7773-7778.
39. Kobayashi, Y.; Hata, H.; Salama, M.; Mallouk, T.; *Nano Letters*, **2007**, 7, 2142-2145.
40. Tan, H.; Ye, E.; Fan, W.; *Advanced Materials*, **2006**, 18, 619-623.
41. Tenne, R.; Margulis, L.; Hodes, G.; *Nature*, **1992**, 360, 444-446.
42. Margulis, L.; Salitra, G.; Tenne, R.; Tallanker, M.; *Nature*, **1993**, 365, 113-114.
43. Remskar, M.; Skraba, Z.; Regula, M.; Ballif, C.; Sanijines, R.; Levy, F.; *Advanced Materials*, **1998**, 10, 246-249.
44. Nath, M.; Govindaraj, A.; Rao, C. N. R.; *Advanced Materials*, **2001**, 13, 283-286.
45. Whitby, R. L. D.; Hsu, W. K.; Watts, P. C. P.; Kroto, H. W.; Walton, D. R. M.; Boothroyd, C. B.; *Applied Physics Letters*, **2001**, 79, 4574-4576.
46. Rosentsveig, R.; Margolin, A.; Feldman, Y.; Popovitz-Bira, R.; Tenne, R.; *Chemistry of Materials*, **2002**, 14, 471-473.
47. Mackie, E. B.; Galvan, D. H.; Adem, E.; Talapatra, S.; Yang, G.; Migone, A. D.; *Advanced Materials*, **2000**, 12, 495-498.
48. Li, Y. D.; Li, X. L.; He, R. R.; Zhu, J.; Deng, Z.; *Journal of the American Chemical Society*, **2002**, 124, 1411-1416.

49. Therese, H. A.; Li, J.; Kolb, U.; Tremel, W.; *Solid State Sciences*, **2005**, 7, 67-72.
50. Zhu, Y.; Q.; Sekine, T.; Brigatti, K. S.; Firth, S.; Tenne, R.; Rosentsveig, R.; Kroto, H. W.; Walton, D. R. M.; *Journal of the American Chemical Society*, **2003**, 125, 1329-1333.
51. Kaplan-Ashiri, I.; Cohen, S. R.; Apter, N.; Wang, Y.; Seifert, G.; Wagner, H.; D.; Tenne, R.; *Journal of Physical Chemistry C*, **2007**, 111, 8432-8436.
52. Rothschild, A.; Cohen, S. R.; Tenne, R.; *Applied Physics Letters*, **1999**, 75, 4025-4027.
53. Zhang, W.; Ge, S.; Wang, Y.; Rafailovich, M. H.; Dhez, O.; Winesett, D. A.; Ade, H.; Shafi, K. V. P. M.; Ulman, A.; Popovitz-Biro, R.; Tenne, R.; Sokolov, J.; *Polymer*, **2003**, 44, 2109-2115.
54. Wang, G. X.; Bewlay, S.; Yao, J.; Liu, H. K.; Dou, S. X.; *Electrochemical and Solid-State Letters*, **2004**, 7, A321-A323.
55. Kam, K. K.; Parkinson, B. A.; *Journal of Physical Chemistry*, **1982**, 86, 463-467.
56. Seifert, G.; Terrones, H.; Terrones, M.; Jungnickel, G.; Frauenheim, T.; *Solid State Communications*, **2000**, 114, 245-248.
57. Scheffer, L.; Rosentzveig, R.; Margolin, A.; Popovitz-Biro, R.; Seifert, G.; Cohen, S. R.; Tenne, R.; *Physical Chemistry Chemical Physics*, **2002**, 4, 2095-2098.
58. Feldman, Y.; Wasserman, E.; Srolovitz, D. J.; Tenne, R.; *Science*, **1995**, 267, 222-225.
59. Hsu, W. K.; Chang, B. H.; Zhu, Y. Q.; Han, W. Q.; Terrones, H.; Terrones, M.; Grobert, N.; Cheetham, A. K.; Kroto, H. K.; Walton, D. R. M.; *Journal of the American Chemical Society*, **2000**, 122, 10155-10158.
60. Zelenski, C. M.; Dorhout, P. K.; *Journal of the American Chemical Society*, **1998**, 120, 734-742.
61. Remskar, M.; Mrzel, A.; Skraba, Z.; Jesih, A.; Ceh, M.; Demsar, J.; Stadelmann, P.; Levy, F.; Mihailovic, D.; *Science*, **2001**, 292, 479-481.
62. Remskar, M.; Mrzel, A.; Sanjines, R.; Cohen, H.; Levy, F.; *Advanced Materials*, **2003**, 15, 237-240.
63. Seifert, G.; Terrones, H.; Terrones, M.; Jungnickel, G.; Frauenheim, T.; *Physical Review Letters*, **2000**, 85, 146-149.

64. Loh, K.; P.; Zhang, H.; Chen, W. Z.; Ji, W.; *Journal of Physical Chemistry B*, **2006**, 110, 1235-1239.
65. Therese, H. A.; Zink, N.; Kolb, U.; Tremel, W.; *Solid State Sciences*, **2006**, 8, 1133-1137.
66. Lavayan, V.; Mirabal, N.; O'Dwyer, C.; Santa Ana, M. A.; Benavente, E.; Sotomayor Torres, C. M.; Gonzalez, G.; *Applied Surface Science*, **2007**, 253, 5185-5190.
67. Zhu, Y. Q.; Sekine, T.; Li, Y. H.; Fay, M. W.; Zhao, Y. M.; Poa, C. H. P.; Wang, W. X.; Roe, M. J.; Brown, P. D.; Fleishcer, N.; Tenne, R.; *Journal of the American Chemical Society*, **2005**, 127, 16263-16272.
68. a.) Chen, J.; Kuriyama, N.; Yuan, H.; Takeshita, H. T.; Sakai, T.; *Journal of the American Chemical Society*, **2001**, 123, 11813-11814; b.) Chen, J.; Li, S. L.; Tao, Z. L.; *Journal of Alloys and Compounds*, **2003**, 356-357, 413-417.
69. Chen, J.; Li, S. L.; Xu, Q.; Tanaka, K.; *Chemical Communications*, **2002**, 1722-1723.
70. Cheng, F.; Chen, J.; Gou, X.; *Advanced Materials*, **2006**, 18, 2561-2564.
71. Dominko, R.; Arcon, D.; Mrzel, A.; Zorko, A.; Cevc, P.; Venturini, P.; Gaberscek, M.; Remskar, M.; Mihailovic, D.; *Advanced Materials*, **2002**, 14, 1531-1534.
72. Nath, M.; Rao, C. N. R.; *Journal of the American Chemical Society*, **2001**, 123, 4841-4842.
73. Zhu, Y. Q.; Hsu, W. K.; Kroto, H. W.; Walton, D. R. M.; *Chemical Communications*, **2001**, 2184-2185.
74. Remskar, M.; Mrzel, A.; Jesih, A.; Levy, F.; *Advanced Materials*, **2002**, 14, 680-684.
75. Nath, M.; Rao, C. N. R.; *Pure and Applied Chemistry*, **2002**, 74, 1545-1552.
76. Galvan, D. H.; Kim, J.; Maple, M. B.; Adem, E.; *Fullerene Science and Technology*, **2001**, 9, 225-232.
77. Nath, M.; Kar, S.; Raychaudhuri, A. K.; Rao, C. N. R.; *Chemical Physics Letters*, **2003**, 368, 690-695.
78. Nath, M.; Rao, C. N. R.; *Chemical Communications*, **2001**, 2236-2237.

79. Flores, E. ; Tlahuice, A.; Adem, E.; Galvan, D. H.; *Fullerene Science and Technology*, **2001**, 9, 9-16.
80. Qiu, L.; Pol, V. G.; Wei, Y.; Gedanken, A.; *Journal of Materials Chemistry*, **2003**, 13, 2985-2988.
81. Wu, X.; Xu, Z.; Zeng, X. C.; *Nano Letters*, **2007**, 7, 2987-2992.
82. Wheeler, B. L.; Leland, J. K.; Bard, A. J.; *Journal of the Electrochemical Society*, **1986**, 133, 358-361; Harris, S.; Chianelli, R. R.; *Journal of Catalysis*, **1984**, 86, 400-412.
83. Coleman, K. S.; Sloan, J.; Hanson, N. A.; Brown, G.; Clancy, G. P.; Terrones, M.; Terrones, H.; Green, M. L. H.; *Journal of the American Chemical Society*, **2002**, 124, 11580-11581.
84. Brorson, M.; Hansen, T. W.; Jacobsen, C. J. H.; *Journal of the American Chemical Society*, **2002**, 124, 1582-1583.
85. Chen, J.; Li, S.; Tao, Z. Gao, F.; *Chemical Communications*, **2003**, 980-981.
86. Chen, J.; Li, S.; Tao, Z.; Shen, Y.; Cui, C.; *Journal of the American Chemical Society*, **2003**, 125, 5284-5285.
87. Chen, J.; Tao, Z.; Li, S.; Fan, X.; Chou, S.; *Advanced Materials*, **2003**, 15, 1379-1382.
88. Therese, H. A.; Rocker, F.; Reiber, A.; Li, J.; Stepputat, M.; Glasser, G.; Kolb, U.; Tremel, W.; *Angewandte Chemie International Edition*, **2004**, 44, 262-265.
89. Rao, C. N. R.; Govindaraj, A.; Deepak, F. L.; Gunari, N. A.; Nath, M.; *Applied Physics Letters*, **2001**, 78, 1853-1855.
90. Miao, J.; Ren, T.; Dong, L.; Zhu, J.; Chen, H.; *Small*, **2005**, 1, 802-805.
91. Li, X.; Chu, H.; Li, Y.; *Journal of Solid State Chemistry*, **2006**, 179, 96-102.
92. Wang, X.; Gao, P.; Li, J.; Summers, C. J.; Wang, Z. L.; *Advanced Materials*, **2002**, 14, 1732-1735.
93. Ye, C.; Meng, G.; Jiang, Z.; Wang, Y.; Wang, G.; Zhang, L.; *Journal of the American Chemical Society*, **2002**, 124, 15180-15181.
94. Park, K. H.; Choi, J.; Kim, H. J.; Lee, J. B.; Son, S. U.; *Chemistry of Materials*, **2007**, 19, 3861-3863.

95. Jiang, X.; Mayers, B.; Herricks, T.; Xia, Y.; *Advanced Materials*, **2003**, 15, 1740-1743.
96. Jiang, X.; Mayers, B.; Wang, Y.; Cattle, B.; Xia, Y.; *Chemical Physics Letters*, **2004**, 385, 472-476.
97. Hu, J.; Bando, Y.; Zhan, J.; Liu, Z.; Goldberg, D.; Ringer, S. P.; *Advanced Materials*, **2005**, 17, 975-979.
98. Niu, H.; Gao, M.; *Angewandte Chemie International Edition*, **2006**, 45, 6462-6466.

## Chapter 2: Surfactant Assisted Synthesis of WS<sub>2</sub> Nanowires

There is a growing interest in the synthesis of novel nanomaterials showing many different structural forms. Inorganic nanomaterials constitute an important class of these structures due to their wide variety of physical and electronic properties. The synthetic methodology for obtaining nanomaterials may be divided into two types: hard and soft chemical routes. The hard chemical routes usually consist of using high temperatures and long reaction times. The soft chemical routes usually offer milder synthetic conditions, one reason that they are becoming more attractive. Among these routes are the use of surfactants and structural directing materials. These structural directing agents have successfully been used to synthesize many different types of nanomaterials. One of the first examples of this synthetic approach is the formation of an ordered mesoporous aluminosilicate by Kresge and co-workers via a surfactant-assisted assembly in 1992.<sup>1</sup> This discovery, on the heels of the discovery of carbon nanotubes by Iijima in 1991<sup>2</sup>, led to a great deal of excitement in nanostructured materials.

The use of surfactants and structural directing agents to aid in the synthesis of one-dimensional materials has been explored. Vanadium oxide nanotubes have been synthesized using hexadecylamine and vanadium triisopropoxide.<sup>3</sup> SiO<sub>2</sub> nanotubes have also been made using a surfactant.<sup>4</sup> In addition to oxidic nanotubes, the layered transition metal dichalcogenides provide a rich toolkit from which to synthesize one-dimensional structures due to their ability to form closed structures as a result of the presence of

dangling bonds at the edges of the layers. CdS and CdSe nanotubes and nanowires have been synthesized using Triton-X surfactant and a mixture of CdO and NaHSe in water.<sup>5</sup> Li and coworkers synthesized WS<sub>2</sub> nanotubes by treating the surfactant cetyltrimethylammonium bromide (CTAB) in combination with thioacetamide and ammonium tungstate hydrothermally followed by pyrolysis.<sup>6</sup> Therese and coworkers produced WS<sub>2</sub> nanotubes by sulfidizing WO<sub>3</sub> nanorods that were synthesized hydrothermally.<sup>7</sup>

Many of the synthetic routes involving surfactants as structural directing agents have resulted in the formation of nanowires. CdS nanowires were formed solvothermally using ethylenediamine as a nonaqueous template and elemental Cd and S at temperatures of 120-190 °C for 3-6 hours.<sup>8</sup> Iron sulfide nanowires have also been formed solvothermally using ethylenediamine as the solvent with FeCl<sub>2</sub> and thioacetamide.<sup>9</sup> Surfactants such as CTAB and trioctylphosphine oxide (TOPO) have also successfully been used to form nanowire structures. Nanowires of tungsten metal have been synthesized by combining Na<sub>2</sub>WO<sub>4</sub> and CTAB in an aqueous solution and treating hydrothermally followed by pyrolysis.<sup>10</sup> PbTe nanowires were synthesized by combining a thin Pb foil and Te powder with CTAB in a 6.6% hydrazine in water solution.<sup>11</sup>

We report a very simple synthetic strategy for the formation of WS<sub>2</sub> nanowires. 1 mmol of ammonium tetrathiotungstate (Aldrich) was dissolved in 15 mL of water. This was then mixed with 60 mL of an aqueous solution containing 2 mmol of the surfactant CTAB. Upon mixing the two solutions, an immediate yellow precipitate formed. The

precipitate was washed with water and ethanol and then vacuum dried overnight at 65 °C. The as-made precipitate was analyzed with XRD. The results of the XRD are presented in Figure 2.1.

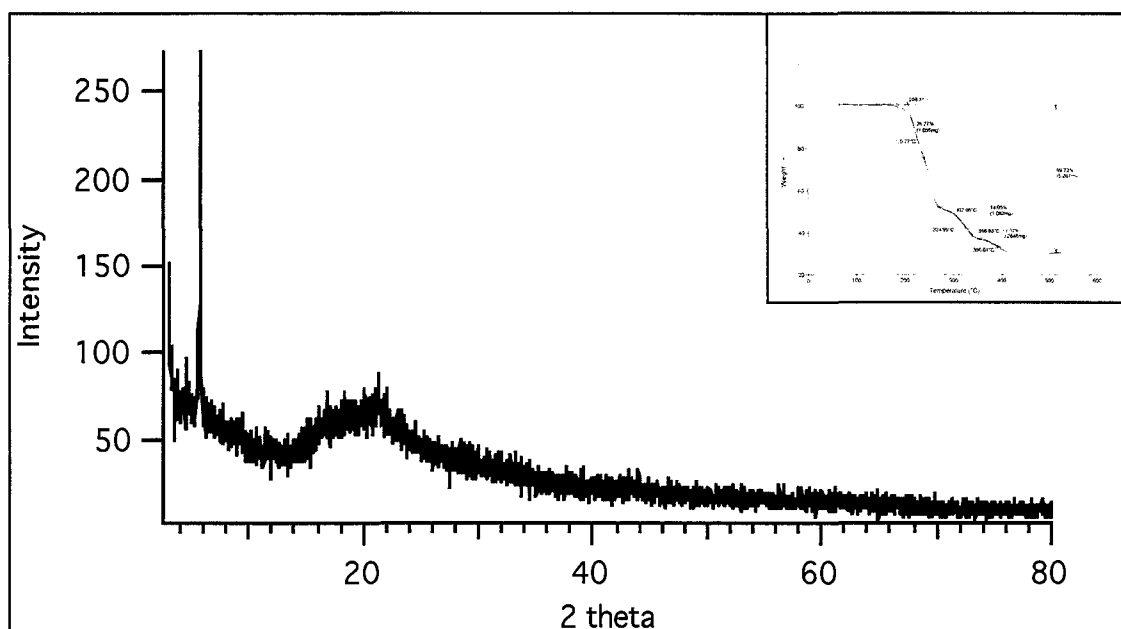


**Figure 2.1.** XRD spectrum of the precipitate formed by combining  $(\text{NH}_4)_2\text{WS}_4$  and CTAB in water. The low angle peak demonstrates the lamellar nature of the sample. The inset shows a TGA of the as-prepared sample.

A low-angle peak at about  $2\theta = 5.74$  is seen in the XRD pattern. This peak is common in striated materials with structural modifiers. In addition to XRD, TGA was performed on the as-prepared precipitate. It shows decomposition with a concomitant 69.7 mass percent loss at 400 °C. This corresponds to the loss of two CTA ions and two S ions, leaving behind  $\text{WS}_2$ .

In many of these experiments, nanowires and nanobelts were synthesized. To see how the morphology of the products was changed, several synthetic parameters were investigated for the pyrolysis of the sample. The pyrolysis temperature was changed from 650 to 850 °C. Higher temperatures improved the yield of nanowires and nanobelts. The flow rate of inert gas through the furnace was also varied, and also seemed to influence the formation of 1-dimensional structures. The reaction times were generally held at 5 hours. Figure 2.2 shows the SEM images of the 1-dimensional WS<sub>2</sub> nanowires formed at different temperatures.

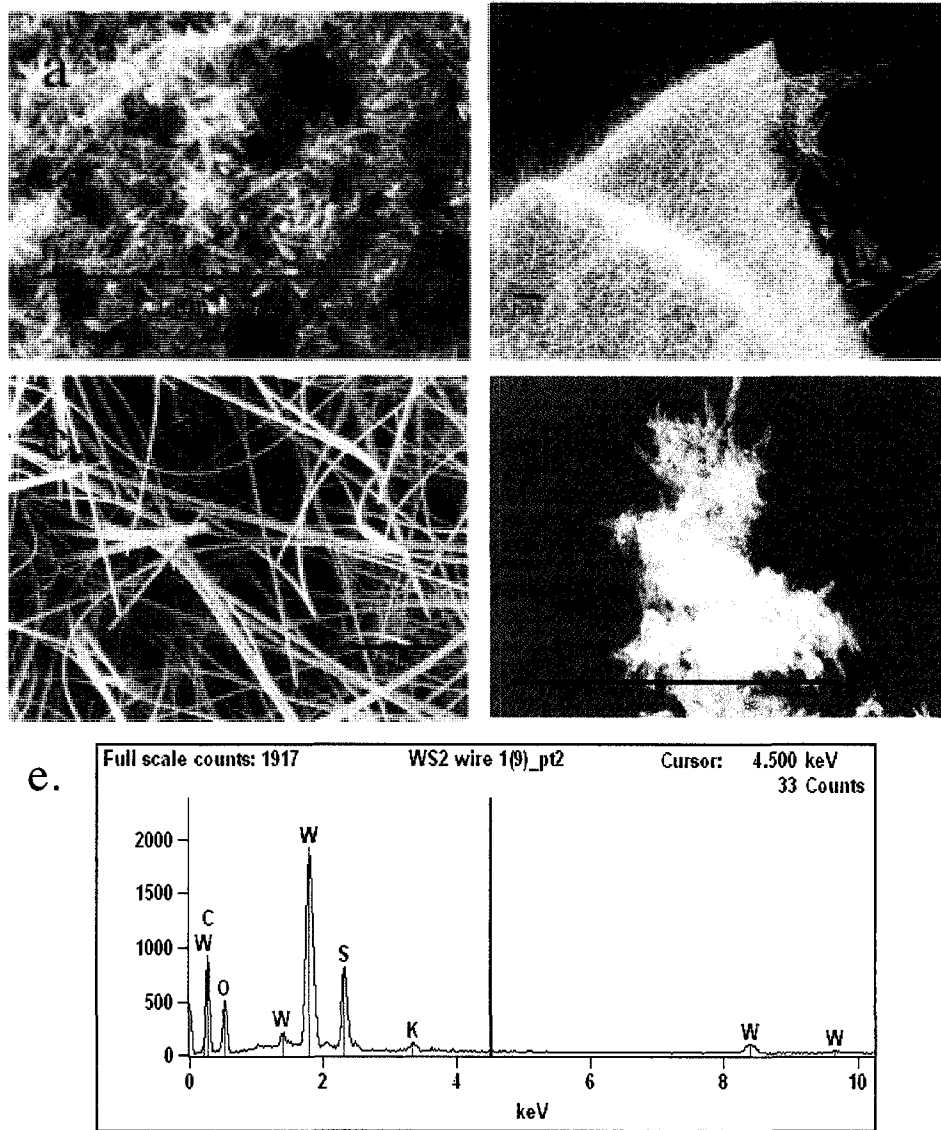


**Figure 2.2** SEM images of the 1-dimensional structures of WS<sub>2</sub> formed at different temperatures: a.) 650 °C, b.) 685 °C, c.) 725 °C, d.) 800 °C and e.) representative EDS of nanowires. All flow rates were 50 sccm N<sub>2</sub> or Ar.

The image in Figure 2.2a shows the beginning of the formation of 1-dimensional structures at 650 °C. These appear to be short nanorods with lengths only up to 150 nm with diameters of about 20 nanometers. In Figure 2.2b, there are many more 1-dimensional structures that have formed with just a 35 °C increase in temperature. These similar structures are also formed when the temperature is increased to 725 °C, as shown

in Figure 2.2c. The dimensions of the nanowires and nanobelts shown in Figure 2.2b and 2.2c are also similar. The diameters are as small as 20 nm and the lengths can be up to 18  $\mu\text{m}$ . Both straight and bent nanowires are present. In both experiments, two or more nanowires appear to merge into each other. The nanowires appear to grow out of the amorphous material they are residing on. In several cases, small areas appear to be nucleation sites from which sea urchin-like structures of nanowires radiate. Figure 2.3 shows these sea urchin-like structures.

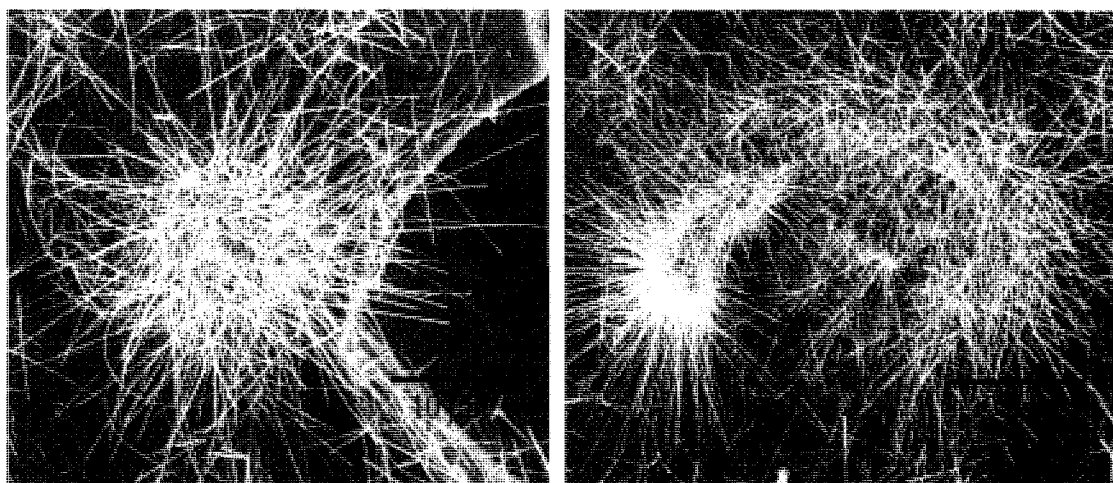
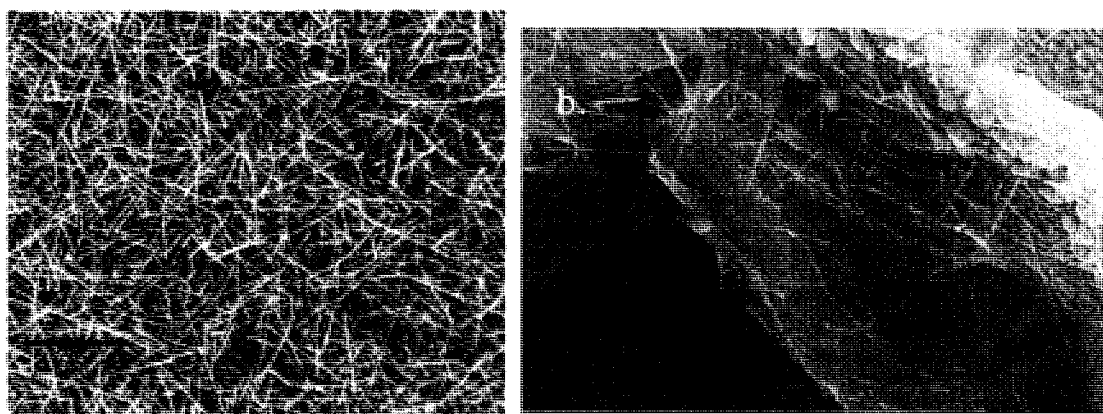


**Figure 2.3** SEM images of sea urchin like  $\text{WS}_2$  wires growing out of the amorphous material.

There also is a higher number of nanowires on the surfaces of the amorphous material. At temperatures above 800  $^{\circ}\text{C}$ , the nanowire yield is drastically reduced, and the material looks similar to that seen with a reaction temperature of 650  $^{\circ}\text{C}$ . The EDS shown in Figure 2.2e is representative of the kinds and amounts of elements present. Notably, the W:S ratio is 1:2. The flow rate of the inert gas through the furnace in all of the

experiments shown in Figure 2.2 was 50 sccm. Both  $N_2$  and Ar were used as the inert gas, but this did not affect the quantity or quality of nanowires formed.

Experiments were also undertaken to determine whether the gas flow rate had an effect on the dimensions or quantity of the nanowires grown. Figure 2.4 shows the SEM images for two of these experiments.



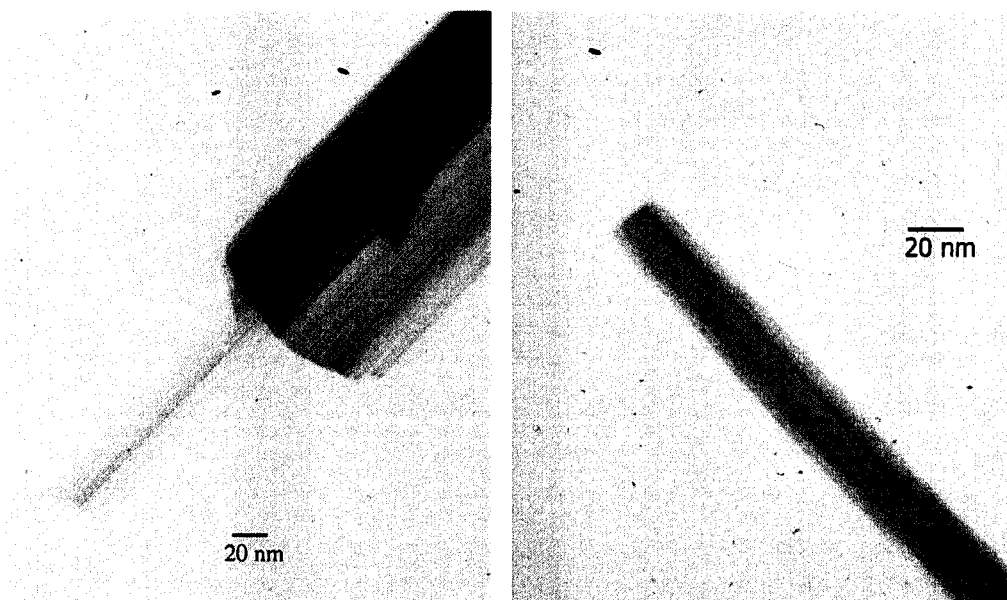
**Figure 2.4.**  $WS_2$  nanowire products formed at different temperatures with high flow rates: a.) shows a bundle of nanowires formed at  $725\text{ }^\circ\text{C}$  ; b.) shows nanowires formed at  $850\text{ }^\circ\text{C}$ . Both gas flows are 200 sccm of  $N_2$ .

Figure 2.4 shows that nanowires are formed at both high flow rates and low inert gas flow rates. There is a large quantity of nanowires in Figure 2.4a. Although there are fewer nanowires in Figure 2.4b, they were still present at temperatures of  $850\text{ }^\circ\text{C}$ . This implies that the higher flow rate of 200 sccm influences the nanowire growth since at temperatures of  $800\text{ }^\circ\text{C}$  with a flow rate of 50 sccm, no nanowires were present. Table 2.1 summarizes the results of the variable synthesis conditions.

Inert Gas	Gas Flow (sccm)	Pyrolysis Temperature (°C)	Result
N <sub>2</sub>	50	650	Nanorods
Ar	50	685	Nanowires and nanobelts
N <sub>2</sub>	50	725	Nanowires and nanobelts
N <sub>2</sub>	50	800	No 1-dimensional structures
Ar	200	700	Nanowires and nanobelts
N <sub>2</sub>	200	850	Some nanowires and nanobelst

**Table 2.1** Summary of the results of the different experimental paramters of temperature and inert gas flow rates. All reaction times were 5 hours.

The table shows the general trend of a range of temperatures resulting in the formation of nanowires and nanobelts. The temperature range of 685 °C to 725 °C results in a large yield of 1-dimensional WS<sub>2</sub> structures. The table also demonstrates the effect of gas flow rate on the synthesis of these nanowires and nanobelts. A higher gas flow rate results in the formation of more 1-dimensional structures than a lower flow rate at higher temperatures. In addition to the SEM analysis, TEM images of the WS<sub>2</sub> nanowires were also taken. Figure 2.5 shows a TEM image of two WS<sub>2</sub> nanowires.



**Figure 2.5.** TEM images of the WS<sub>2</sub> nanowires synthesized at 725 °C: a.) shows a nanowire that appears to be growing out of a larger one; b.) shows an individual WS<sub>2</sub> nanowire. Both small nanowires are about 20 nm in diameter.

As shown in Figure 2.5, the nanowire morphology is confirmed; the 1-dimensional structures are solid throughout their length. Figure 2.5a shows a WS<sub>2</sub> nanowire that appears to be growing out of a larger nanobelt. Distinct lines can be seen along the length of the wire as well. These are interference patterns in the nanowire due to the thickness. The larger structure appears to have different thicknesses and areas of concavity along the axis. It does not appear to be perfectly flat or perfectly cylindrical. Figure 2.5b shows an individual WS<sub>2</sub> nanowire. This nanowire also has distinct striations running along the long axis. Both smaller nanowires have diameters of about 20 nm.

In the initial reaction between  $\text{CTA}^+$  cations and  $\text{WS}_4^{4-}$  anions, we speculate a simple cation exchange reaction between the ammonium and cetyltrimethylammonium groups. The result is a  $\text{WS}_4^{4-}$  ion surrounded by four  $\text{CTA}^+$  ions. The long chain hydrocarbons associate with other hydrocarbon chains in the hydrophilic environment. Since these hydrophobic groups have a cationic head group, they are attracted to the thiotungstate anions. This has the effect of pulling out the  $\text{WS}_4^{4-}$  anions from the solution in a precipitate containing both. Upon precipitation of the solid material from the solution, some order is retained in the solid in the form of a lamellar structure. This order is reflected in the XRD pattern of the precipitate indicating a periodicity of about 1.54 nm. The C-C bond length is about 1.5 angstroms, and there are 15 carbon atoms in the  $\text{CTA}^+$  cation giving a length of about 2.25 nm. However, this length reflects the C-C bonds with bond angles of  $180^\circ$ , not the expected  $104.5^\circ$  resulting in a shortened overall length.

When the washed and dried precipitate is placed in the furnace, it is exposed to a gas flow rate with high temperature. As previously mentioned the nanowires are more prevalent on the surface of the bulk material. This implies that the conditions on the surface are quite different from the conditions within the bulk material. One possible reason for the formation of the  $\text{WS}_2$  nanowires is as follows. As indicated by the TGA on a washed and dried sample, when the temperature of the reaction exceeds  $400^\circ\text{C}$ , the CTA groups and some sulfur leave as gaseous products. What remains are tungsten/sulfur groups with some charge associated with them. The temperature of the

reaction is not great enough to melt or sublime these materials. They are only a short distance away from other tungsten/sulfur species and condense with each other to form 1-dimensional WS<sub>2</sub> wires. The higher flow rates have the effect of sweeping away the decomposition products more quickly and initiate a more complete synthesis of nanowire and nanobelt structures. Based on the above hypothesis, it is likely that if the dried precipitate were ground into a very fine powder that a much greater yield of WS<sub>2</sub> nanowires would result from the higher surface area, and further experiments are warranted to verify this.

In conclusion, we have synthesized WS<sub>2</sub> nanowires and nanobelts by a surfactant-assisted synthesis. We have explored and optimized the reaction parameters of time and gas flow rate and have found conditions that are more conducive to a high yield of nanowires. The optimal conditions are temperatures of about 700 °C with inert gas flow rates about 200 sccm. Our simple synthetic route has several advantages: it does not require an intermediate hydrothermal reaction step, as ordered phases occur upon the mixing of only 2 reactants, and it is a bulk technique.

## References

1. Kresge, C. T.; Leonowicz, M. E.; Roth, W. J.; Vartuli, J. C.; Beck, J. S.; *Nature*, **1992**, 359, 710-712.
2. Iijima, S.; *Nature*, **1991**, 354, 56-68. Spahr, M. E.; Bitterli, P.; Nesper, R.; Muller, M.; Krumeich, F.; Nissen, H. U.; *Ang. Chem. Intl. Edn.*, **1998**, 37, 1263-1265.
3. Krumeich, F.; Muhr, H.-J.; Niederberger, M.; Bieri, F.; Schnyder, B.; Nesper, R.; *Journal of the American Chemical Society*, **1999**, 121, 8324-8331.
4. Ono, Y.; Nakashima, K.; Sano, M.; Kanekiyo, Y.; Inoue, K.; Hojo, J.; Shinkai, S.; *Chemical Communications*, **1998**, 1477-1478.
5. Rao, C. N. R.; Govindaraj, A.; Deepak, F. L.; Gunari, N. A.; Nath, M.; *Applied Physics Letters*, **2001**, 78, 1853-1855.
6. Li, Y. D.; Li, X. L.; He, R. R.; Zhu, J.; Deng, Z.; *Journal of the American Chemical Society*, **2002**, 124, 1411-1416.
7. Therese, H. A.; Li, J.; Kolb, U.; Tremel, W.; *Solid State Sciences*, **2005**, 7, 67-72.
8. Li, Y.; Liao, H.; Ding, Y.; Qion, Y.; Yang, L.; Zhou, G.; *Chemistry of Materials*, **1998**, 10, 2301-2303.
9. Nath, M.; Choudhury, A.; Kundu, A.; Rao, C. N. R.; *Advanced Materials*, **2003**, 15, 2098-2101.
10. Li, Y.; Li, X.; Deng, Z.; Zhou, B.; Fan, S.; Wang, J.; Sun, X.; *Angewandte Chemie International Edition*, **2002**, 41, 333-335.
11. Zhang, L.; Yu, J. C.; Mo, M.; Wu, L.; Kwong, K. W.; Li, Q.; *Small*, **2005**, 1, 349-354.

## Chapter 3: Synthesis and Characterization of MoS<sub>2</sub> and WS<sub>2</sub> Nanotubes

The discovery of carbon nanotubes by Iijima in 1991 catalyzed a great deal of research into the synthesis and properties of 1-dimensional materials.<sup>1</sup> The research on carbon nanotubes has resulted in not only the discovery of novel properties of carbon nanotubes themselves, but to the potential applications of other 1-dimensional materials. Tenne and co-workers suggested that other layered materials could also form nanotubes. This was first demonstrated in WS<sub>2</sub> in 1992.<sup>2</sup> Following this discovery, the same researchers demonstrated that MoS<sub>2</sub> nanotubes could also be synthesized.<sup>3</sup> Both WS<sub>2</sub> and MoS<sub>2</sub> belong to the class of layered transition metal dichalcogenides (LTMDs). The LTMDs exhibit a wide range of physical and electrical properties.<sup>4</sup> Both MoS<sub>2</sub> and WS<sub>2</sub> exhibit trigonal prismatic geometry and are semiconducting with bandgaps of 1.2 and 1.3 eV, respectively. These materials have found applications as catalysts and solid lubricants. Tenne and co-workers were the first investigators to synthesize these nanotubes. However, the synthetic routes of flowing H<sub>2</sub>S gas over the respective oxides of these materials did not allow for the preparation of uniform sized materials. The resulting products encompassed both inorganic fullerene like particles as well as nanotubes.

Experiments probing the electrical properties of these materials have been undertaken in the past. The current voltage characteristics of WS<sub>2</sub> nanotubes were investigated with scanning tunneling microscopy.<sup>5</sup> These experiments showed WS<sub>2</sub> nanotubes to be semiconducting and confirmed theoretical calculations predicting smaller band gaps with decreasing diameters of the nanotubes.<sup>6</sup> For nanotubes of MoS<sub>2</sub>, there has been some investigation of their electrical properties.

Remskar and co-workers performed scanning tunneling microscopy on individual single-walled MoS<sub>2-x</sub>I<sub>y</sub> nanotubes prepared by a chemical vapor transport reaction.<sup>7</sup> These tubes were determined to be metallic, agreeing with theoretical calculations that all MoS<sub>2</sub> nanotubes with diameters greater than 2 nm would be semiconducting, while nanotubes with smaller diameters would be metallic.<sup>8</sup>

Nath and Rao used ammonium tetrathiomolybdate and tetrathiotungstate powders and decomposed them at high temperatures under a hydrogen and nitrogen gas flow to make closed structures of MoS<sub>2</sub> and WS<sub>2</sub>.<sup>9</sup> In addition, a route demonstrated by Zelenski and Dorhout utilized an anodic alumina membrane as a hard template.<sup>10</sup> The pores of the membrane were loaded with ammonium tetrathiomolybdate precursor solution and the solvent driven off. The resulting products were nearly monodisperse nanotubules of MoS<sub>2</sub>. The diameter of the nanotubules corresponded to the size of the pores of the membrane. The lengths of the nanotubules were also uniform.

We have used the anodic alumina membranes as templates to make both MoS<sub>2</sub> and WS<sub>2</sub> nanotubes. In a similar experimental approach to Zelenski and Dorhout, we

used the single-source tetrathiomallate precursors dissolved in a solvent and loaded the alumina membranes. In a typical experiment, a 0.1 M solution of the single source tetrathiomallate precursor dissolved in dimethylformamide (DMF) was added dropwise onto an alumina membrane via a syringe. The DMF was evaporated over a hotplate and the loaded template was then placed on a quartz boat in a flow through furnace. The sample was heated at 450 ° C for 1 hour under a flow of 90% N<sub>2</sub>/ 10 % H<sub>2</sub> and then allowed to cool to room temperature. The chemical reaction taking place may be written as follows:



where M = Mo, W.

After removing the sample from the furnace, the shiny black membrane was placed in a solution of 2 M NaOH for several hours. The basic solution was carefully removed and the solid material was rinsed several times with deionized water until a neutral pH was achieved. The water was removed and the sample placed under methanol for future analysis.

Figure 3.1 shows a scanning electron micrograph of a bundle of WS<sub>2</sub> nanotubes. The tubes have open ends and diameters generally conforming to the diameter of the template pores. The surfaces appear smooth and relatively defect free. The EDS spectrum verifies a W:S ratio of 1:2. Upon analysis of the samples with TEM, the appearance of a bamboo type structure becomes apparent. In addition to the bamboo

appearance, the presence of lattice fringes is clearly visible. The distance between layers corresponds to the 001 plane of  $\text{WS}_2$ .

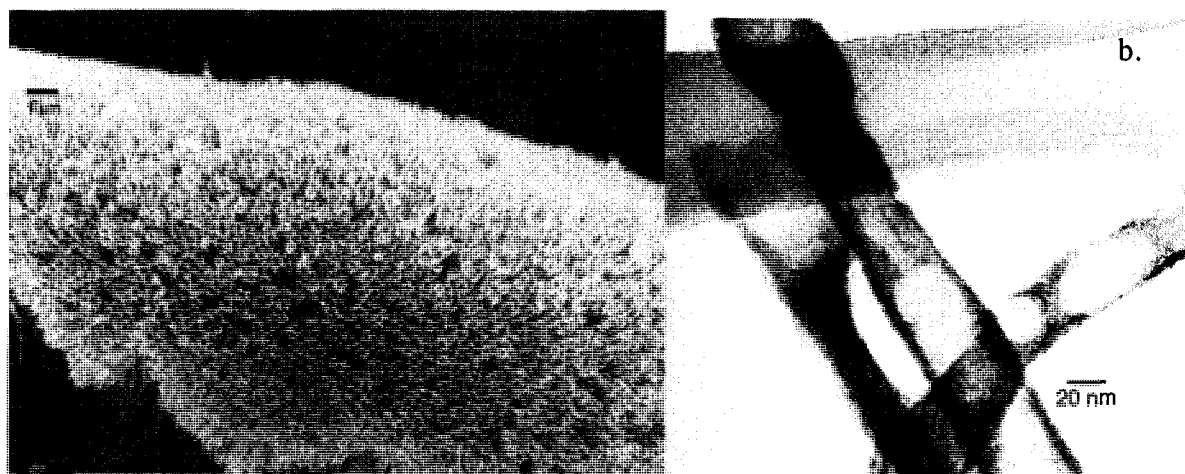


**Figure 3.1** a.)SEM of bundle of  $\text{WS}_2$  nanotubes made by using anodic aluminum oxide template; b) TEM of  $\text{WS}_2$  nanotubes using 30 nm pore anodic aluminum oxide template.

The  $\text{MoS}_2$  nanotube products can be seen in Figure 3.2. Once again the nanotubes exhibit a bamboo type appearance, which is commonly seen in nanotubes synthesized in the pores of alumina templates. The EDS characterization indicates a Mo:S ratio of 1:2. Nanotubes of diameters close to 30 nm have been synthesized using custom alumina templates with corresponding diameter pore sizes. These tubes appear much more flexible than their larger diameter counterparts. The tubes are bent and curved rather than straight and rigid. This may be due to the bamboo type nature of the tubes, which create localized areas of flexibility.

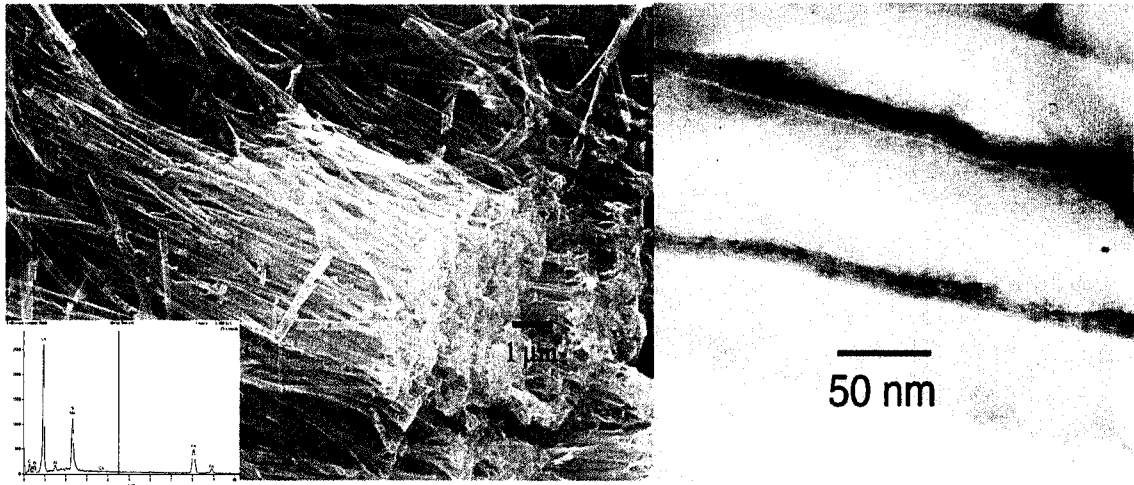


**Figure 3.2.** MoS<sub>2</sub> nanotubes formed by anodic aluminum oxide template: a.) shows an SEM of the as-prepared nanotubes. Inset: EDS characterization of the nanotubes indicating Mo:S ratio of 1:2. b.) shows high-magnification of MoS<sub>2</sub> nanotubes using alumina membranes with pore sizes of s 60 nm.

The MoS<sub>2</sub> nanotubes have a very similar appearance to their WS<sub>2</sub> counterparts with respect to the bamboo type appearance along the tube axis. The TEM shows lattice fringes with distances of 6.5 angstroms corresponding to the 001 planes of MoS<sub>2</sub>.

In an effort to improve the morphology of the nanotubes, a wide variety of synthesis parameters were adjusted. The variables of temperature, time, concentration, and pore diameters were investigated. Table 3.1 lists these parameters with some description of the resulting nanotubes.

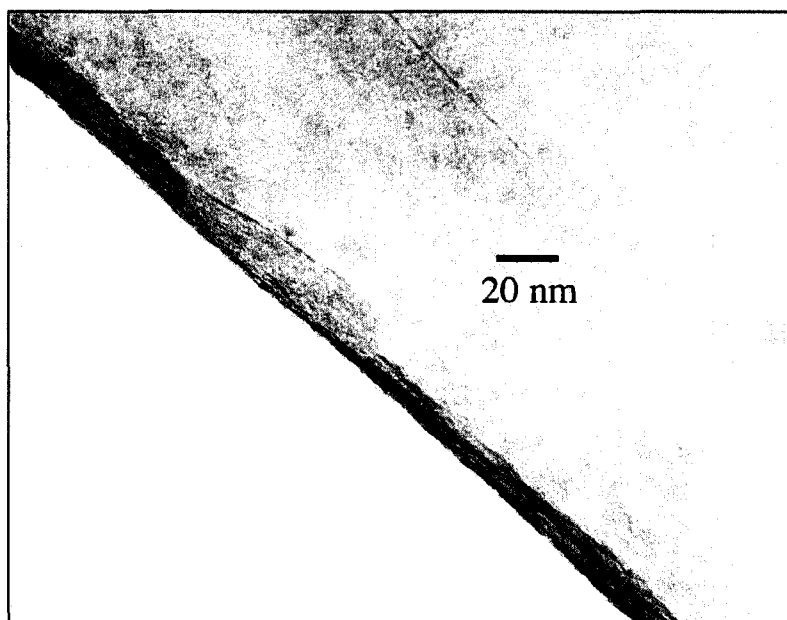
Precursor Metal	Concentration (M)	Template Pore Size ( $\mu\text{m}$ )	Loading	Temperature ( $^{\circ}\text{C}$ )	Time	Result
Mo	0.1	0.2	D31DES3X	450	80-85 min	Wires, solid looking
Mo	0.1	0.02	2DES	450	70 min	Bamboo tubes, rough walls
Mo	0.1	0.2	2DES	450	24 hr	Tube fragments
Mo	0.1	0.1	2DES	450	2.5 hr	Bamboo tubes, wires
Mo	0.1	0.1	D12DES2X	450	2.5 hr	Bamboo tubes
Mo	0.1	0.1	D13DES2X	450	3.5 hr	Bamboo tubes
Mo	0.1	0.1	D12DES2X	450	3.5 hr	Bamboo tubes
Mo	0.1	0.03	D3	450	2.5 hr	Bamboo tubes, flexible
Mo	0.1	0.1	2DES	700	2.5 hr	Bamboo tubes, fewer dislocations
Mo	0.1	0.1	2DES	525	3 hr	Bamboo tubes
W	0.1	0.02	2DES	450	90 min	Bamboo tubes
W	0.1	0.03, 0.05	2DES	450	1 hr	Bamboo tubes, flexible
W	0.1	0.02, 0.1, 0.2	D12DES	450	7 hr	Bamboo tubes
W	0.1	0.03	1DES3X	450	18 hr	Few tubes
W	0.1	0.1	2DES	700	2.5 hr	Bamboo tubes, fewer dislocations
W	0.1	0.1	2DES	600	2 hr	Bamboo tubes
W	0.02	0.1	1DES, 1DES2X, 1DES3X	700	1.5 hr	Thinner walled bamboo tubes
W	0.005	0.03	1DES3X	725	1.5 hr	Thinner walled bamboo tubes

**Table 3.1** Reaction parameters for synthesis of  $\text{MoS}_2$  and  $\text{WS}_2$  tubes. Loading key: D31DES3X = dipped 3 times, 1 drop each side 3 times.

Despite the many synthetic parameters investigated, the nanotube morphology did not change significantly. At higher temperatures (above 650 °C), the number of edge dislocations - discontinuous layers - along the length of the nanotubes decreased. The yield of nanotubes at higher temperatures was lower. No combination of parameters completely eliminated the bamboo-like structure of these nanotubes. The use of the smaller pore size templates appears to increase the frequency of the bamboo-like appearance per tube. When reviewing the literature, virtually all nanotubes synthesized using the anodic alumina membrane technique result in this morphology.<sup>11</sup> Although decreasing the concentration of the precursor did result in nanotubes with thinner walls, the fewest number of layers attainable was approximately 12. This is likely true because the concentration of the solution was still too high to be able to form nanotubes consisting of a few layers. When using very small concentrations, it was difficult to find the nanotubes after dissolution of the template in base. The concentration was low enough that the resulting dissolved template appeared to be a colorless homogenous solution.

It is difficult to draw conclusions for choosing the reaction condition parameters that yield the highest quality of nanotubes. However, given the fact that there is some improvement in the number of edge dislocations at higher temperature, the most attractive synthetic route would feature temperatures of around 525 °C. Additionally, a lighter loading (dipping the membrane once in the precursor solution) using concentrations of below 0.1M would be desirable for thinner walled tubes. The larger

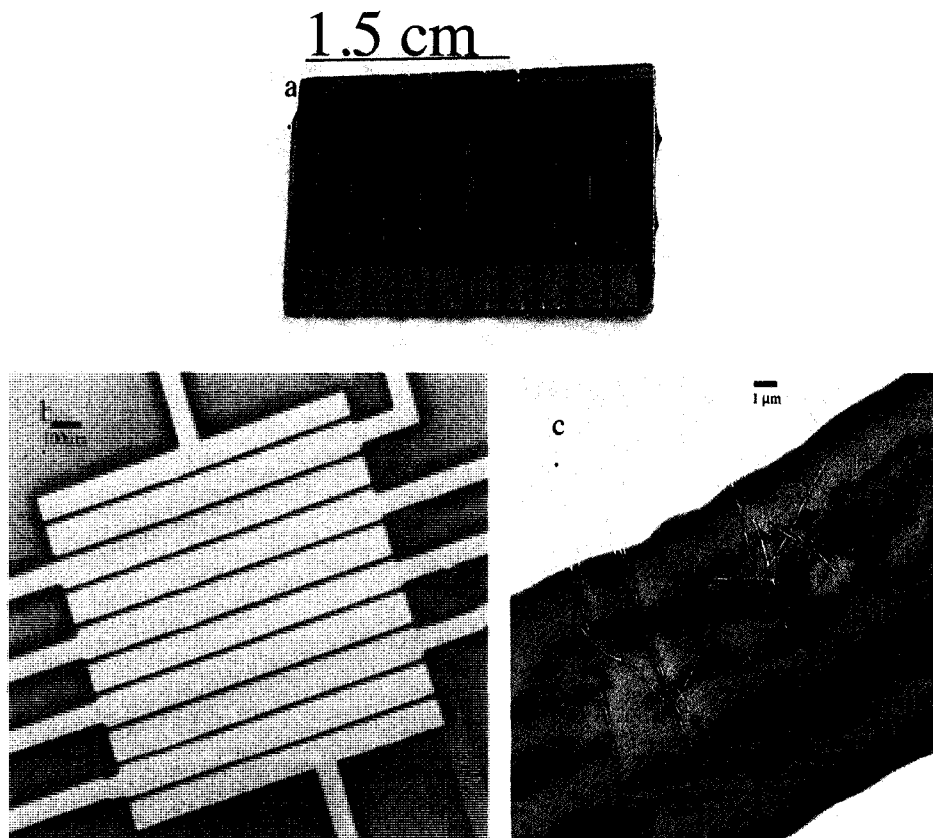
pore size templates to achieve a higher number of smooth walled tubes would also be advisable. Figure 4.3 shows a high magnification TEM image of a MoS<sub>2</sub> nanotube that has been pyrolyzed at 700 ° C. The edge dislocations have diminished to some extent as can be seen in the image, however, the yield of nanotubes was lower.



**Figure 3.3.** High magnification TEM of a MoS<sub>2</sub> nanotube that has been pyrolyzed at 700 ° C for 2.5 hours.

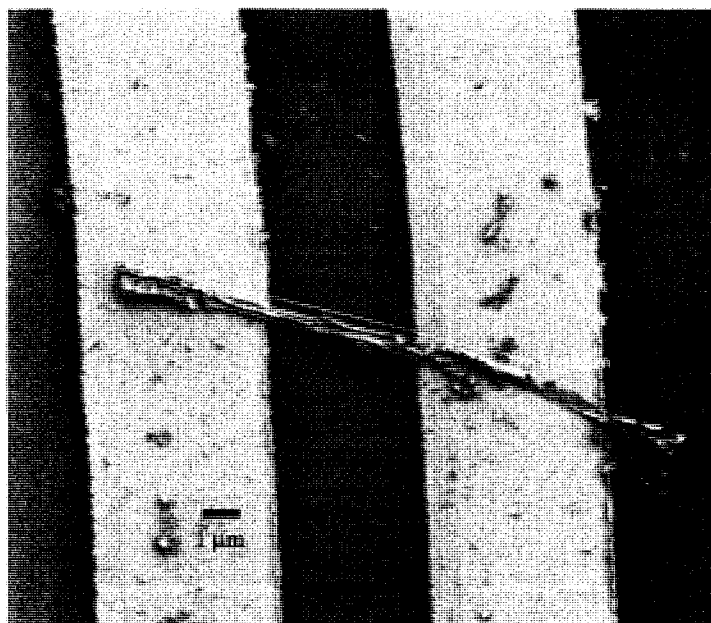
Upon achieving the best quality of nanotubes possible with the anodic aluminum oxide membrane technique, efforts were underway to investigate the electrical properties of these nanotubes. As with the synthesis part of the study, several techniques were looked at for the purpose of measuring the electrical properties of the MoS<sub>2</sub> nanotubes.

The first efforts involved using optical lithography to make an interdigitated array of electrodes on which a suspension of nanotubes was placed. The interdigitated array was fabricated in the clean-room in the engineering department at Colorado State University. A silicon wafer with a 500 nm thermal oxide was used as the substrate. The mask consisted of a transparency film with the interdigitated array pattern printed on it. A mask aligner was used to transfer the pattern to the positive photoresist covering the substrate. After development, an adhesive layer of Ti followed by 30 nm of Au was electron beam evaporated onto the sample. The resulting chip is pictured in Figure 3.4.



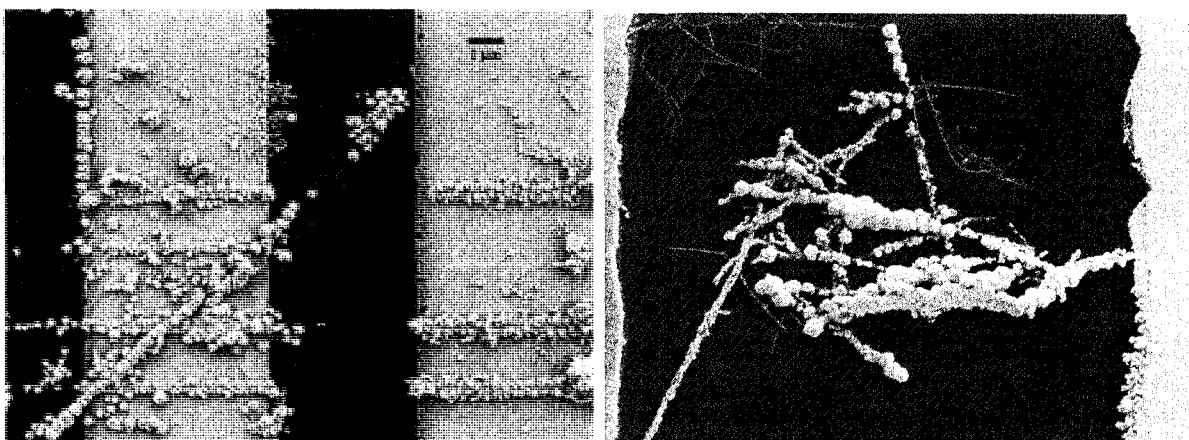
**Figure 3.4.** Series of images showing the original interdigitated array fabricated in the clean-room at Colorado State University: a.) the as-made IDA; b.) SEM image of the center array; c.) SEM image showing MoS<sub>2</sub> nanotubes on the IDA.

Figure 3.4c highlights one of the issues encountered when trying to make electrical contact to the nanotubes. No tubes were long enough to span the distance of 18 to 20  $\mu\text{m}$  between the gold contacts. Based on the simple nature of the photomask, an interdigitated array with the spacing between electrodes being less than 15  $\mu\text{m}$  was not achievable. A different approach had to be taken. We were able to obtain an interdigitated array commercially that would suit our requirements. The chips were purchased from Abtech, and featured four gold electrodes that were 5  $\mu\text{m}$  wide spaced 5  $\mu\text{m}$  apart. Based on this new chip, we were able to place a nanotube across the new interdigitated array. Figure 3.5 shows a nanotube that spans the distance between the two adjacent electrodes.



**Figure 3.5.** MoS<sub>2</sub> nanotube spanning two gold contacts on Abtech IDA.

We attempted to measure the electrical properties of the nanotube using a high-impedance electrometer. Unfortunately, the results indicated that no good electrical contact was made between the Au electrodes and the nanotubes, therefore a resistance indicative of an open-circuit resulted. Additional experiments were carried out with the intention of laying down gold over the nanotube in areas where it was specifically touching the electrode. These involved trying to plate Au over the nanotube from a solution. The nanotubes stayed in place over the electrodes even in a stirred solution, so that the plating experiments could be undertaken. A 3-electrode cell was used with the working electrode connected to the IDA from Abtech. A gold plating solution from Tecnic was used to electrodeposit the gold. The chip was configured such that two of the four gold contacts were connected. The amount of gold electrodeposited was calculated from the amount of charge that was passed. Care was taken to try and achieve a slow and uniform electrodeposition. Figure 3.6 shows an SEM image of the results of electrodeposition of Au on a MoS<sub>2</sub> nanotube.



**Figure 3.6.** Results of efforts to electroplate Au over a MoS<sub>2</sub> nanotube. The Au nucleated along the length of the nanotube.

As can be seen in the figure, the Au was deposited along the length of the nanotubes instead of only on the areas where the nanotubes were in contact with the Au electrodes. Ultimately, the use of electron beam lithography solved the problem of contacting individual nanotubes.

The electron beam lithography system used was the NPGS system by Joe Nability. A bi-layer of PMMA was used as the electron beam resist. The first layer was 3% 495 k MW PMMA in chlorobenzene. The second layer was 3% 950 k MW PMMA in chlorobenzene. The purpose of the bi-layer is to facilitate the final lift-off of the resist after metallization. Considerable effort was required in optimizing the conditions for e-beam lithography since it had not been previously done at CSU. Details are given in Appendix A. Two point electrical property measurements were carried out on the MoS<sub>2</sub> nanotubes at room temperature. The nanotubes used in the study of the electrical property measurements were synthesized at a temperature of 525 °C in the pores of 100 nm diameter Al<sub>2</sub>O<sub>3</sub> membranes from Whatman.

Previous electrical property measurements on semiconducting nanowires have revealed three different kinds of current voltage characteristics: almost symmetric, almost rectifying, and almost linear.<sup>12</sup> Each of these cases results from the type of the contact present: an ohmic contact, or a Schottky barrier. The height of the barrier should depend on the work function of the metal, the presence of surface states, the presence of an interfacial insulating surface layer, and the electron affinity of the semiconductor.<sup>13</sup> If the semiconductor surface is free from defects and is non-reactive with the metal, the

Schottky barrier height should depend mostly on the work function of the metal and the I-V curve should be symmetric. Surface states can be comprised of areas of oxygen contamination or metal-semiconductor reactions that occur during metallization. Their cumulative interaction with the metal can have the effect of raising or lowering the barrier height. It may also occur that Schottky barriers form on either contact, but with different barrier heights due to the aforementioned conditions. This may result in nearly symmetric behavior in which a system passes more current in one direction than the other. Contaminants may act as dopants to effectively lower the barrier height.<sup>14</sup> If the barrier height is lowered at both contacts, the resulting current voltage curve may be nearly linear. Finally, it may occur that one contact through a combination of factors becomes ohmic while the other contact is a Schottky barrier. The resulting current voltage curve would be nearly rectifying, or blocking the passage of current in one direction.

The electrical property measurements of MoS<sub>2</sub> nanotubes in this study reveal almost symmetric and almost linear I-V characteristics, with the majority of the measurements being almost symmetric. Typical current voltage curves for these MoS<sub>2</sub> nanotubes are shown in Figure 3.7.

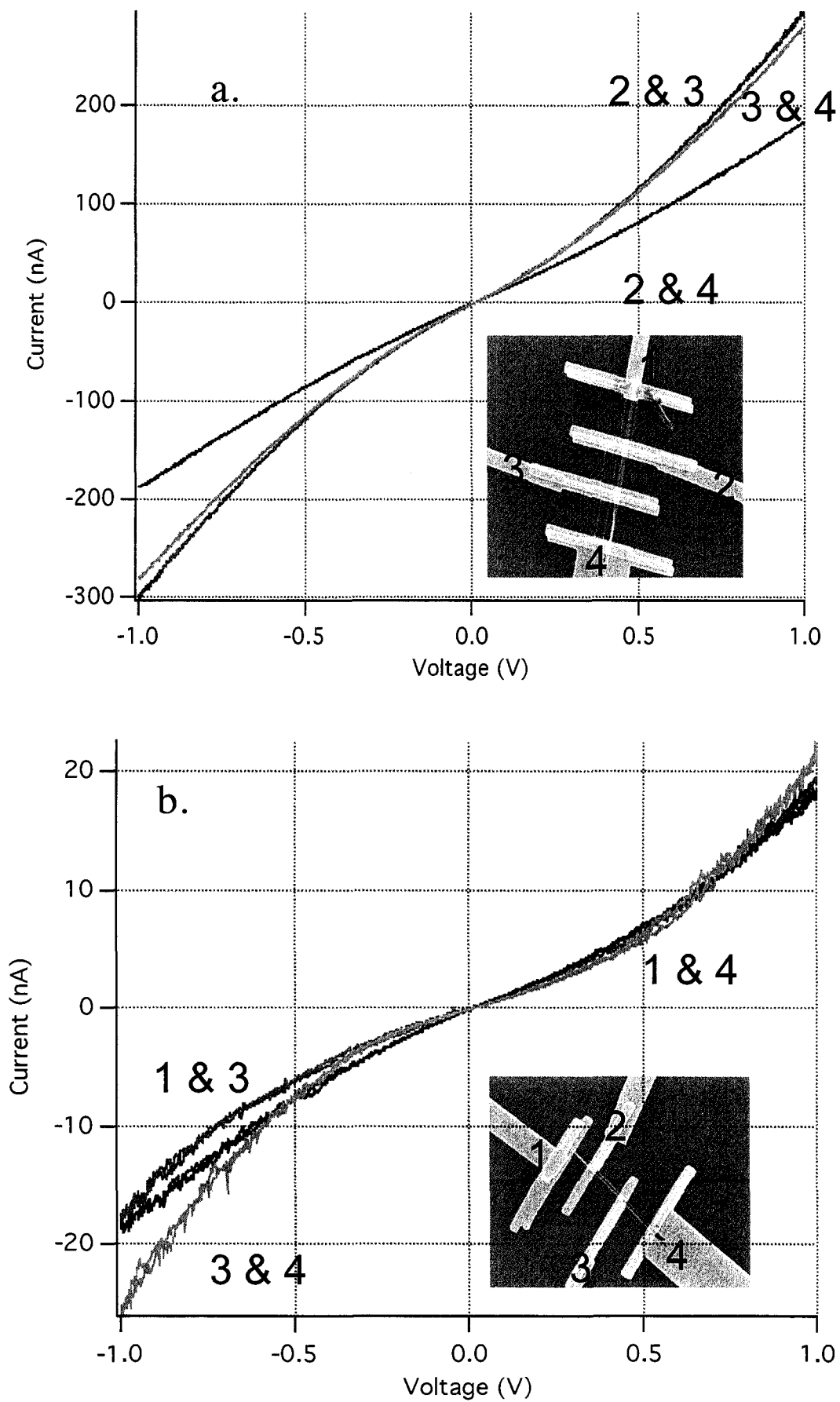


**Figure 3.7.** Current voltage curves of MoS<sub>2</sub> nanotubes; a.) contact one is open; b.) contact 2 is open. Insets show SEM of contacted nanotubes.

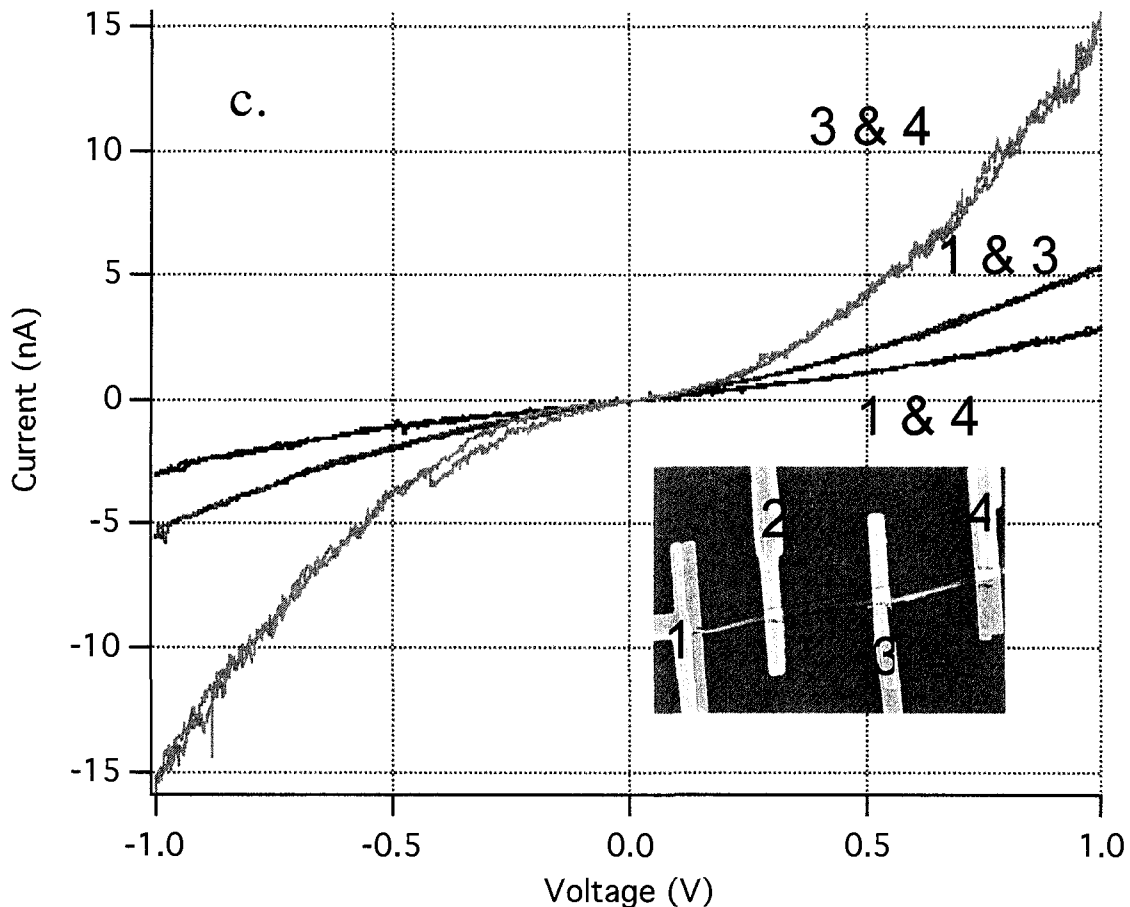


**Figure 3.7 c.** Current voltage curves of MoS<sub>2</sub> nanotubes; contact 2 is open. Inset shows SEM image of contacted

The current voltage curves in the figures are all nearly symmetric. In Figure 3.7, all of the nanotubes appear to be contacted in four places, but only three contacts showed a measurable current in each nanotube. In looking at the insets of the figures, there is some variation in the diameters of the nanotubes. This is a result of the anodic aluminum oxide membrane. The pores of the commercial membranes are frequently narrower on either side. This may result in a wire-like structure due to the plugging of the pores by the precursor during the loading step. This effect may also have an influence on the shape of

the current voltage curves. If the tubes were entirely uniform throughout the diameter, the current voltage curves might be more symmetric. However, there is an asymmetry in virtually all of the curves. Considering that both of the contacts are made of a Cr adhesion layer followed by a layer of Au, it is difficult to attribute the asymmetry to metals of different work functions. In Figure 3.7c, the nanotube appears to either branch, or in fact to be two adjacent tubes between the third and fourth contacts. The tube also appears to be hemicylindrical where it touches the fourth contact. A summary of the current voltage measurements is listed in Table 3.2.

Tube	Segment Length ( $\mu\text{m}$ )	Resistance at 1 V ( $\text{M}\Omega$ )	Linear Resistance ( $\text{M}\Omega/\mu\text{m}$ )	Current Density ( $\text{mA}/\text{cm}^2$ )
7a	4.78	5.4	1.1	$9.39 \times 10^3$
7a	2.10	3.5	1.7	$4.46 \times 10^4$
7a	1.68	3.4	2.0	$5.51 \times 10^4$
7b	6.54	55.6	8.5	$8.77 \times 10^2$
7b	3.83	52.6	13.7	$1.58 \times 10^3$
7b	1.81	46.7	25.0	$3.77 \times 10^3$
7c	13.72	351	25.6	66.1
7c	8.45	188	22.2	$2.01 \times 10^2$
7c	4.18	64.1	15.3	$1.19 \times 10^3$

**Table 3.2.** Summary of current voltage measurements on MoS<sub>2</sub> nanotubes.

The table shows the trend of increasing resistance as a function of the length of the nanotube segments. This behavior is consistent with the expected result. The longest nanotube measured was 13.72  $\mu\text{m}$  and showed the highest resistance. The resistances of the nanotubes are quite varied. However, given the uneven morphology of the nanotubes, this is not surprising. The TEM images reveal many edge dislocations due to the low synthesis temperature of 525 °C. The number of layers in the individual nanotubes may also vary due to the loading conditions. Even though a single concentration of precursor was used, applying exactly the same amount to the entire membrane was not possible

with the dropping technique most commonly used. Additionally, as mentioned previously, the diameters of the nanotubes are not uniform throughout their lengths. The values for resistance include the contact resistance, which could not be accounted for in the two-electrode configuration.

In conclusion, we have synthesized nanotubes of WS<sub>2</sub> and MoS<sub>2</sub> within the pores of anodic aluminum oxide membranes. Nanotubes of diameters ranging from 50 nm to 200 nm were achieved. The experimental conditions for the synthesis of these nanotubes were investigated. In order to achieve the highest quality of nanotube by this method several factors should be considered: the loading should be accomplished through dipping the membrane in the precursor solution; the synthesis temperatures should be between 650 and 700 °C; and using membranes with pore sizes of 100 nm. In addition to the optimization of the synthetic conditions, two point room temperature electrical property measurements were taken on individual MoS<sub>2</sub> nanotubes. The nanotubes are characterized by a relatively high resistance, which is not unexpected for semiconducting systems. The linear resistance of the MoS<sub>2</sub> nanotubes range from about 1 MΩ/μm to about 25 MΩ/μm. The wide range of resistances can be attributed to the many imperfections in the nanotubes including edge defects, areas of curvature, and their bamboo-like structures. The measured values also include the contact resistances. In comparison to multiwalled carbon nanotubes (MWCNTs), these numbers are quite high. The linear resistance in MWCNTs range from 0.03 MΩ/μm to 0.41 MΩ/μm.<sup>15</sup> In comparison to Si nanowires, the linear resistance of the MoS<sub>2</sub> nanotubes is very similar.

Heath has performed transport experiments on Si nanowires and a typical value for the linear resistance of these wires is  $5.8 \text{ M}\Omega/\mu\text{m}$ .<sup>16</sup> These measurements represent the first measurements on individual nanotubes of  $\text{MoS}_2$ .

## References

1. Iijima, S.; *Nature*, **1991**, 354, 56-68.
2. Tenne, R.; Margulis, L.; Hodes, G.; *Nature*, **1992**, 360, 444-446.
3. Margulis, L.; Salitra, G.; Tenne, R.; Tallanker, M.; *Nature*, **1993**, 365, 113-114.
4. Wilson, J.; Yoffe, A.; *Advances in Physics*, **1969**, 269, 193-335.
5. Scheffer, L.; Rosentzveig, R.; Margolin, A.; Popovitz-Biro, R.; Seifert, G.; Cohen, S. R.; Tenne, R.; *Physical Chemistry Chemical Physics*, **2002**, 4, 2095-2098.
6. Seifert, G.; Terrones, H.; Terrones, M.; Jungnickel, G.; Frauenheim, T.; *Solid State Communications*, **2000**, 114, 245-248.
7. Remskar, M.; Mrzel, A.; Sanjines, R.; Cohen, H.; Levy, F.; *Advanced Materials*, **2003**, 15, 237-240.
8. Seifert, G.; Terrones, H.; Terrones, M.; Jungnickel, G.; Frauenheim, T.; *Physical Review Letters*, **2000**, 85, 146-149.
9. Nath, M.; Govindaraj, A.; Rao, C. N. R.; *Advanced Materials*, **2001**, 13, 283-286.
10. Zelenski, C. M.; Dorhout, P. K.; *Journal of the American Chemical Society*, **1998**, 120, 734-742.
11. a.) Kyotani, T.; Tsai, L.-f.; Tomita, A.; *Chemistry of Materials*, **1996**, 8, 2109-2113;  
b.) Peng, T.; Yang, H.; Chang, G.; Dai, K.; Hirao, K.; *Chemistry Letters*, **2004**, 33, 336-337.
12. Zhang, Z. Y.; Jin, C. H.; Liang, X. L.; Chen, Q.; Peng, L.-M.; *Applied Physics Letters*, **2006**, 88, 073102-1 – 073102-3.
13. Freeouf, J. L.; Woodall, J. M.; *Applied Physics Letters*, **1981**, 39, 727-729.
14. Cui, Y.; Duan, X.; Hu, J.; Lieber, C. M.; *Journal of Physical Chemistry B*, **2000**, 104, 5213-5216.
15. a.) Ebbesen, T. W.; Lezec, H. J.; Hiura, H.; Bennett, J. W.; Ghaemi, H. F.; Thio, T.; *Nature*, **1996**, 382, 54-56; b.) Dai, H.; Wong, E. W.; Lieber, C. M.; *Science*, **1996**, 272, 523-526.
16. Yu, J-Y.; Chung, S-W.; Heath, J. R.; *Journal of Physical Chemistry b*, **2000**, 104, 11864-11870.

## Chapter 4: Template Synthesis of ReS<sub>2</sub> Nanotubes and Electrical Property Measurements

David B. Seley, Manashi Nath and B. A. Parkinson

Department Of Chemistry  
Colorado State University  
Fort Collins, CO 80523

### Preface

This chapter is a publication that will shortly be submitted to *Chemistry of Materials*. I did all of the experimental work and contributed to the writing. M. Nath contributed helpful discussions and to the writing.

### Abstract

Nanotubes of ReS<sub>2</sub> have been synthesized for the first time using the pores of an anodic aluminum oxide membrane. The single source precursor [(C<sub>4</sub>H<sub>9</sub>)<sub>4</sub>NReS<sub>4</sub>], was loaded into the membrane pores and pyrolyzed at 450°C to yield nanotubes. Two point electrical property measurements were performed on the resulting individual nanotubes and yielded I-V curves that were linear, nearly symmetric, and diode-like.

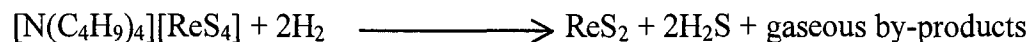
The family of transition metal dichalcogenides with a layered structure, where the metal is sandwiched between layers of chalcogen atoms, exhibit a wide range of physical and electronic properties<sup>1</sup> and have continued to attract considerable research interest due to their potential applications including catalysis, electrochemical hydrogen storage, solid-state lubricants.<sup>2</sup> The layered structure, where the trigonal prismatic or octahedrally coordinated metal is sandwiched between hexagonal layers of chalcogen atoms, suggests that carbon fullerene-like and nanotube structures might also be formed from these materials. Following the discovery that these layered materials can indeed fold to form nested or closed shell geometries,<sup>3</sup> nanotubes, nanowires and nanoclusters of the transition metal dichalcogenides have been synthesized with a wide variety of methods.<sup>4</sup> The incorporation of transition metals with d-electron configurations will provide these nanomaterials with a wider range of electronic properties than are available from carbon or isoelectronic BN nanostructures.

ReS<sub>2</sub> is a diamagnetic, indirect gap semiconductor with a slightly different layered structure than the more common MoS<sub>2</sub> or CdI<sub>2</sub> structures.<sup>5</sup> ReS<sub>2</sub> has Re-Re bonds, forming Re<sub>4</sub> parallelogram units that break the usual hexagonal symmetry. It exhibits highly anisotropic optical, electrical and mechanical properties, and has possible applications as a sulfur-tolerant hydrogenation and hydrodesulfurization catalyst, in a photoelectrochemical solar cell and as a material for fabrication of polarization sensitive photodetectors in the visible wavelength region.<sup>6,7</sup> Although nanotubes of various transition metal disulfides have been studied extensively over the last two decades, there

are only two reports on the synthesis of ReS<sub>2</sub> nanotubes and closed cages.<sup>8,9</sup> In this communication we report the synthesis of ReS<sub>2</sub> nanotubes synthesized from a single source molecular precursor decomposed inside the pores of an anodic aluminium oxide (AAO) membrane.

The single source molecular precursor used for the synthesis of the nanotubes was tetrabutylammonium tetrathiorhenate, [(C<sub>4</sub>H<sub>9</sub>)<sub>4</sub>NReS<sub>4</sub>], purchased from Strem Chemicals and used as is. Alumina membranes (Anodisc) (AAO) with pore sizes 0.02, 0.1 and 0.2 μm were obtained from Fisher Scientific, while membranes with pore sizes 0.03-0.07 μm were acquired from Dr. Hideki Masuda (Tokyo Metropolitan University, Japan). Tetrabutylammonium tetrathiorhenate was dissolved in a suitable solvent, such as dimethylformamide (DMF), to make a solutions with concentrations ranging from 0.005 M to 0.1 M. Alumina membranes with pore sizes ranging from 0.03 to 0.2 μm were then loaded with the DMF solution by adding two drops on each side of the membrane via a 1 cc syringe. The loaded membranes were then placed in a horizontal flow through furnace and pyrolyzed at 450°C for 1 hour under a flow of 90% N<sub>2</sub> + 10% H<sub>2</sub>. After the completion of the reaction, the furnace was allowed to cool to room temperature over a period of several hours. The AAO membrane was then dissolved by soaking in 2M NaOH for several hours followed by washing the residues with deionized water until the wash showed a neutral pH.

The chemical reaction can be written as follows:



The rhenium precursor concentration was varied from 0.01M to 0.005M, and the pore size of the AAO membranes was varied. Irrespective of Re precursor concentration, the obtained nanotubes had thick walls with a uniform diameter along the length of the nanotube. TEM images showed that the nanotube walls were composed of small randomly oriented grains (Fig. 4.1a). High-magnification TEM images revealed lattice fringes within the grains indicating a degree of crystallinity in the nanotube walls (Fig. 4.1b).

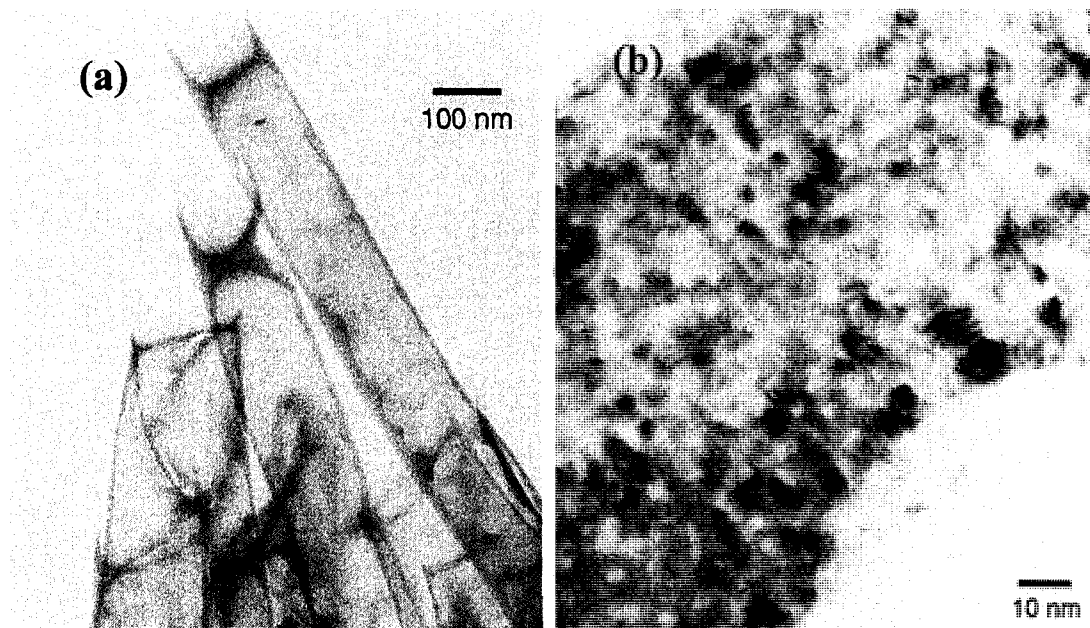


**Figure 4.1** (a) TEM image of open-ended nanotubes of  $\text{ReS}_2$  with granular walls obtained at higher concentration of the precursor solution; (b) High-magnification TEM image of the granular walls showing agglomeration of crystallites.

The distance between lattice fringes is approximately 6Å corresponding to the (100) spacing of bulk  $\text{ReS}_2$ .<sup>9</sup> Some of the nanotubes showed one closed tip with a spherical cap while the rest were open at both ends. Occasionally the walls of the nanotubes show a positive curvature towards the interior of the tube indicating the tendency to form cavities or bamboo-like structures within the nanotubes. These bamboo-like structures have been frequently observed in the  $\text{MoS}_2$  nanotubes synthesized in AAO pores,<sup>10</sup> and has been attributed to the assembly on the precursor particles along the walls of the alumina membrane prior to the decomposition. The EDS analysis performed on the nanotubes show a uniform distribution of Re and S in the structure with a ratio of ~1:2, thus confirming a nominal composition of  $\text{ReS}_2$  for the nanostructures.

As the precursor solution is loaded inside the pores of the AAO membrane it leads to a simple assembly of the cations and anions inside the pores. Pyrolysis thus leads to condensation of the anionic moieties within the pores of the AAO membrane forming the walls of the nanotube while the organic moieties are decomposed and removed, resulting in the solid walled nanotubes. The presence of randomly oriented crystalline domains in the granular walls of the solid walled tubes may be explained by the low annealing temperature.

The dependence of the nanotubular structure on the pore size of the template was also investigated using pore sizes ranging from 0.02-0.07, 0.1 and 0.2  $\mu\text{m}$ . While the templates with larger pore sizes yielded nanotubes, depending on the precursor concentration, the templates with narrower pores did not produce any nanotubes. The

product obtained using the 0.02-0.07  $\mu\text{m}$  pore size templates were mostly thin solid nanowires and few nanotubes with granular wires (Fig. 4.2).

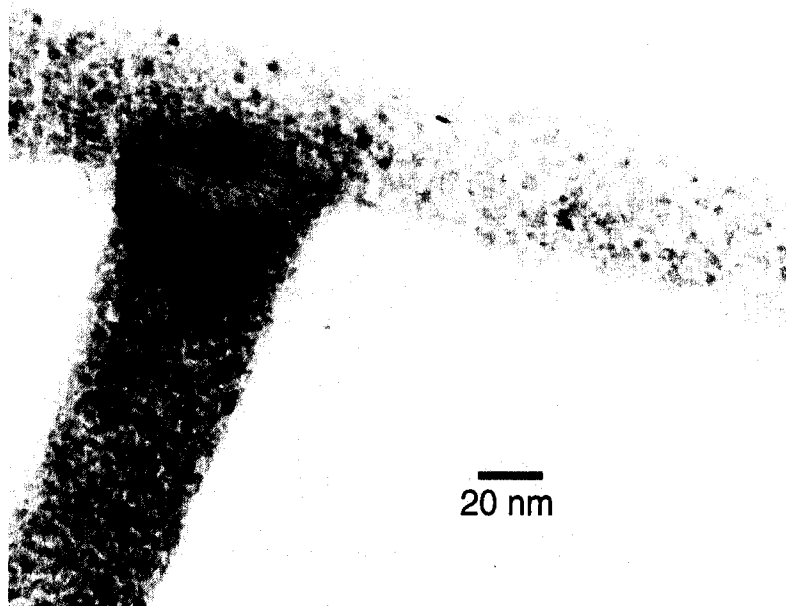


**Figure 4.2.** TEM image of  $\text{ReS}_2$  nanowires formed using the small pore AAO templates.

The formation of the nanowires suggests that the precursor solution might clog the narrower pores. Using large pore membranes on the other hand leads to collection of the precursor near the walls of the pore, resulting in hollow tubules templated by the walls of the pores. Ideally narrower pores should lead to smaller diameter nanotubes with thicker walls. However the strain associated with thicker, smaller diameter nanotubes<sup>11</sup> is perhaps not be accommodated by the more rigid  $\text{ReS}_2$  structure under these reaction conditions, leading to solid nanowires, whereas  $\text{MoS}_2$  nanotubes, prepared

from the  $(\text{NH}_4)_2\text{MoS}_4$  precursor under the same reaction conditions, can form tubes in these smaller pores.<sup>10</sup>

In addition to the synthesis of these nanotubes, we were interested in measuring the electrical properties of individual nanotubes. Two point electrical property measurements were performed on individual  $\text{ReS}_2$  nanotubes at room temperature. The nanotubes were suspended in a solution of methanol and then drop cast onto a Si wafer with a 100 nm thermal oxide coating. A bi-layer of PMMA was spin-coated onto the wafer and electron beam lithography was used to define the electrical contacts. Details can be found in Appendix A. After developing with MIBK:IPA (1:3), a 20 nm Cr adhesion layer and a 70 nm Au layer were thermally evaporated onto the sample. Measurements were conducted using an Ivium Compactstat potentiostat. Physical contact to the gold pads was accomplished using a micromanipulator probe station.

Three different types of I-V behavior were observed for the nanotubes. Figure 4.3 shows I-V curves for an individual nanotube of  $\text{ReS}_2$ . The nearly symmetrical I-V curves are typical for semiconducting materials due to the formation of Schottky barriers at the contacts. This type of behavior was seen in half of the nanotubes we measured. Interestingly, Figure 4.3 also shows the same nanotube exhibiting diode-like behavior. This I-V behavior might be expected if there are two different metals at either contact with 2 different work functions. However, both contacts are Cr/Au with the same thickness.

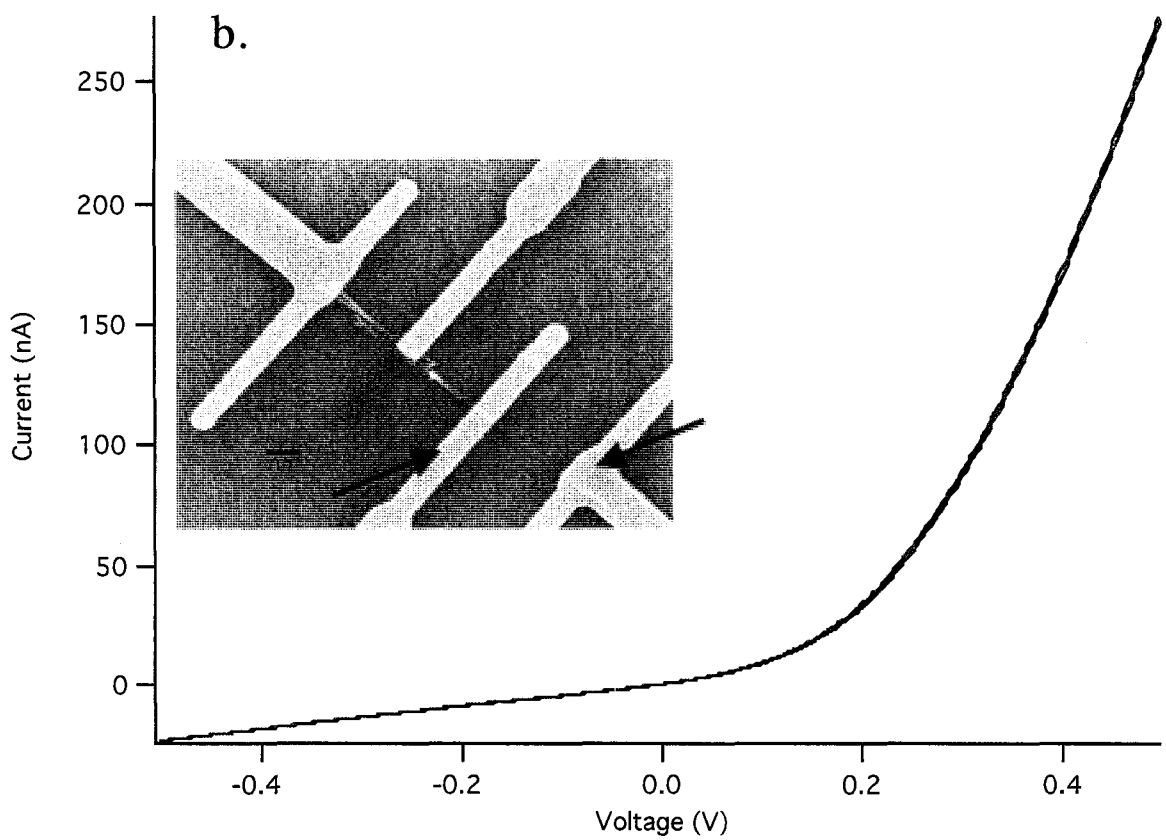
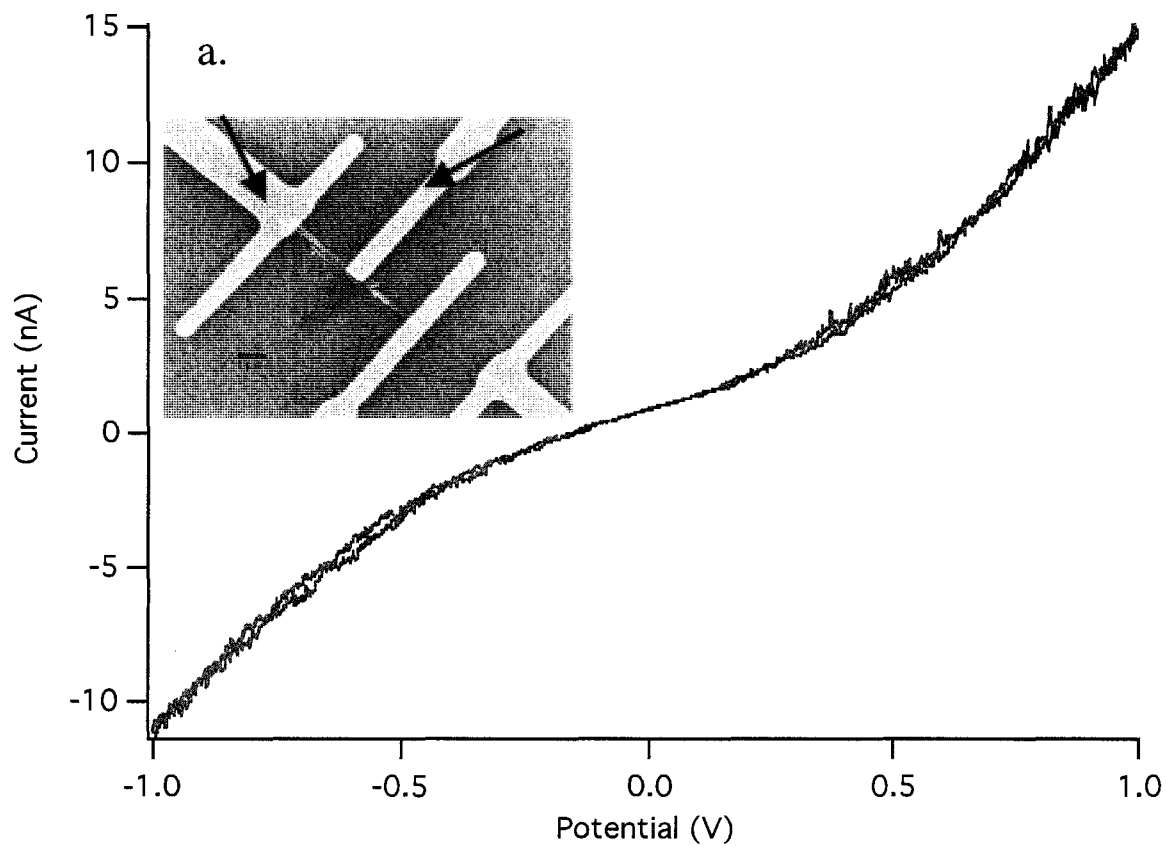


**Figure 4.3.** Current voltage characteristics of a  $\text{ReS}_2$  nanotube: a.) shows nearly asymmetric I-V behavior; b.) shows diode-like behavior. Both types of behavior seen in a single nanotube.

Another interesting feature of the two current voltage curves shown in Figure 4.3 is the difference in the magnitude of current. In Figure 4.3a, the voltage sweep is from -1 to 1 volt and the maximum current passed is about 15 nA. In Figure 4.3b, where the current is not blocking, about 250 nA is passed at a potential of 0.5 V. In looking at the SEM images, it is clear that the tube in Figure 5.3a branches at the first contact. This does not result in an unusual I-V curve, however. At the second contact, there is branching again, but it is not clear whether the branched portion is contacted by the gold. The tube in Figure 4.3b looks very uniform, without any branching or obvious defects. Nonetheless, the current voltage curve is still blocking in one direction.

In addition, on some tubes we measured, I-V curves were linear, with the nanotubes acting as resistors. This linear I-V behavior was observed in 5 of the 10 nanotubes we measured. On one of the nanotubes exhibiting the linear I-V curve, we were able to back calculate the resistance of two of the contacts and the middle segment of the nanotube due to the fact that we had made 4 good contacts to the nanotube. Figure 4.4 shows the current voltage characteristics of this nanotube.

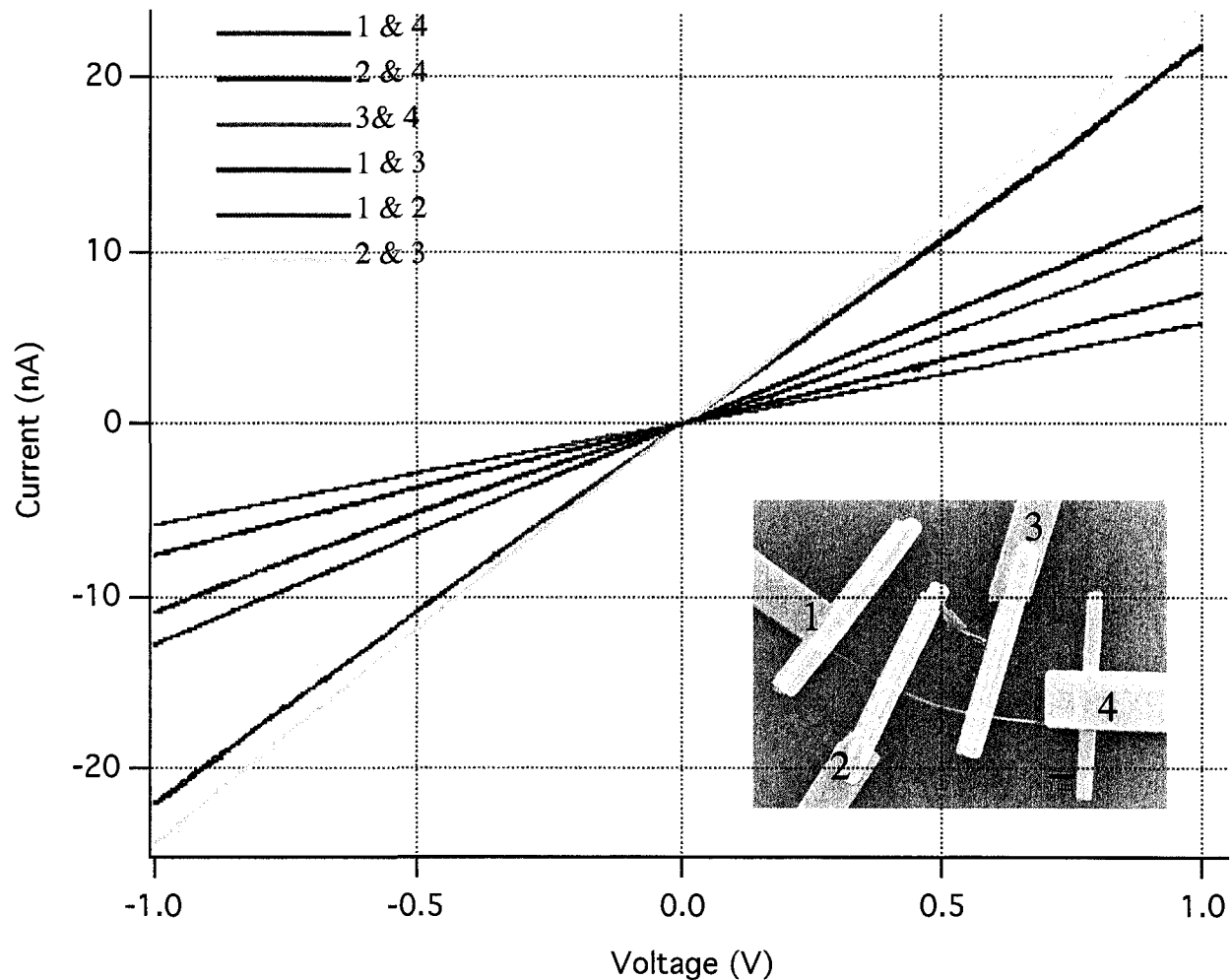


**Figure 4.4.** Current voltage characteristics of individual  $\text{ReS}_2$  nanotube behaving as a resistor. Inset shows SEM image with numbered contacts.

The resistances of the second and third gold contacts, as well as the intrinsic resistance of the nanotube spanning those two contacts were calculated. The resistance of the second contact was calculated to be  $4.5 \text{ M}\Omega$ . The resistance of the third contact was calculated to be  $1.5 \text{ M}\Omega$ . The intrinsic resistance of the middle segment of the nanotube was calculated to be  $36 \text{ M}\Omega$ . We were unable to calculate the resistances of the other segments of the nanotube or outside contacts due to the lack of more data points. However, we are still pleased to have calculated the intrinsic resistance of the nanotube

segment. Since the length of the nanotube segment is known, as well as the cross-sectional area of the nanotube, we can calculate the resistivity of the nanotube. The resistivity of the nanotube segment of ReS<sub>2</sub> is calculated to be about 75 MΩ m. For comparison, Tiong and co-workers have measured the bulk ReS<sub>2</sub> resistivity.<sup>12</sup> They measured the resistivity of ReS<sub>2</sub> along the different crystallographic planes. The resistivity parallel to the c-axis was found to be about 10<sup>7</sup> Ω m. This is understandable considering the van der Waals space between the sulfur atoms. Parallel and perpendicular to the b-axis, the resistivity was much lower. These values were 10 to 100 Ω m. Our calculated resistivity is much higher than might be expected considering the nanotubes preferentially grow in the direction of the c-axis. However, given the morphology of the nanotubes this is not unreasonable. The nanotubes have many edge dislocations along the length of the tube. There are also pea-pod areas reminiscent of bamboo within the tubular structures. The surfaces of the nanotubes appear grainy and will also contribute to the high resistivity of the nanotubes. The nanotube segment is also slightly curved which may contribute to the resistivity.

A summary of the electrical property measurements on several tubes is shown in Table 4.1.

IV Curve Characteristics	Lengths ( $\mu\text{m}$ )	Resistance ( $\text{M}\Omega$ )	Linear Resistance ( $\text{M}\Omega/\mu\text{m}$ )	Current Density ( $\text{mA}/\text{cm}^2$ )
Linear	2.1	63	30	$2.01 \times 10^3$
Linear	2.0	93	47	$1.43 \times 10^3$
	2.3	46	20	$2.52 \times 10^3$
	2.5*	36*	14	$2.95 \times 10^3$ *
	5.5	132	24	$3.65 \times 10^2$
	5.8	79	14	$5.77 \times 10^2$
	8.8	172	20	$1.60 \times 10^2$
Almost symmetric	1	62	62	$4.28 \times 10^3$
Almost symmetric	1.4	16	11	$9.68 \times 10^3$
Almost symmetric	2.2	67	30	$1.80 \times 10^3$
Almost symmetric	2	690	345	$1.92 \times 10^2$
	2	149	75	$8.92 \times 10^2$
	4	158	40	$4.19 \times 10^2$
Diode-like	2.4	1.8	0.75	$3.04 \times 10^4$

**Table 4.1.** Summary of current voltage measurements on individual  $\text{ReS}_2$  nanotubes. The asterisk indicates the nanotube's intrinsic resistance.

As seen in Table 4.1, the linear I-V curves follow a general trend of increasing resistance with increasing length. However, with the exception of the one nanotube segment whose intrinsic resistance was calculated, all other values for resistance include the contact resistance. Also, electrons may follow a different path from contact to contact, perhaps encountering higher areas of resistance along those paths. As mentioned previously, the nanotubes likely have many defects and have areas along the tube axes where a higher number of defects may reside. The nanotubes are not well crystallized given the low pyrolysis temperature of 450 °C.

The ReS<sub>2</sub> nanotubes exhibited 3 different types of I-V curves: almost symmetric, almost linear, and almost rectifying. The different shapes of the I-V curves reflect the nature of the contact – ohmic or a Schottky barrier. The ohmic contacts result in linear IV curves. This type of contact may be due to the presence of impurities that act as dopants in the nanotubes.<sup>13</sup> A Schottky barrier is lowered enough in heavily doped semiconductors to be able to achieve an ohmic contact. The almost symmetric IV curves represent two contacts with Schottky barriers. This is the typical result of a metal coming into contact with a semiconductor. The IV curves are not exactly symmetric, and this could be a result of one barrier being a little higher than the other. The height of the barrier depends on the work function of the metal, the presence of surface states on the semiconductor, and the semiconductor's electron affinity.<sup>14</sup> The likely cause of the nearly asymmetric behavior is the presence of surface states on the nanotube. The nearly rectifying current voltage curve likely results from one contact being ohmic and the other

contact having a Schottky barrier. As mentioned previously, the ohmic contact likely is a result of impurities in the nanotubes acting as dopants. On the other side of the nanotube, a barrier exists and blocks the passage of current.

The current densities of the ReS<sub>2</sub> nanotubes ranged from less than 1 A/cm<sup>2</sup> to 30 A/cm<sup>2</sup>. In comparison to multiwalled carbon nanotubes (MWCNTs), the current densities are much lower. Dai and co-workers have reported current densities of MWCNTs on the order of 10<sup>6</sup> A/cm<sup>2</sup>.<sup>15</sup> We have also calculated the resistivity of a segment of a ReS<sub>2</sub> nanotube. This resistivity was 75 MΩ m. The resistivities of MWCNTs have been reported to be on the order of 10 - 50 Ω m.<sup>15</sup> The resistivities of Si nanowires were also compared to the ReS<sub>2</sub> nanotubes. The Si nanowire resistivities can be as high as 10<sup>3</sup> Ω m in undoped nanowires to 10<sup>-5</sup> Ω m in heavily doped nanowires.<sup>16</sup>

Preliminary experiments were undertaken to investigate whether these nanotubes exhibit a photocurrent and also whether their resistivities change as a function of ammonia concentration. These preliminary experiments indicated that no change occurred with the exposure of white light or gas. However, considering the semiconducting nature of ReS<sub>2</sub>, further experiments are warranted.

In conclusion, we have reported the first example of ReS<sub>2</sub> nanotubes formed within the pores of an AAO membrane from a single-source precursor. Since ReS<sub>2</sub> is a semiconducting material, the dependence of the band gap on the morphology of the nanotube would be worthwhile to investigate. The structural diversity of these semiconducting nanotubes can have important implications in the electronic properties of

these materials, which in turn will affect the applicability of these nanotubes in suitable devices.

Additionally, we have performed two point room temperature electrical property measurements on individual nanotubes of  $\text{ReS}_2$ . We have seen three different types of current voltage curves, almost linear, almost symmetric, and diode-like, in this single system and possible explanations for these transport properties were proposed. We have also been able to calculate the resistivity of a single nanotube segment and compared it with reported data for bulk  $\text{ReS}_2$ . This resistivity was compared to the resistivities of MWCNTs and Si nanowires. The current density of  $\text{ReS}_2$  nanotubes was also compared to MWCNTs.

**Acknowledgement:** The authors would like to acknowledge financial assistance from NSF project CTS-0529323 and Dr. Hideki Masuda for supplying some of the alumina templates.

## References:

1. Wilson, J., Yoffe, A. J.; *Adv. Phys.*, **1969**, 269, 193.
2. Chianelli, R. R.; Berhault, G.; Santiago, P.; Mendoza, D.; Espinosa, A.; Yacaman, M. J.; *Mater. Technol.*, **2000**, 15, 54.
3. Tenne, R.; Margulis, L.; Genut, M.; Hodes, G.; *Nature*, **1992**, 360, 444.
4. Tenne, R.; Rao, C. N. R.; *Phil. Trans. R. Soc. Lond. A.*, **2004**, 362, 2099; Rao, C. N. R.; Nath, M.; *Dalton Trans.*, **2003**, 1.
5. Lamfers, H.-J.; Meetsma, A.; Wiegers, G. A.; de Boer, J. L.; *J. Alloys Compd.*, **1996**, 241, 34.
6. Liang, W. Y.; *J. Phys. C*, **1973**, 6, 551; Friemelt, K.; Lux-Steiner, M.-Ch; Bucher, E.; *J. Apl. Phys.*, **1973**, 24, 73.
7. Broadbent, H. S.; Slangh, L. H.; Jarvis, N. L.; *J. Am. Chem. Soc.*, **1954**, 74, 1519; Harris, S.; Chianelli, R. S.; *J. Catal.*, **1984**, 86, 400; Koffeyberg, F. P.; Dwight, K.; Wold, A.; *Solid State Commun.*, **1979**, 30, 433; Wheeler, B. L.; Leland, J. K.; Bard, A. J.; *J. Electrochem. Soc.*, **1986**, 133, 358.
8. Brorson, M.; Hansen, T. W.; Jacobsen, C. J. H.; *J. Am. Chem. Soc.*, **2002**, 124, 11582.
9. Coleman, K. S.; Sloan, J.; Hanson, N. A.; Brown, G.; Clancy, G. P.; Terrones, M.; Terrones, H.; Green, M. L. H.; *J. Am. Chem. Soc.*, **2002**, 124, 11580.
10. Zelenski, C. M.; Dorhout, P. K.; *J. Am. Chem. Soc.*, **2000**, 120, 734.
11. Seifert, G.; Kohler, T.; Tenne, R.; *J. Phys Chem. B*, **2002**, 106, 2497.
12. Tiong, K. K.; Ho, C. H.; Huang, Y. S.; *Solid State Communications*, **1999**, 111, 635-640.
13. Zhang, Z. Y.; Jin, C. H.; Liang, X. L.; Chen, Q.; Peng, L.-M.; *Applied Physics Letters*, **2006**, 88, 073102-1 – 073102-3.
14. Freeouf, J. L.; Woodall, J. M.; *Applied Physics Letters*, **1981**, 39, 727-729.
15. Dai, H.; Wong, E. W.; Lieber, C. M.; *Science*, **1996**, 272, 523-526.
16. Yu, J-Y.; Chung, S-W.; Heath, J. R.; *Journal of Physical Chemistry b*, **2000**, 104, 11864-11870.

## Chapter 5: ReSe<sub>2</sub> Nanotubes Synthesized From Sacrificial Templates

David B. Seley, Manashi Nath, and B. A. Parkinson  
Department of Chemistry  
Colorado State University  
Fort Collins, CO 80523

### Preface

This chapter is a publication that will be submitted to *Chemistry of Materials*. I did all of the experimental work and contributed to the writing. M. Nath contributed discussions and to the writing.

### Abstract:

ReSe<sub>2</sub> nanotubes have been synthesized for the first time by using Se nanotubes as sacrificial templates. Under hydrothermal conditions ammonium perrhenate reacts with the surface of the Se nanotubes to yield ReSe<sub>2</sub> nanotubes. The ReSe<sub>2</sub> nanotube walls are composed of randomly oriented crystalline ReSe<sub>2</sub> flakes, thus producing a high surface area of “fuzzy” nanotubes.

## 5.1 Introduction

Since the discovery of carbon nanotubes by Iijima in 1991,<sup>1</sup> and subsequent discovery by Tenne in 1992 that other layered materials can form nanotubes,<sup>2</sup> the search for inorganic nanotubes and nanowires has been accelerated. The layered transition metal dichalcogenides (TMDCs) are an important class of inorganic materials exhibiting a wide variety of optical, electronic, magnetic, and catalytic properties.<sup>3</sup> The typical structure of these metal dichalcogenides is analogous to graphite where each graphene sheet has been replaced by the  $ME_2$  ( $E = S, Se, Te$ ) sandwich layer where the metal can have different coordination. Many of these TMDCs have been shown to form nanotubes including  $MoS_2$ ,  $WS_2$ ,  $ReS_2$ , and  $NbS_2$ .<sup>4-6</sup> Rhenium dichalcogenides,  $ReS_2$  and  $ReSe_2$ , are two such TMDCs, which crystallize in the triclinic space group with a distorted  $CdCl_2$  structure with intralayer Re-Re bonds.<sup>7</sup>  $ReS_2$  and  $ReSe_2$  are both diamagnetic indirect gap semiconductors with bandgaps of about 1.32 and 1.2 eV, respectively.<sup>3</sup>  $ReE_2$  ( $E = S, Se$ ) possesses extremely anisotropic electrical, optical and mechanical properties.<sup>8</sup> The in-plane optical and electrical anisotropy in  $ReE_2$  seems to be related to the layered structure where “diamond chains” containing the Re-Re bonds form along the  $b$ -axis (Figure 5.1).<sup>9</sup> The material shows optical dichroism making it useful for fabrication of polarization sensitive photodetectors in the visible wavelength region.<sup>10</sup> These materials have also been explored as the photoelectrode in photoelectrochemical solar cells.<sup>11</sup>

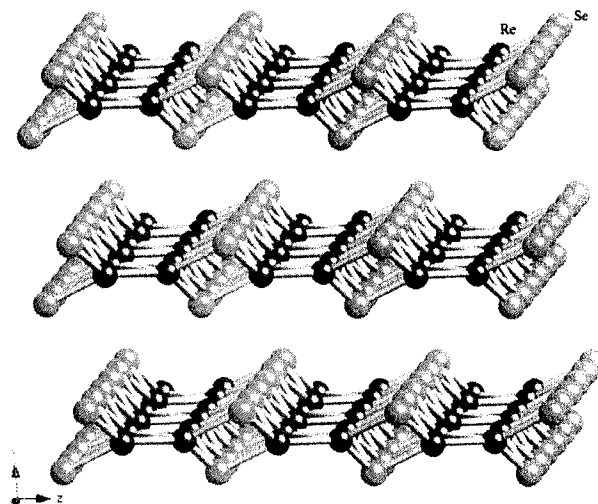


**Figure 5.1.** Layered structure of triclinic  $\text{ReSe}_2$  viewed down the  $b$ -axis showing the arrangement of the  $\text{Re}_4$  units.

Inorganic nanotubes have been synthesized by a variety of techniques including pyrolysis, sol-gel, solvothermal and template-mediated synthesis methods.<sup>12</sup> In the template-mediated synthesis, the material either precipitates and grows inside the pores of a hard template (e.g. anodic aluminium oxide membrane or MCM-41) or around a soft template like a carbon nanotube. The ease of removal of the template with minimal degradation to the nanotube of interest determines the effectiveness of the synthesis route. In this respect, sacrificial templates, which are involved in the chemical reaction and are consumed during the reaction, are very advantageous for inorganic nanotube synthesis. These syntheses are typically carried out under milder conditions than with the hard templates. Generally, a nanowire or nanotube of one of the reactants is used as the template, and a second precursor reacts with the surface to form the final product. The sacrificial template method has been effectively adopted to synthesize CdS nanotubes or CdTe nanotubes using  $\text{Cd}(\text{OH})\text{Cl}$  or  $\text{Cd}(\text{OH})_2$  nanowires as the template.<sup>13,14</sup> Xia's group

has effectively demonstrated that Se nanowires can be ideal templates for the synthesis of new 1-D materials including Ag<sub>2</sub>Se, CdSe, Pd<sub>17</sub>Se<sub>15</sub>, and RuSe<sub>2</sub>.<sup>15</sup>

In this communication, we report the first synthesis of ReSe<sub>2</sub> nanotubes using a sacrificial template approach where as-grown Se nanotubes have been used as templates to grow the ReSe<sub>2</sub> nanotubes by solvothermal methods. Apart from having potential applications as electrodes and photoelectrodes,<sup>11</sup> the ReSe<sub>2</sub> nanotubes are also attractive as a chemical sensor due to their large and accessible van der Waals surfaces.

The ReSe<sub>2</sub> nanotubes have been synthesized in two steps. In the first step, Se nanotubes are synthesized in a water-ethylenediamine mixture. In the second step, the as-synthesized Se nanotubes are reacted with ammonium perrhenate [NH<sub>4</sub>ReO<sub>4</sub>] in ethanol medium, under solvothermal conditions at 135°C for 6 days. The chemical reaction taking place can be written as follows:



## 5.2 Experimental Methods

*Se nanotubes:*

The Se nanotubes were made by a procedure similar to a reported one.<sup>16</sup> In a typical experiment, 40 mg (0.5 mmoles) of elemental Se was dissolved in 20 ml of ethylenediamine by magnetic stirring for several hours until complete dissolution occurs. The yellow-amber solution was then added dropwise to 15 ml of deionized water, which was being ultrasonically treated. The appearance of amorphous selenium was immediately apparent as the ethylene diamine/Se/H<sub>2</sub>O mixture became reddish. This

solution was ultrasonically treated for about 1 hour or until a metallic looking film appeared on the surface of the solution. The solution was then removed from the ultrasonic bath and allowed to sit overnight in the dark. A dark solid film-like material fell to the bottom of the vial. The supernatant solution was removed carefully and the film-like material was washed with ethanol and air-dried. Large quantities of Se nanotubes were observed in the 25 mg (0.3 mmoles) dark film-like product. (Fig 5.2a)

*ReSe<sub>2</sub> nanotubes by solvothermal method:*

40 mg of NH<sub>4</sub>ReO<sub>4</sub> (0.15 mmoles) was dissolved in 10 ml of absolute ethanol with sonication and the solution was transferred to a Teflon lined acid digestion bomb. Se nanotubes were then added to this solution and stirred for several minutes. The autoclave was then sealed and placed in an oven at 135 °C for a period of 6 days. Upon removal from the oven, the autoclave was allowed to cool down to ambient conditions. A black precipitate was isolated from the product by centrifugation and was washed several times with water and ethanol. Powder x-ray diffraction and SEM of the black precipitate revealed that it contained the ReSe<sub>2</sub> nanotubes. A small amount of the precipitate was dispersed in ethanol and added on formvar coated holey Cu grids for TEM studies.

### **5.3 Results and Discussion**

The as-synthesized Se nanotubes have smooth walls and exhibit both open and closed ends. It was observed that the majority of the nanotubes have a faceted geometry. A cross-sectional view at the open ends of the nanotube revealed that they are either triangular or hexagonal as shown in Figure 5.2a. Triangular or hexagonal cross-sections

are very common for Se nanotubes and can be attributed to the stability and orientation of the different crystal faces of the *t*-Se phase.<sup>15</sup> The diameter and length of the Se nanotubes is in the range of 80 – 300 nm and 1 – 2  $\mu\text{m}$  respectively. The nanotube walls were quite thin when compared to the diameter, being in the range of 50-70 nm. We have characterized the Se nanowires by Raman spectroscopy which shows the expected spectra for Se.

After the solvothermal reaction, the overall morphology of the triangular and hexagonal selenium nanotube precursor was preserved in the  $\text{ReSe}_2$  nanotubes, but the wall thickness was considerably reduced. The nanotube morphology is similar to other nanotubes that have been made via a sacrificial template. The  $\text{ReSe}_2$  nanotubes have a distinctly rough surface as shown in Figure 5.2b. EDS analysis on individual nanotubes yielded a Re:Se ratio of 1:2. XRD and Raman spectroscopy showed no elemental Se, indicating that there is no excess Se in the nanotubes. The XRD pattern of the  $\text{ReSe}_2$  nanotubes is shown in Figure 5.2c. The diffraction peak at  $2\theta = 13.87^\circ$ , characteristic of  $\text{ReSe}_2$  [JCPDS file, card no. 18-1086], was clearly visible in the pattern. The peaks were very broad and some of the closely spaced diffraction peaks ( $2\theta = 30\text{-}60^\circ$  range) were masked by several broad peaks. This indicates that the diffraction pattern arises from an ensemble of very small crystalline domains or crystallites. This observation could be directly correlated to the “furry” appearance of the nanotube walls as discussed in the following paragraph.

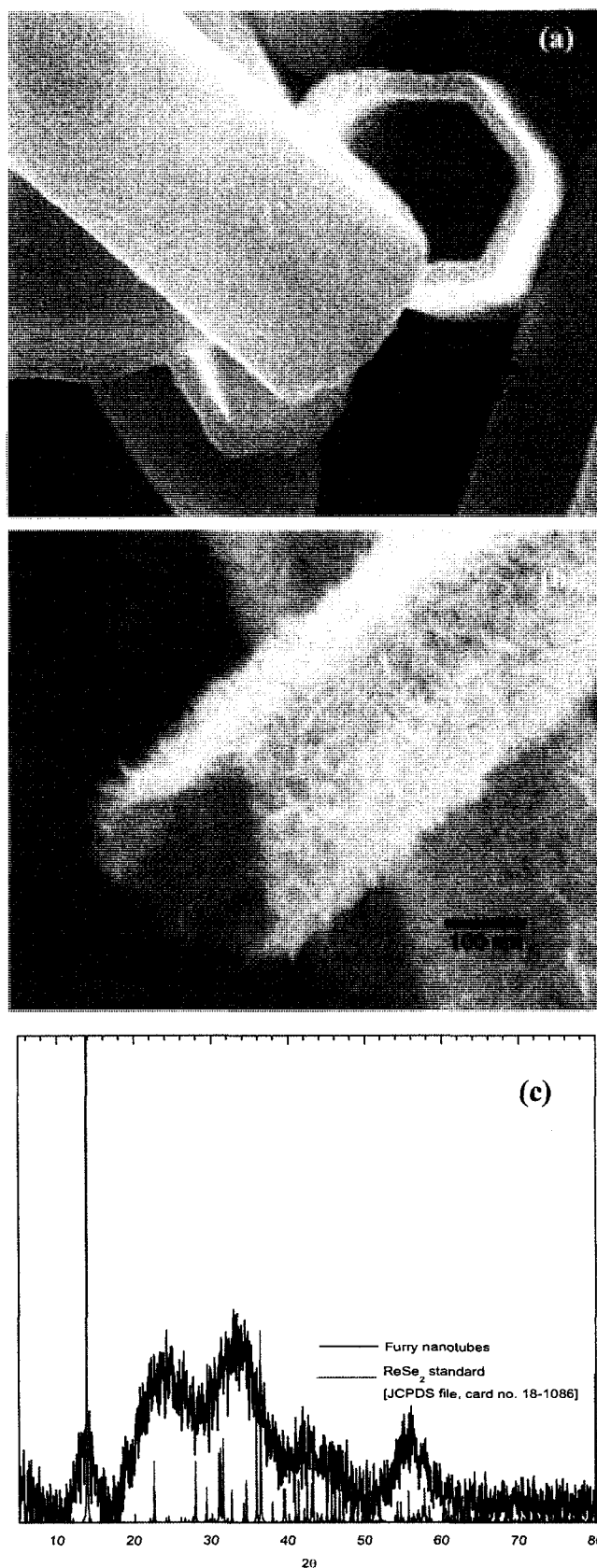


**Figure 5.2.** (a) SEM micrograph of Se nanotube precursor. A hexagonal nanotube is seen. (b) SEM micrograph of a ReSe<sub>2</sub> nanotube showing the “furry” walls. (c) Powder XRD pattern of the furry nanotubes exhibiting broad peaks which shows close resemblance to the standard pattern of ReSe<sub>2</sub> plotted below.

The “furry” appearance occurs along the entire length of the nanotube. TEM was used to observe the nanotube walls more closely. Figure 5.3a shows a TEM image of a closed and an open ended ReSe<sub>2</sub> nanotube, while Figure 5.3b shows a high-magnification image of the nanotube wall, showing that the tube wall is composed of small, thin crystalline flakes arranged randomly over the entire surface. High resolution TEM of the surface flakes on the nanotubes reveals lattice fringes with a spacing of about 5.5 Å (Figure 5.3b), corresponding to the d (001) lattice spacing of ReSe<sub>2</sub>. The flakes were generally 4-5 layers thick and 10-15 nm in width. Since extensive electron microscopy did not reveal the presence of any other morphology in the sample besides the furry nanotubes, it can be concluded that the nano-crystallites on the nanotube surface gives rise to the broad peaks in the XRD pattern. A rough estimation of the particle size determined from the broadening of the (100) peak by Scherrer formula gives a value of approximately 10 nm, which agrees very well with the size of the flakes as observed in TEM. This “furry” nanotube could be very interesting from technological point of view considering its very large surface area.

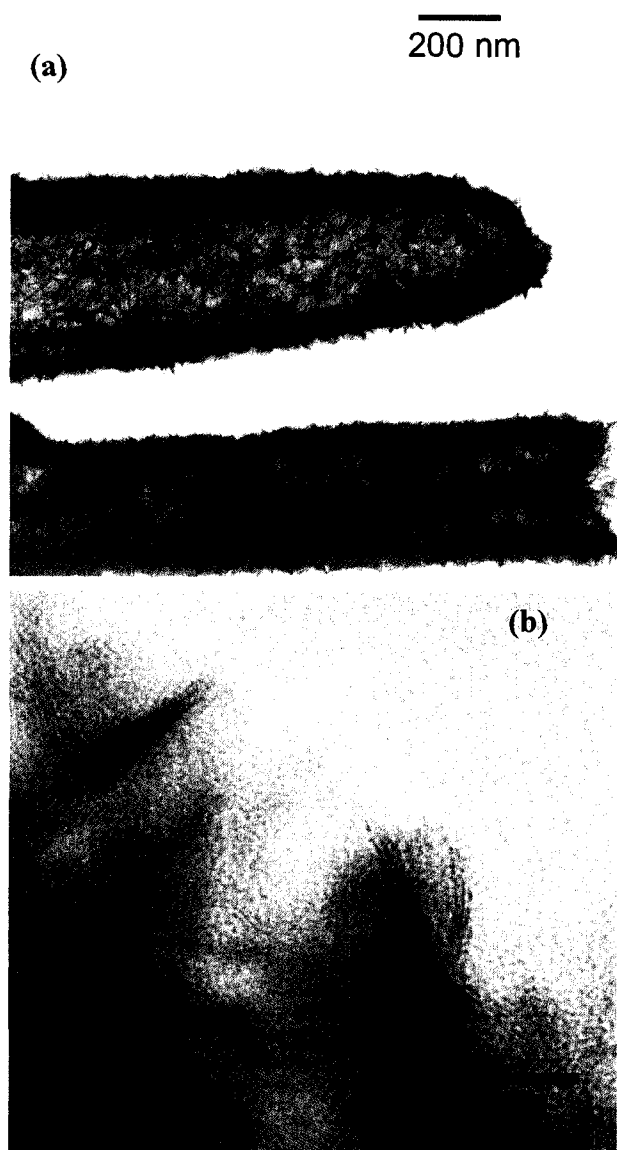


**Figure 5.3.** (a) Low magnification TEM image of the ReSe<sub>2</sub> nanotubes showing both open and closed ended nanotubes. (b) High-resolution TEM of the walls of the ReSe<sub>2</sub> nanotubes. The lattice fringes show a spacing of 5.4 Å.

The furry appearance of the nanotube walls occurs both on the inner and outer surfaces, indicating that the Re-precursor reacts homogenously over the exposed surface of the Se nanotube. As the ammonium perrhenate goes into solution, it produces  $\text{ReO}_4^-$  species that reacts with the Se nanotubes according to Eq. 5-1. It was expected that the perrhenate ion will react slowly on the surface of the Se nanotubes, eventually forming a shell of Re-Se layers on the Se nanotube, which will ultimately give the hollow  $\text{ReSe}_2$  nanotubes when the entire Se nanotube is consumed. The “furry” appearance may be due to the non-selective and rapid reaction between  $\text{ReO}_4^-$  and Se under solvothermal conditions, leading to creation of many nucleation sites on the surface of the precursor nanotube. Simultaneous growth from the nucleation sites leads to randomly oriented flakes lining the walls of the final  $\text{ReSe}_2$  nanotube. We studied the effect of annealing on the walls of the  $\text{ReSe}_2$  nanotubes. The morphology of the tube walls does not show any major change on annealing at  $600^\circ\text{C}$  under  $\text{N}_2$  (200 sccm) flow for 1 hour. However, the Re:Se ratio changes from 1:2 to 1:1.4. This indicates that the  $\text{ReSe}_2$  nanotubes may lose some Se, which is not uncommon in selenide compounds.<sup>17</sup> We are also varying other reaction parameters to see whether milder conditions would lead to a more controlled reaction on the surface of the Se nanotube and result in  $\text{ReSe}_2$  nanotubes with smooth continuous walls.

#### **5.4 Conclusions**

In conclusion, we have synthesized  $\text{ReSe}_2$  nanotubes for the first time using Se nanotubes as sacrificial templates. Since the  $\text{ReSe}_2$  nanotubes imitate the initial

morphology and diameter of the Se nanotube precursor, it should be possible to tune the diameter and length of the nanotubes by controlling these parameters in the sacrificial templates. Many synthetic methods are available to achieve smaller diameter nanowires and nanotubes of Se. The high surface area of the “furry”  $\text{ReSe}_2$  nanotubes reported here, may prove useful for catalytic or gas sensing applications. Efforts are currently underway to obtain baseline electrical property measurements on these nanotubes.

## References

1. Iijima, S. *Nature*, **1991**, *318*, 162.
2. Tenne, R.; Margulis, L.; Genut, M.; Hodes, G. *Nature*, **1992**, *360*, 444.
3. Wilson, J.; Yoffe, A. J. *Adv. Phys.*, **1969**, *269*, 193.
4. Tenne, R.; Margulis, L. *Nature* **1993**, *365*, 113; Coleman, K. S.; Sloan, J.; Hanson, N. A.; Brown, G.; Clancy, G. P.; Terrones, M.; Terrones, H.; Green, M. L. H. *J. Am. Chem. Soc.*, **2002**, *124*, 11580.
5. Brorson, M.; Hansen, T. W.; Jacobsen, C. J. H. *J. Am. Chem. Soc.*, **2002**, *124*, 11582.
6. Nath, M.; Rao, C. N. R. *J. Am. Chem. Soc.*, **2001**, *123*, 4841.
7. Lamfers, H.-J.; Wieggers, G. A.; de Boer, J. L. *J. Alloys and Compounds*, **1996**, *241*, 34.
8. Ho, C.H.; Huanaga, Y. S.; Liao, P.C.; Tiong, K.K. *J. Phys. Chem. Solids*, **1999**, *60*, 1797; Friemelt, K.; Lux-Steiner, M.-Ch.; E. Bucher, *J. Appl. Phys.*, **1973**, *24*, 73; W.Y., Liang *J. Phys. C*, **1973**, *6*, 551.
9. Ho, C. H.; Huang, Y. S.; Tiong, K. K. *Journal of Alloys and Compounds*, **2001**, *317-318*, 222.
10. Friemelt, K.; Lux-Steiner, M.-Ch.; Bucher, E. *J. Appl. Phys.*, **1993**, *74*, 5266
11. Wheeler, B. L.; Leland, J. K.; Bard, A. J. *J. Electrochem. Soc.*, **1986**, *133*, 358.
12. Nath, M.; Rao, C. N. R.; *Dalton Trans*, **2003**, 1.
13. Miao, J. J.; Ren, T.; Dong, L.; Zhu, J. J.; Chen, H. Y. *Small*, **2005**, *1*, 802; Li, X.; Chu, H.; Li, Y. *Journal of Solid State Chemistry*, **2006**, *179*, 96.
14. Niu, H.; Gao, M. *Ang. Chem. Int. Ed.*, **2006**, *45*, 6462.
15. Gates, B.; Wu, Y.; Yu, Y.; Yang, P.; Xia, Y. *J. Am. Chem. Soc.*, **2001**, *123*, 11500; Jiang, X.; Mayers, B.; Herricks, T.; Xia, Y. *Adv. Mat.*, **2003**, *15*, 1740; Jiang, X.; Mayers, B.; Wang, Y.; Cattle, B.; Xia, Y. *Chem. Phys. Lett.*, **2004**, *385*, 472.
16. Chen, Y-T.; Zhang, W.; Zhang, F-B.; Zhang, Z-X.; Zhou, B-J.; Li, H-L. *Mater. Lett.* **2004**, *58*, 2761.

17. Ruckh, M.; Kessler, J.; Oberacker, T. A.; Schock, H. W. *Jpn. J. Appl. Phys.* **1993**, *32*, 65; Pyrzynska, K. *Microchim Acta* **2002**, *140*, 55.

## **Chapter 6: Electrical Property Measurements of Individual ReSe<sub>2</sub> Nanotubes**

### **Abstract**

We have recently synthesized ReSe<sub>2</sub> nanotubes for the first time by using Se nanotubes as sacrificial templates. These nanotubes are characterized by a very high surface area due to the presence of ReSe<sub>2</sub> flakes along the walls of the nanotubes. In this paper, we have measured the two point room temperature electrical properties of individual nanotubes of ReSe<sub>2</sub>. Additionally, we have performed preliminary photocurrent and gas sensor measurements of these tubes with promising results.

The pursuit of novel 1-dimensional structures such as nanotubes has been vigorous since the discovery of carbon nanotubes by Iijima in 1991.<sup>1</sup> In 1992, Tenne found that other layered materials could also form nanotubes.<sup>2</sup> The materials that Tenne investigated are in the class of layered transition metal dichalcogenides. These materials feature a transition metal sandwiched between two chalcogen atoms forming one layer analogous to a sheet of graphene in graphite. They exhibit a wide variety of optical, catalytic, and electronic properties.<sup>3</sup> Many of the LTMDs have been shown to be able to form nanotubes due to the presence of dangling bonds at the edges of the individual layers or sheets. Nanotubes of tungsten and molybdenum disulfides and diselenides have been synthesized.<sup>2,4</sup> Rhenium disulfide nanotubes have been synthesized, and very recently, newly discovered rhenium diselenide nanotubes have been created.<sup>5,6</sup>

Rhenium diselenide is a layered transition metal dichalcogenide with an indirect gap of 1.2 eV that has a distorted CdCl<sub>2</sub> structure that results in triclinic symmetry.<sup>7</sup> Tiong and co-workers have studied the optical and electrical properties of bulk ReSe<sub>2</sub>.<sup>8</sup> They have found ReSe<sub>2</sub> to have highly anisotropic optical, electrical, and physical properties. Although a good deal of research has been done on the bulk material, there are no studies of the electrical properties of 1-dimensional structures of ReSe<sub>2</sub>.

Recently, we have synthesized ReSe<sub>2</sub> nanotubes using Se nanotubes as sacrificial templates via a solvothermal route.<sup>6</sup> We report here the first electrical property measurements of these interesting nanotubes.

The research thus far on the transport properties of 1-dimensional materials has been dominated by carbon nanotubes.<sup>9</sup> Perusal of the literature reveals scant research on the electrical property measurements of nanotubular systems with the exception of carbon nanotubes. In the past few years, however, the electrical properties of many 1-dimensional nanowires have been characterized.<sup>10 - 12</sup> The shapes of the current voltage curves exhibited by these systems can be classified as nearly linear, nearly symmetric, and nearly rectifying. ZnO nanowires can be p- or n- doped to yield nearly linear current voltage curves, and upon applying strain can exhibit nearly rectifying behavior.<sup>13</sup> A system that does manifest the three different types of current voltage behavior would be interesting from a research point of view and would have the desirable qualities for different electronic applications.

The study of 1-dimensional systems has been facilitated typically by lithographic techniques. One of the most useful of these techniques is electron beam lithography (EBL). EBL allows the researcher to contact specific nanotubes, rather than ensembles or random samples of the material. It has been used to successfully contact both carbon nanotubes and other nanowires.<sup>14</sup> In our efforts to characterize the electrical properties of ReSe<sub>2</sub> nanotubes, we used EBL to contact the nanostructures. We used a bi-layer of 495 k MW PMMA and a 950 k MW PMMA spun on at 4000 and 4500 rpm for 50 seconds with a bake treatment at 180 °C for 6 minutes after each resist application. The exposed PMMA was developed with a 1:3 ratio of MIBK:IPA followed by lift-off with acetone. Details of electron beam writing can be found in Appendix A.

The nanotubes were synthesized using a technique previously described. Briefly, Se nanotubes were synthesized by adding a solution of Se dissolved in ethylenediamine to deionized water in an ultrasonic bath. An ethanolic solution of  $\text{NH}_4\text{ReO}_4$  was added to the Se nanowires and treated solvothermally at  $135\text{ }^\circ\text{C}$  for 6 days. An SEM micrograph showing the as-made  $\text{ReSe}_2$  nanotubes is shown in Figure 6.1.

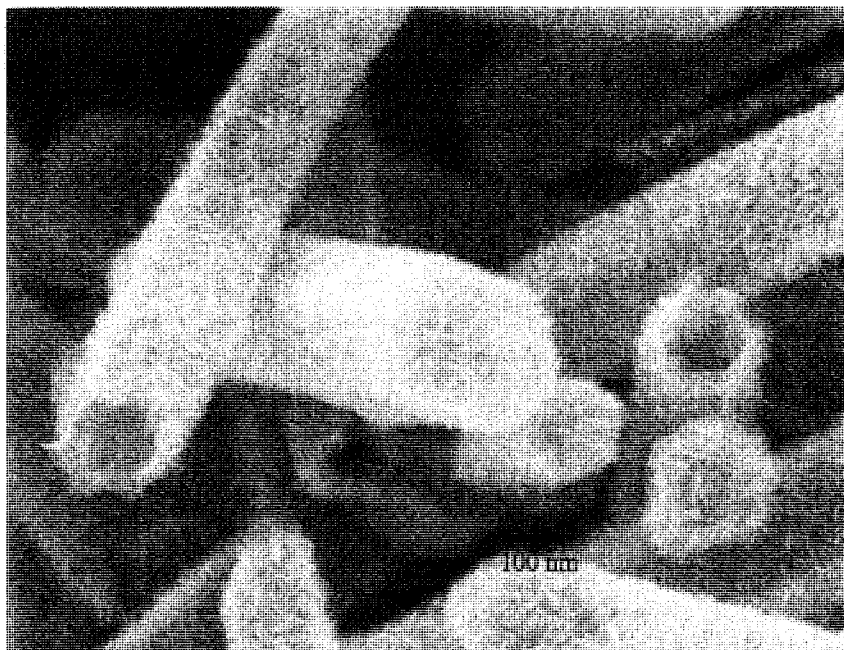


**Figure 6.1** SEM micrograph of as-synthesized  $\text{ReSe}_2$  nanotubes.

The nanotubes are characterized by a “fuzzy” looking surface, created by the presence of  $\text{ReSe}_2$  flakes throughout the length of the tube. The Se nanotube morphology has been preserved in the  $\text{ReSe}_2$  nanotubes, resulting in hexagonal and triangular nanotubes with open or closed ends.

The  $\text{ReSe}_2$  nanotubes were dispersed in IPA and dropped onto a Si wafer with a 100 nm thermal oxide coating. The two-point electrical property measurements were

carried out at room temperature using an Ivium Soft potentiostat and a micromanipulator probe station. The reference and counter electrodes were connected together on one contact and the working electrode connector was attached to the other end of the nanotube. The nanotubes exhibited nearly rectifying, nearly symmetric, and nearly linear current voltage behavior. Figure 6.2 shows the current voltage curves for a set of nearly rectifying nanotubes.

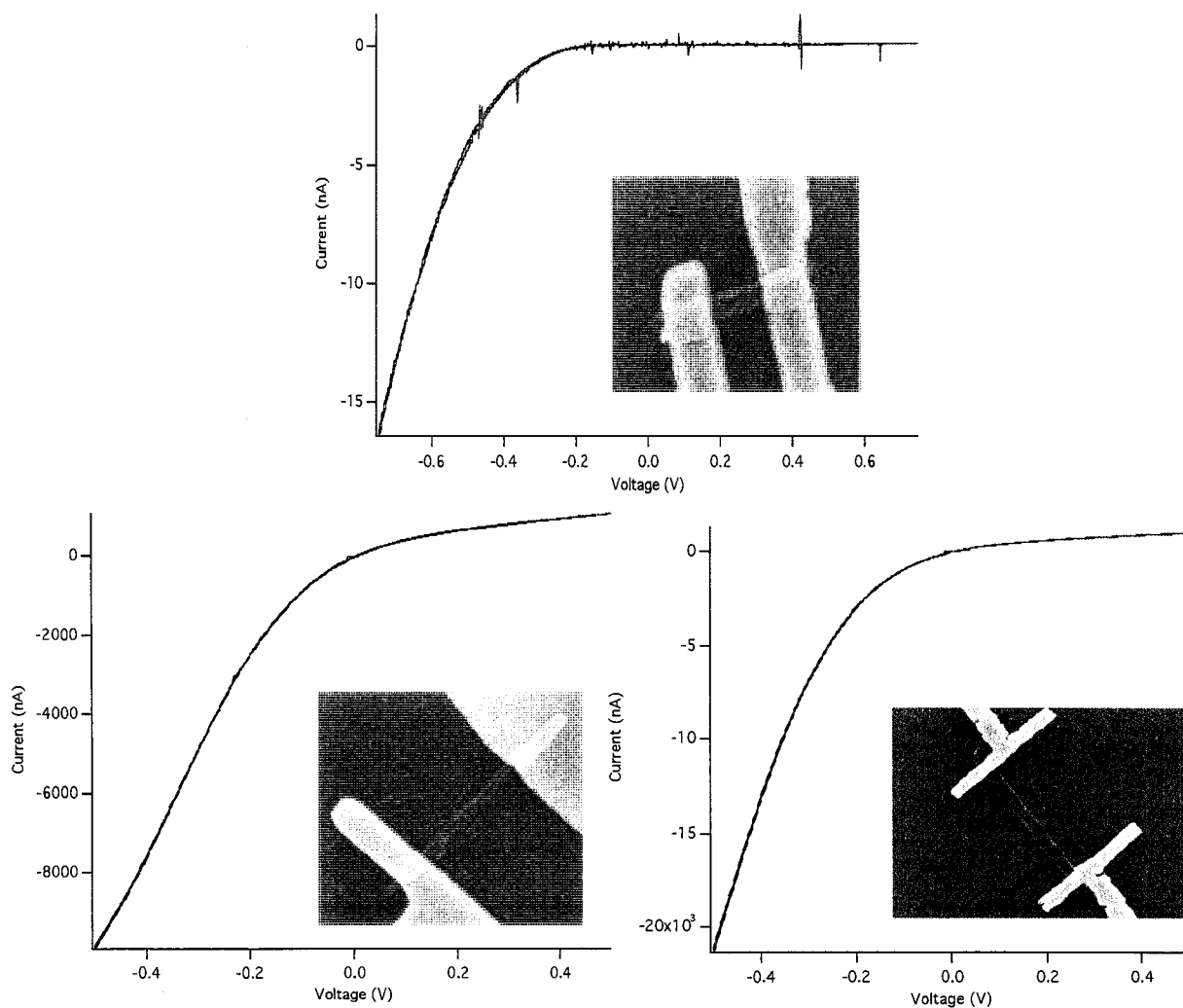


**Figure 6.2** Current voltage curves of  $\text{ReSe}_2$  nanotubes exhibiting nearly rectifying behavior.

From the current voltage curves it can be seen that the nanotubes display a wide range of currents, from 15 nA to 20  $\mu$ A. The direction of the current was reversed and the expected behavior with the nanotube blocking in the opposite direction was seen. The nanotubes in the images are from about 1  $\mu$ m to 3  $\mu$ m long. It can be seen that the nanotube in the top image is triangular in shape, while the shape of the lower nanotubes is indeterminate, but expected to be hexagonal since the majority of the Se nanotubes were hexagonal. Both contacts are Cr/Au, so there is no difference in the work functions of the metals at the two ends of the nanotubes, which would explain the rectifying nature of the I-V curves. There does not appear to be a length -dependence on the resistance of the nanotubes.

We have also seen nearly linear I-V behavior in the nanotubes. Figure 6.3 shows a series of current voltage curves for a nanotube displaying nearly linear behavior. The nanotube is also shown in the figure.

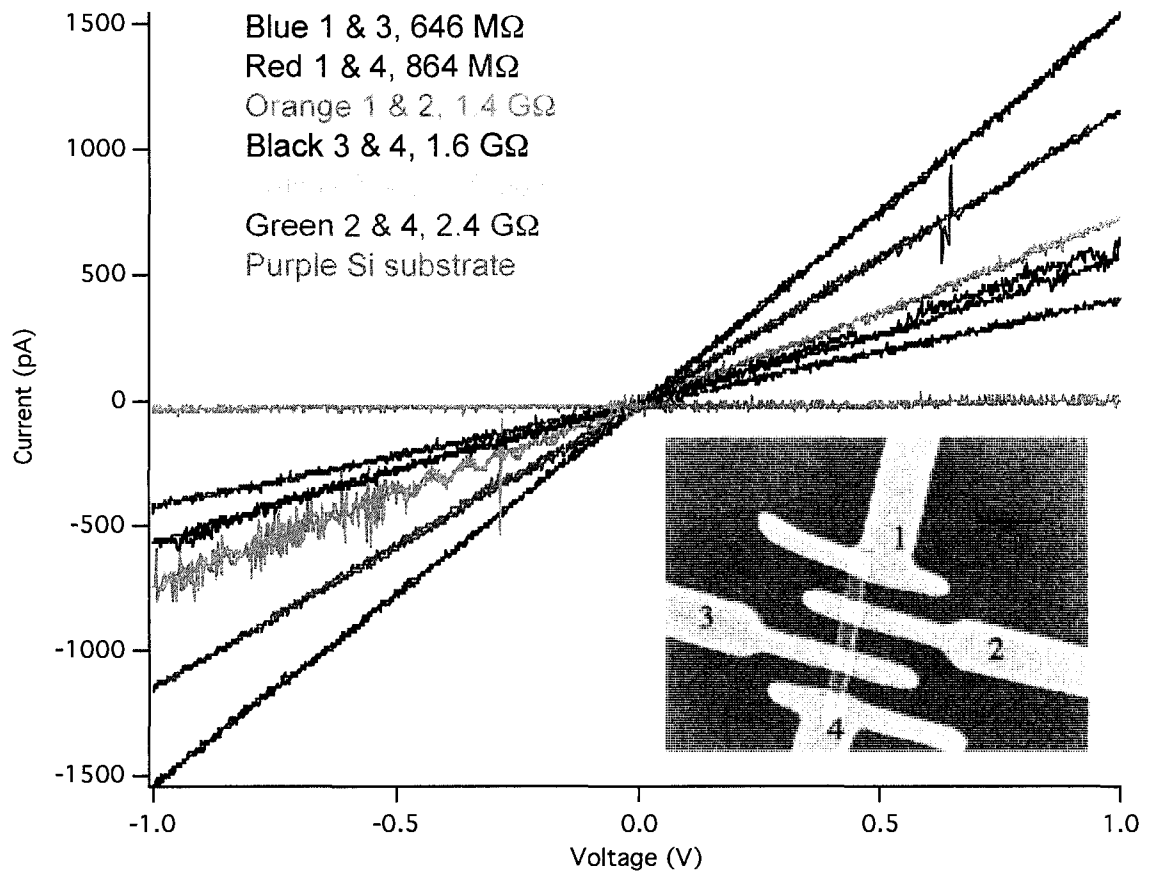


**Figure 6.3** Nearly linear current voltage curves of a single  $\text{ReSe}_2$  nanotube. Shown also are the resistances of the segments of the nanotube. The Si substrate with the 100 nm thermal oxide is shown for reference.

The currents achieved in this nanotube are much lower than the currents seen in the nearly rectifying nanotubes. Given the low currents associated with this nanotube, a control I-V curve of the Si wafer using contacts that were spaced by 5  $\mu\text{m}$  with the 100 nm thermal oxide is included. It is clear that this reference represents an open-circuit. The I-V curves are noisy likely because of the low currents. Additionally, there is no

length dependence on the resistance of the nanotube segments. The contacts are numbered according to the measured resistances. The smallest current corresponds to a resistance of about  $650 \text{ M}\Omega$ , which is  $\frac{1}{2}$  of the largest current recorded.

Lastly, we have also observed nearly symmetric current voltage curves in the  $\text{ReSe}_2$  nanotubes. Figure 6.4 shows this behavior.

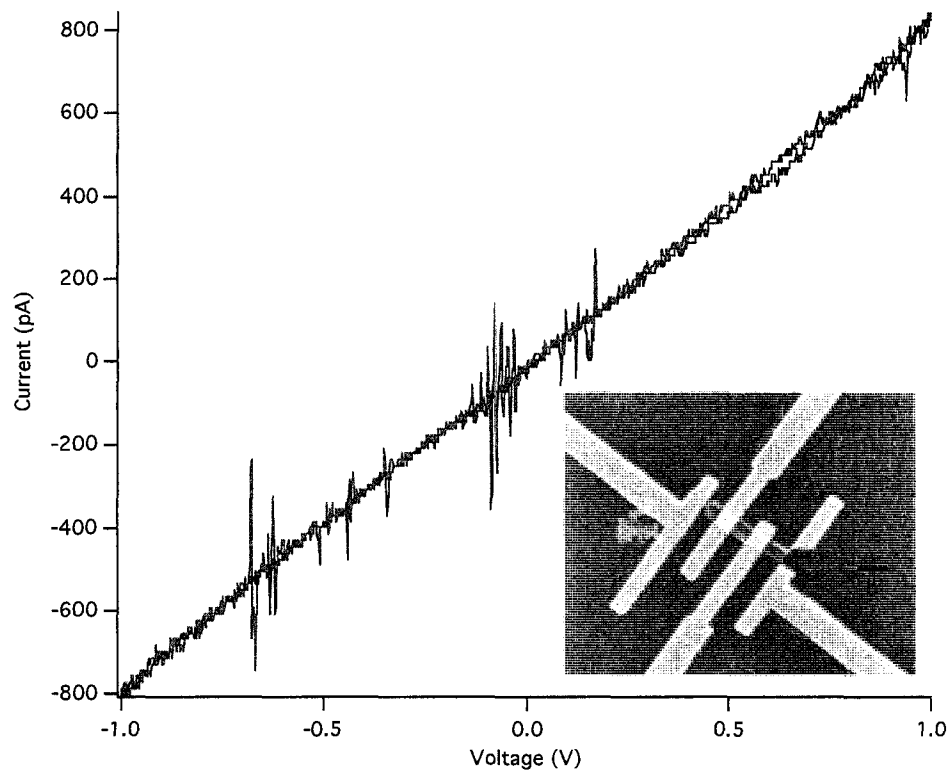


**Figure 6.4** Nearly symmetric current voltage curve of an individual  $\text{ReSe}_2$  nanotube.

From the current voltage curve, it can be seen that there is some curvature of the line near  $-0.5 \text{ V}$  and  $0.5 \text{ V}$ . The two contacts being addressed are the middle two contacts. Once

again, the curve is quite noisy, likely because of the small currents being measured; this tube only passes currents up to 800 pA at  $\pm 1$  V bias.

These ReSe<sub>2</sub> nanotubes have shown a remarkable spectrum of current voltage characteristics. None of the measurements indicated a strong relationship between the length of the nanotube segment measured and the resulting currents. Certainly, the electrons can take different paths from contact to contact, resulting in this high variation of current magnitude. Given the large variation in the “fuzzy” morphology, there may be multiple paths for the electrons to travel depending on the resistance of the paths. The polycrystalline nature may explain the nearly rectifying behavior of some of these nanotubes. The presence of different sizes and directions of the crystallites, as well as the inherent anisotropy of ReSe<sub>2</sub> may have the effect of disallowing current to flow in one direction. If the contact is primarily to the faces of the platelets and the next adjacent platelet is oriented in the same direction (face to face platelet contact), then the resistance would be higher due to the electron flow across the van der Waals gap. If the contact is primarily on the edges and the next adjacent platelet is located in an edge to edge orientation, then the resistance should be lower.

There does not appear to be a nanotube shape dependence on the current voltage characteristics. The only nanotube whose shape can be determined with certainty shows nearly rectifying behavior similar to the nanotubes that are definitely not triangular. It also does not appear that the open or closed ended nanotubes behave differently from

each other. Since these are composite nanotubes, it is not expected that shape would be important when considering the resistances.

Given that  $\text{ReSe}_2$  is a semiconductor, we performed experiments to determine whether the tubes could generate a photocurrent. Figure 6.5 shows the preliminary current voltage curve with the presence of light.

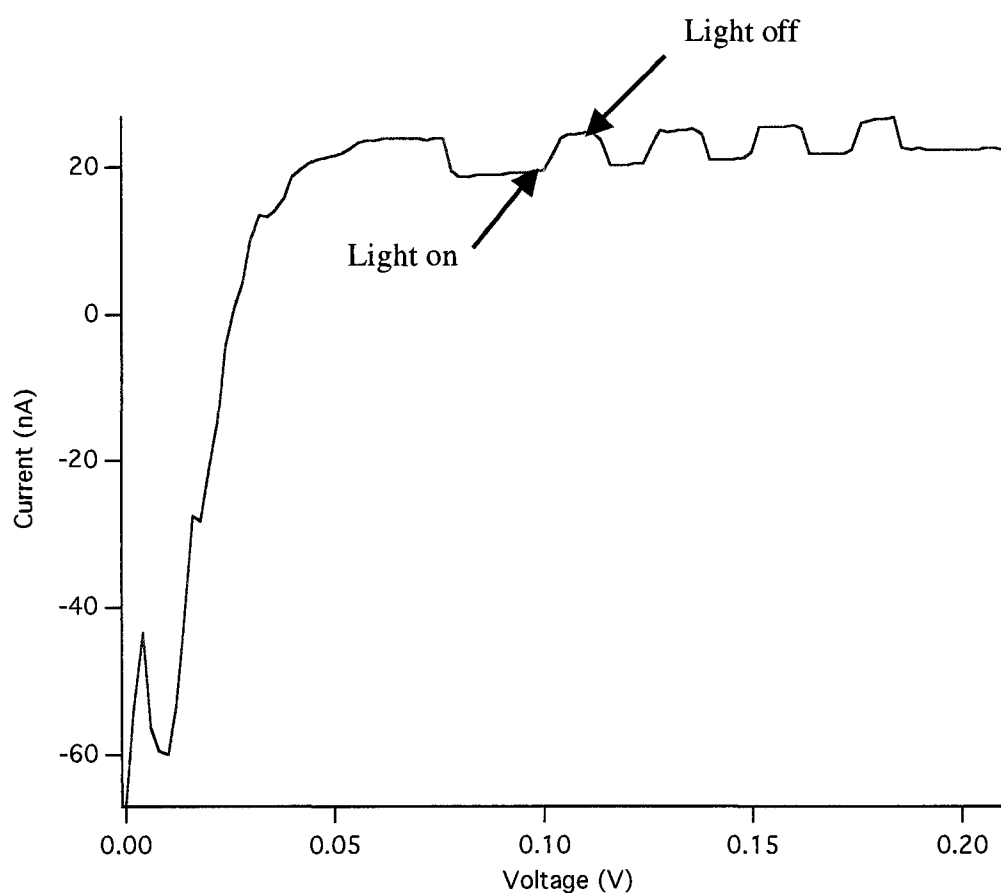


Figure 6.5 Current voltage curve of an individual  $\text{ReSe}_2$  nanotube exhibiting a photocurrent. The peaks indicate the presence of light from a halogen lamp.

The current voltage curve clearly indicates the effect of shining a light on the contacted nanotube. The peaks of the curve indicate the increased current response when light impinges on the nanotube. This exciting result prompted us to determine how much photocurrent could be generated within the nanotubes. Figure 6.6 shows two more current voltage curves and the effect of shining light on the nanotubes.

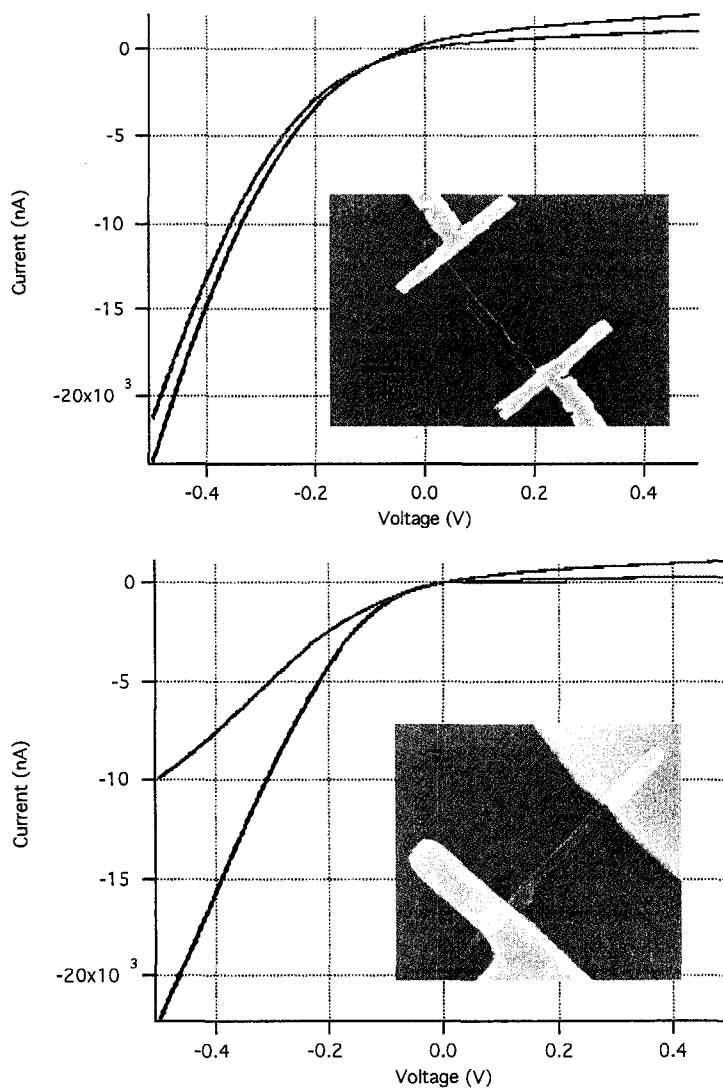
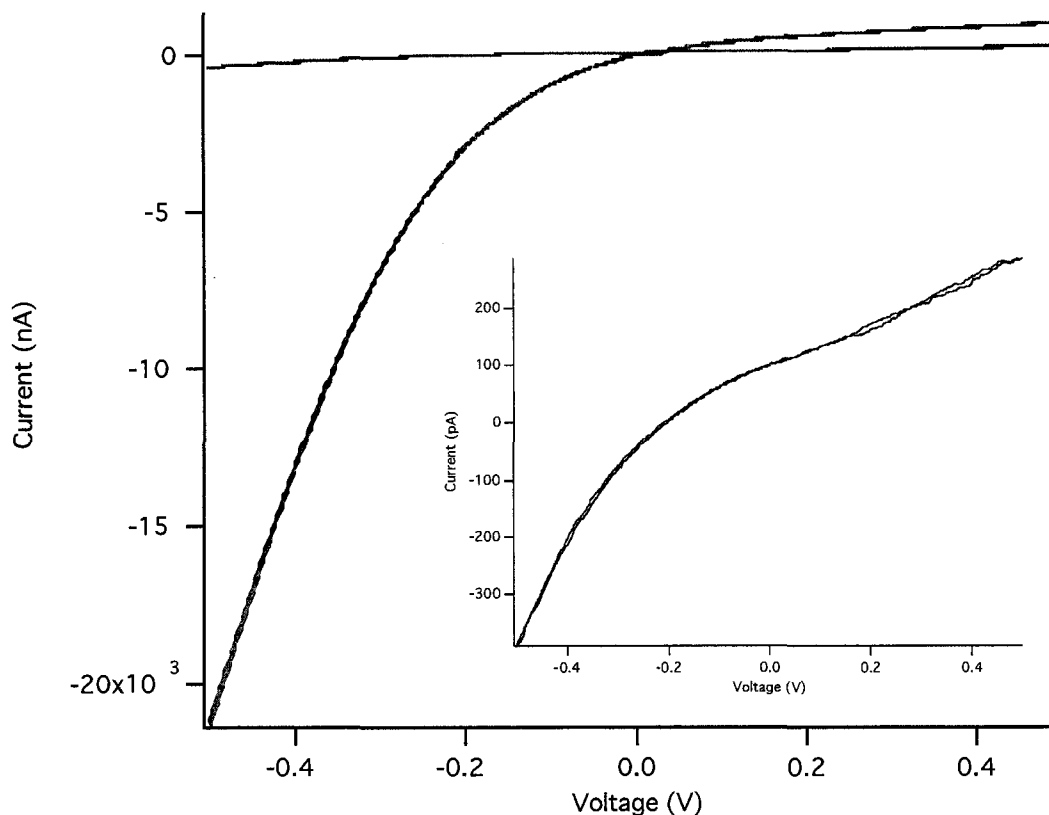


Figure 6.6 Two ReSe<sub>2</sub> nanotubes showing a photocurrent. Blue curves indicate I-V characteristics with light shining on nanotubes. Red curves indicate I-V characteristics under ambient conditions.

In the current voltage curves, the blue lines indicate light shining on the nanotubes, while the red lines represent the current voltage curves without light shining on the tubes. The curves shown in Figure 6.6 clearly show the increase in current when light is shining on the nanotubes. The top current voltage curve shows a modest increase in current in the negative direction of about 12%. In the positive direction, the increase in current is closer to a 95% increase. The bottom current voltage curve is interesting. It shows a huge increase in current in the negative direction of about 125%. However, in the positive direction, there is no increase in current. This may in part be due to the nature of the ReSe<sub>2</sub> crystallites present on that end of the nanotube. The ReSe<sub>2</sub> nanotubes exhibit photoconductivity. Light will enhance the current through the length of the tube, but we saw no response at short-circuit with just the light shining on the tube.

Based on the high surface area of the nanotubes, we were interested in the possibility of these nanotubes acting as gas sensors. The experimental set-up was very simplistic. We placed a beaker of concentrated NH<sub>4</sub>OH in close proximity to the nanotube while we swept the voltage from -0.5 V to 0.5 V. The effect of ammonia can easily be seen in the resulting current voltage curve shown in Figure 6.7.



**Figure 6.7** Current voltage curve of an individual  $\text{ReSe}_2$  nanotube showing the effect of ammonia on the transport properties. Blue curves indicate exposure to ammonia; red curves indicate ambient conditions. The inset shows a different scale indicating the effect of ammonia.

The blue curve indicates the presence of ammonia, and the red curve indicates the nanotube transport properties without ammonia. This figure shows a drastic change in the transport properties of the nanotube with the presence of ammonia. The ammonia has the effect of virtually “shutting off” the current. This result is not unlike an early result investigating carbon nanotubes as ammonia sensors.<sup>15</sup> The current decreases 4 orders of magnitude from about  $20 \mu\text{A}$  to about  $400 \text{ pA}$  in the negative direction. After the  $\text{NH}_3$  was removed, the I-V curves recovered, indicating the reversibility of the sensor.

These very preliminary studies on the ability of the ReSe<sub>2</sub> nanotubes to exhibit a photocurrent and to act as ammonia sensors are promising. In both instances, the transport properties of the nanotubes changed significantly. The nanotubes were relatively durable upon applying a bias to them. This is somewhat surprising, considering their polycrystalline nature and given the fact that before measurements, some of the tubes were destroyed by the electron beam during writing or during the lift-off step of lithography.

Very recently, we have gone back and examined some of the nanotubes interrogated in these experiments with the SEM. We have seen an interesting change in morphology of some of the nanotubes. Figure 6.8 shows these differences.

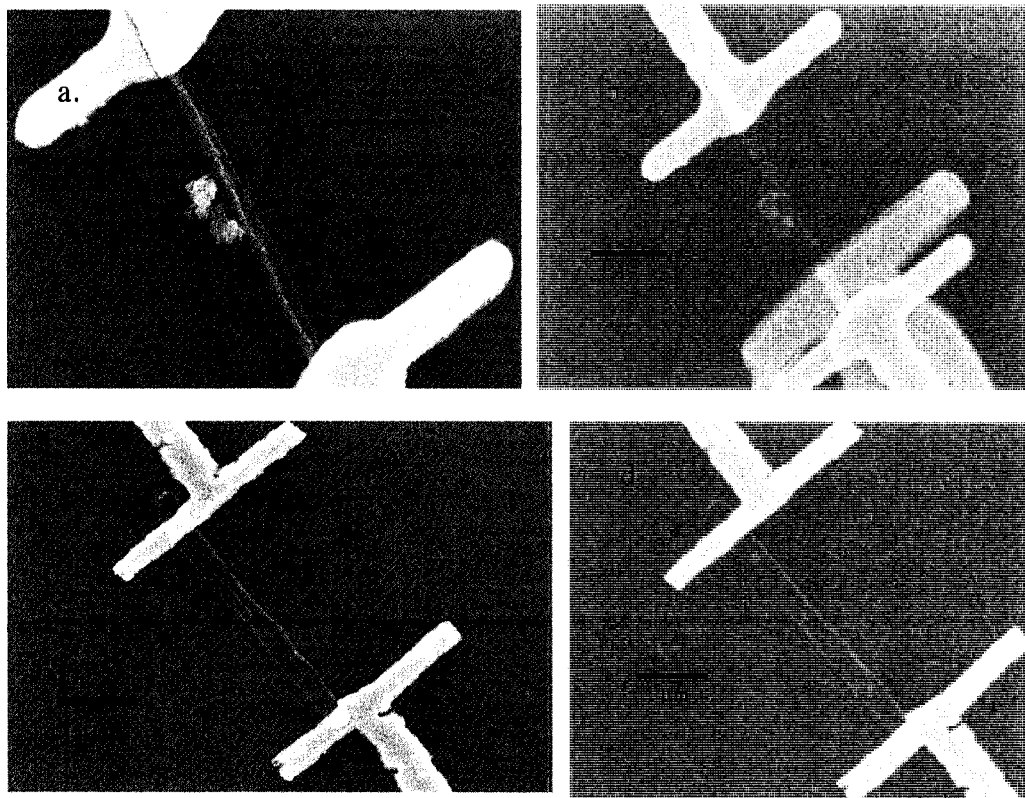


**Figure 6.8** SEM micrographs of 2 nanotubes before and after electrical property measurements; a.) and b.) show 1 nanotube before and after measurements, respectively; c.) and d.) show a different nanotube before and after, respectively.

In Figure 6.8a, there is a small group of crystallites touching the nanotube. These are likely  $\text{ReSe}_2$  based on the original SEM images and EDS data. These can be clearly seen in the image to consist of smaller particles with many edges resembling the “fuzzy” nature of the  $\text{ReSe}_2$  nanotubes. This group of particles has changed into larger crystallites in 6.8b after measurements of the electronic properties. The tube itself shows many edges and crystallites before the measurements, but afterwards, it also has larger crystallites seemingly emanating from the edge of the tube wall. In Figure 6.8c and d, more evidence of this phenomenon is shown. Before measurements in 6.8c, the tube has no large crystallites on its body. However, after measurements in 6.8d, two distinct crystallites are seen to have formed on the tube wall. Both of these crystallites appear to be triangular in shape, although one is larger than the other. Looking closely at the tube, there doesn't seem to be a preexisting shape that precedes the formation of these larger particles. We speculate that they are comprised of  $\text{ReSe}_2$  or Re. We do not believe them to be Se, which has been shown to decompose from selenides.<sup>16</sup> Our own experiments of annealing the nanotubes at temperatures of 600 °C for 1 hour resulted in a lower Se content based on EDS of the tubes after annealing. These larger crystallites present on both tubes shown may be the result of current induced recrystallization or decomposition. There are likely local areas of heating while the current is being passed through the tube. These localized areas could provide enough energy to anneal some smaller crystallites into larger ones. Considering that the nanotubes were synthesized over a year ago there may be some propensity to explain the formation of these larger crystallites by the

passing of time. However, these tubes have been viewed and measured when they had been sitting around for 10 months. There was no indication of any larger crystallite formation in those nanotubes.

In conclusion, we have measured the two point room temperature electrical properties in individual nanotubes of  $\text{ReSe}_2$  nanotubes. The nanotubes exhibit three kinds of current voltage behavior: nearly linear, nearly symmetric, and nearly rectifying. The nearly rectifying behavior may be attributed to the presence of different sized  $\text{ReSe}_2$  crystallites growing out in different directions from the nanotube body.  $\text{ReSe}_2$  has highly anisotropic electrical properties and this may also contribute to the nearly rectifying behavior.

We have also performed some preliminary experiments investigating the nanotube's change in resistance with the influence of light and gaseous analytes. The nanotubes do exhibit an increase in current when exposed to white light. The nanotubes also show a change in their electrical properties when exposed to ammonia gas.

Finally, we have noticed what we believe to be a current induced recrystallization of the nanotubes after electrical property measurements have been performed. These unique nanotubes warrant further study into their optical and electrical properties, and should find applications taking advantage of their behavior under a wide variety of conditions.

## References

1. Iijima, S. *Nature*, **1991**, 318, 162.
2. Tenne, R., Margulis, L.; Genut, M.; Hodes *Nature*, **1992**, 360, 444.
3. Wilson, J., Yoffe, A. J.; *Adv. Phys.*, **1969**, 269, 193.
4. a.) Margulis, L.; Salitra, G.; Tenne, R.; Tallanker, M.; *Nature*, **1993**, 365, 113-114; b.) Nath, M.; Rao, C. N. R.; *Chemical Communications*, **2001**, 2236-2237.
5. a.) Coleman, K. S.; Sloan, J.; Hanson, N. A.; Brown, G.; Clancy, G. P.; Terrones, M.; Terrones, H.; Green, M. L. H.; *Journal of the American Chemical Society*, **2002**, 124, 11580-11581; b.) Brorson, M.; Hansen, T. W.; Jacobsen, C. J. H.; *Journal of the American Chemical Society*, **2002**, 124, 1582-1583.
6. Seley, D. B.; Nath, M.; Parkinson, B. A.; submitted for publication.
7. Lamfers, H.-J., Wiegers, G. A., de Boer, J. L. *J. Alloys and Compounds*, **1996**, 241, 34.
8. a.) Ho, C. H.; Huang, Y. S.; Tiong, K. K.; Liao, P. C.; *Physical Review B*, **1998**, 58, 16130-16135; b.) Tiong, K. K.; Ho, C. H.; Huang, Y. S.; *Solid State Communications*, **1999**, 635-640.
9. a.) Ebbesen, T. W.; Lezec, H. J.; Hiura, H.; Bennett, J. W.; Ghaemi, H. F.; Thio, T. *Nature*, **1996**, 382, 54-56; b.) Dai, H.; Wong, E. W.; Lieber, C. M.; *Science*, **1996**, 272, 523-526; c.) Tans, S. J.; *Nature*, **1998**, 393, 49-52.
10. Wang, D.; Lu, J. G.; Jones Otten, C.; Buhreo, W. E., *Applied Physics Letters*, **2003**, 83, 5280-5282.
11. Zhang, D.; Li, C.; Han, S.; Liu, X.; Tang, T.; Jin, W.; Zhou, C.; *Applied Physics Letters*, **2003**, 82, 112-114.
12. Kim, J.; Shin, D. H.; Lee, E-S.; Han, C-S.; Park, Y. C.; *Applied Physics Letters*, **2007**, 90, 253103-1 – 253103-3.
13. He, Jr H.; Hsin, C. L.; Liu, J.; Chen, L. J.; Wang, Z. L.; *Advanced Materials*, **2007**, 19, 781-784.
14. a.) Harnack, O.; Pacholski, C.; Weller, H.; Yasuda, A.; Wessels, J. M.; *Nano Letters*, **2003**, 3, 1097-1101; b.) Cui, Y.; Duan, X.; Hu, J.; Lieber, C. M.; *Journal of Physical Chemistry B*, **2004**, 104, 5213-5216; c.) Yu, J-W.; Chung, S-W.; Heath, J. R.; *Journal of Physical Chemistry b*, **2000**, 110, 11864-11870.

15. Kong, J.; Franklin, N. R.; Zhou, C. W.; Chapline, M. G.; Peng, S.; Cho, K. J.; Dai, H. J.; *Science*, **2000**, 287, 622-625.
16. Ruckh, M.; Kessler, J.; Oberacker, T. A.; Schock, H. W. *Jpn. J. Appl. Phys.* **1993**, 32, 65; Pyrzynska, K. *Microchim Acta*, **2002**, 140, 55.

## Chapter 7: Concluding Remarks and Future Work

This research project entailed the synthesis and electrical property measurement of chalcogenide nanotubes and nanowires. The synthesis methods all used some form of templating approach, which is ideal for the creation of such nanostructures. The syntheses of nanotubes of MoS<sub>2</sub>, WS<sub>2</sub>, and ReS<sub>2</sub> involved using the pores of anodic aluminum oxide membranes to direct the 1-dimensional growth. The use of the surfactant CTAB was enlisted as a structural modifier for the synthesis of WS<sub>2</sub> nanowires. Finally, the first examples of ReSe<sub>2</sub> nanotubes were synthesized using Se nanotubes as sacrificial templates in a solvothermal synthesis.

The use of anodic aluminum oxide membranes as templates for nanotube synthesis is quite straightforward. However, these nanotube products are not very crystalline and have many defects within and along the nanotube walls. I do not think it is likely that nanotubes of a very high quality will ever be synthesized using this approach since changing many synthesis conditions did not make significant difference in the nanotubes. The use of the surfactant CTAB to yield WS<sub>2</sub> nanowires is quite interesting. There seems to be a variety of 1-dimensional structures attainable with this method, including nanobelts, nanoribbons, and nanowires. Additionally, the nanowires appear to contain a residual coating of carbon leftover from the synthesis. These two factors – lack of structural control and difficulty removing the surfactant – make this synthetic technique less attractive than other techniques. The use of Se as sacrificial

templates is a very interesting and promising approach. There is much information in the literature about the control of the size distribution of these 1-dimensional structures.

The two point room temperature electrical property measurements of some of the nanotubes made during the course of this project were both exciting and promising. By using the technique of electron beam lithography, virtually any nanotube could be contacted if its length is greater than 2  $\mu\text{m}$  long. A wide variety of current voltage behaviors were observed and additional experiments on the  $\text{ReSe}_2$  nanotubes were undertaken. These nanotubes showed both an enhanced current when light impinged on them, as well as a definite change in transport properties when exposed to ammonia.

Given the current state of the project with so many tools in place, there are several different areas worth exploring in the future. These directions include aspects of both synthesis and measurement of the optical and electrical properties. The synthesis using the Se nanotube sacrificial template is quite promising as previously mentioned. The  $\text{ReSe}_2$  nanotubes synthesized in this project displayed a “furry” appearance due to the presence of  $\text{ReSe}_2$  crystallites along the nanotube walls. It should be possible to make these nanotubes more uniform by varying such things as the rhenium concentration in the reaction. There are several ways to control the morphology of this material.<sup>1</sup> Both nanowires and nanotubes of Se can be synthesized allowing for different morphologies in the final product. There are a variety of the layered transition metal diselenides that either have not been synthesized in the form of nanotubes, or are of great interest due to their electrical properties. Selenides of hafnium and vanadium have not been synthesized

in the form of nanotubes.  $\text{NbSe}_2$  is a superconducting material and further studies into the synthesis of these kinds of nanotubes would be of interest especially if the properties of individual tubes can be measured.

Along this same vein, tellurium is very similar chemically to selenium. Nanowires and nanotubes of this material have also been made by different synthetic routes.<sup>2</sup> There are many ditelluride nanotubes that have yet to be made including zirconium, hafnium, vanadium, and niobium ditellurides. Other tellurides are promising thermoelectric materials and there are many applications of these semiconducting systems.<sup>3</sup> Using Te nanotubes as sacrificial templates to make new materials would be a logical direction to follow.

There are several new directions for the electrical property measurements of these materials. One of the most obvious next steps is to perform some variable temperature measurements on the different 1-dimensional systems. This would provide an opportunity to verify that all of the materials are in fact semiconducting, and perhaps obtain some information on the band gaps and carrier mobilities of the materials. A base fabricated from Teflon could be used to hold the substrate in place and contacts could be soldered to the macroscopic contacts, which are in electrical contact to the nanotubes. A thermocouple could be placed close to the sample to record the temperature. This device could be lowered into a dewar of liquid nitrogen or helium and the transport properties monitored as a function of temperature.

Electron beam lithography allows for the ability to contact the nanotubes in a four-point configuration. Using a current source and a potentiostat, the contact resistances of the Cr/Au could be determined. The current would be applied through the two tube ends, and the voltage drop between the two inside contacts could be measured. This would effectively eliminate the contact resistance and answer any questions about the intrinsic resistance of the nanotubes.

The nanotubes that have been contacted on a Si wafer could be made to act as field effect transistor if a gate electrode was added to the back of the wafer. This device would allow for the determination of the dominant carrier. For example, if the gate voltage were negative and a higher current was seen in the I-V curves, the nanotubes would be defined as p-type. It would be interesting to determine the p- or n- nature of all of the 1-dimensional systems investigated in this project.

There are certainly ways to take a more quantitative approach to the gas sensing nature of these systems. Although it would require a greater effort to design such a system, it is definitely possible. The requirements would be a vacuum system, a substrate heater for the Si wafer, some mass flow controllers to monitor the concentration of the gases, and the wiring coming from the substrate to the outside world to a current measuring device that can measure low currents. Different gases should affect the resistances of the nanotubes in different ways depending on whether the gas is electron donating or electron withdrawing.

Photocurrent studies can also be done on these materials with most of the equipment being available in the Parkinson lab. A high intensity light source with different filters would provide the light of different wavelengths. A potentiostat and a lock-in amplifier would likely be required due to the low currents expected, as well as a chopper for the impinging light. These experiments should not only provide information on the quantity of photocurrent generated, but would also allow for the determination of the optical gap.

## References

1. Gates, B.; Mayers, B.; Cattle, B.; Xia, Y.; *Advanced Functional Materials*, **2002**, 12, 219-227.
2. a.) Mayers, B.; Xia, Y.; *Advanced Materials*, **2002**, 14, 279-282; b.) Liu, Z.; Li, S.; Yang, Y.; Hu, Z.; Peng, S.; Liang, J.; Qian, Y.; *New Journal of Chemistry*, **2003**, 27, 1748-1752.
3. a.) Deng, Y.; Cui, C-W.; Zhang, N-L.; Ji, T-H.; Yang, Q-L.; Guo, L.; *Solid State Communications*, **2006**, 138, 111-113; b.) Ikeda, T.; Collins, L. A.; Ravi, V. A.; Gascoin, F. S.; Haile, S. M.; Snyder, G. J.; *Chemistry of Materials*, **2007**, 19, 763-767.

## **Appendix A: Electron Beam Lithography**

Appendix A is dedicated to the discussion of the electron beam lithography system at Colorado State University in the Electron Microscopy Center. It should be used as a tutorial for beginning to understand the operation of the Nanometer Pattern Generation System software as well as using the hardware (SEM) for the purpose of electron beam writing. This chapter specifically discusses the required steps in using the electron beam lithography system to make contacts to individual nanotubes and nanowires.

## A.1 Introduction

Electron beam lithography (EBL) has found wide use in the fabrication of nanometer-sized features. It is used in the semiconductor industry to make masks for subsequent optical lithography. Electron beam lithography has advantages over traditional optical lithography due to the diffraction limit of high-energy electrons versus light. EBL has been an invaluable tool in the pursuit of measuring the electrical properties of carbon and other kinds of nanotubes. In this case, EBL is used as a direct-write technique in which the electron beam creates a pattern of electrodes over an individual nanotube. The small feature sizes attainable with EBL make 4-point measurements achievable on individual nanotubes that are shorter in length than the limits optical lithography allows.

Many researchers have taken advantage of this technique for these specific applications. One of the first examples of using EBL to make contacts to an individual nanotube is that of Dai using a carbon nanotube <sup>1</sup>. Since that time, there have been many different examples of measuring the electrical properties of individual nanotubes utilizing EBL as a tool <sup>2-5</sup>.

One of the most obvious challenges in utilizing EBL to make contact to individual nanotubes is the problem of knowing the exact position of the nanotube on the substrate and making a precise line in the electron beam resist without exposing the resist while trying to locate the tubes. This problem has been overcome by a combination of a grid of numbers for reference that has been designed in a computer aided design (CAD) program

and a macro in the software program Igor, that functions to describe the position of the nanotube on the substrate.

The equipment required to perform EBL is readily available at Colorado State University in the electron microscopy center. A scanning emission microscope (JEOL 6500 FE-SEM) provides the high-energy electron beam for writing. The software driving the SEM is provided by the Nanometer Pattern Generation System (NPGS) created by Joe Nability. This software includes a CAD program for designing patterns and also tells the electron beam where to write. This software is located on a computer in the Electron Microscope Center and all of the subsequent references to writing or incorporating the positions of the nanotubes will be carried out on this computer. The SEM is equipped with a beam blanker that disables the electron beam from exposing the sample when it is not desirable to do so. There is also a picoammeter to measure the beam current from the SEM, which is important to know when writing on the samples since it determines the electron exposure.

The photoresist most commonly used in EBL is (poly)-methyl methacrylate (PMMA). This is a positive electron beam resist, meaning that where the beam shines, the polymer is eventually removed. The main reason that PMMA is used is because it is the highest resolution e-beam resist, meaning that the smallest feature sizes can be made using this resist<sup>6</sup>. Different molecular weight ranges can be used depending on the particular application. Generally speaking, for the smallest feature sizes, a thin layer (<100 nm) of 950,000 MW PMMA works the best.

The following section will describe specifically the process used with respect to making electrical contacts to individual nanotubes in the Parkinson group at CSU. A more detailed discussion will follow when describing the specifics of the software. Si wafers with an insulating thermal oxide of 100 nm thickness are cut into  $\sim 1$  cm pieces. The chips are then rinsed with acetone and methanol, followed by a deionized water rinse and blow-drying. Two layers of different molecular weight PMMA are then spun-coated onto the substrates. The first layer consists of 3% solution of 495,000 MW PMMA dissolved in chlorobenzene spun on at 4000 rpm for 50 seconds. Once the PMMA is on the chip, the chip is placed on a hot plate at 180°C for 6 minutes to drive off the chlorobenzene solvent. The sample is then placed in the spin-coater again and a 3% solution of 950,000 MW PMMA dissolved in chlorobenzene is spun onto the chip at 4500 rpm for 50 seconds. The chip is then placed on the hot plate for another 6 minutes. The purpose of the two layers is to provide a cleaner lift-off of the resist after metallization.

Once the chips have been prepared for e-beam writing, they are taken to the SEM. The same pattern is written on every chip prepared. This pattern consists of an array of bracketed numbers from 1 to 100. In the four corners of the 800  $\mu\text{m}^2$  pattern, are four alignment marks consisting of two squares each of 25  $\mu\text{m}^2$ . As their names indicate, these features are used to align the pattern within the SEM for future use. Before writing the pattern, the beam current must be determined for use in the NPGS software run file.

Once the microscope has been aligned, and all other parameters set, the writing may ensue.

After the pattern has been written, the chip is placed in a developing solvent of methyl-isobutyl ketone (MIBK) and isopropanol (IPA) in a ratio of 1:3, respectively. The pattern is developed for 60 seconds, followed by a 20 second rinse using IPA. The chip is then rinsed with deionized water and blown-dry. The pattern may now be inspected using an optical microscope to determine the quality of the pattern. If the features on the pattern appear rounded, the pattern has been overexposed – a higher dose of electrons impinged upon the sample than required. If the pattern is underexposed, that will be evident by the presence of residual PMMA indicated by areas of lighter color than that of the substrate. Once the pattern is deemed acceptable, chromium and gold are thermally evaporated onto the sample. Lift-off of the metallized sample is accomplished by soaking the chip in acetone for several hours. This process may take less time if mild ultrasonic treatment is applied to the chip.

After lift-off, a suspension of nanotubes is dropped onto the substrate. The tubes are then located with an optical microscope or the SEM. Images are taken of the sample that must include at least the lower left bracketed number as well as the upper right bracketed number. This is necessary for the subsequent use of the Igor macro in which the location of the nanotubes is communicated to the CAD program. Subsequent to the locating of nanotubes, the process of spinning on two layers of PMMA is repeated. It is

prudent to check under the optical microscope after this process to determine if any of the nanotubes moved from their original position.

## **A.2 NPGS Software**

The software used to direct the electron beam is the Nanometer Pattern Generation System, designed by Joe Nabity. There are several important aspects of the software that will be discussed. The first part of the software is the CAD program designated Design CAD Light. This program is used to design the objects that are to be written by the electron beam. A scale denotes microns within the program. A pattern is generally drawn and then saved as a file for later reference by the NPGS software's Run File. The most commonly used tool to draw objects is the "Filled Polygon" tool. Any shape may be created, however, it is useful to check for errors in the pattern as it is drawn. If errors exist and aren't discovered until pattern is finished, it is very difficult to determine which shape was faulty. When saving the pattern, it is necessary to use the NPGS icon and save it under that heading (NPGS – Save File). Do not use the familiar File-Save combination. Arrays of objects can also be made in this CAD program.

Once a pattern is designed and saved, the CAD program is exited. The "Edit Run File" icon is then accessed and a pattern must be chosen for writing. This pattern is the one previously designed and saved in the CAD program. Default parameters are loaded into the run file, which represent things such as the magnification, the beam current, the dose of electrons, the kind of dose, the number and kind of entities, etc. Most of these

default parameters must be changed to represent the current microscope conditions. The magnification parameter represents the highest magnification allowed for the pattern's dimensions. This can be lowered, but not increased. It is critical that the microscope's actual magnification reflects the magnification represented in the run file, or the resulting pattern will not be written to the size desired.

The beam current should be set at the measured beam current at the spot size and accelerating voltage used for the pattern. The beam current is measured through a Farraday cup and a picoammeter. Zoom in with the microscope into the Farraday cup. The picoammeter's scale is in nanoamperes (nA). Therefore, a reading of 0.046 on the picoammeter is equivalent to 46 picoamperes (pA). It is useful to make note of the beam current at different spot sizes. This will give you an indication of whether something is not working correctly with the SEM.

The dose typically used is an area dose, not a line dose. With a bi-layer of PMMA, the reasonable area dose was found to be  $455 \mu\text{C}/\text{cm}^2$ . If there are doubts about the exposure dose – a pattern that is very spread out or a pattern that leaves residual PMMA on the wafer after development – there is a run file that will help determine the correct dose. This run file is called Sample 3. It is a repeating pattern of different shapes set to different doses. This pattern can be written and then developed to determine the appropriate dose for the sample. Figures 3.1 and 3.2 show the run file for Sample 3, and the corresponding CAD file for Sample 3.

Project: Chandler		NPGS Runfile: SAMPLE3.rf0		page 1 of 1	
Number of entries to process	2	Write to Sample	Yes	Write to Sample	Yes
Also Advanced Modes	No	Write to Sample	Yes	Write to Sample	Yes
<p>1. Entry Type ..... Comment</p> <p>Display Mode ..... Never</p> <p>Comment Name ..... Explanation</p> <p>This run file will expose the pattern "Sample3.ac2" with 6 different doses that are increasing in an exponential fashion.</p> <p>The doses are set to range from 100 <math>\mu\text{C}/\text{cm}^2</math> to too high, while the best dose is expected to be near 200 <math>\mu\text{C}/\text{cm}^2</math>.</p> <p>Note the on field emission BEVs, the low doses may actually produce an array of dots with a spacing of 50 nm.</p> <p>Proximity effects are typically easy to see in the underexposed and overexposed pattern elements, however, the best dose will show little, if any, proximity effect.</p>					
2. Entry Type	Pattern	Layer 1	Normal Writing		
Pattern Name	sample3	Origin Offset (X,Y)	( $\mu\text{m}, \mu\text{m}$ )	0	
Number of times to repeat pattern	1	Magnification		500	
XY Move to Pattern Center	0,0	Center-to-Center Distance	( $\mu\text{m}$ )	49.44	
		Line Spacing	( $\mu\text{m}$ )	49.44	
		Configuration Parameter		1	
		Measured Beam Current	(pA)	20.0	
		Dwell: Color 1 (1000 000 255)	( $\mu\text{sec}$ )	122.210	
		Area Dose	( $\mu\text{C}/\text{cm}^2$ )	100.000	
		Dwell: Color 2 (128 000 128)	( $\mu\text{sec}$ )	161.250	
		Area Dose	( $\mu\text{C}/\text{cm}^2$ )	131.951	
		Dwell: Color 3 (255 000 000)	( $\mu\text{sec}$ )	212.750	
		Area Dose	( $\mu\text{C}/\text{cm}^2$ )	174.110	
		Dwell: Color 4 (255 085 000)	( $\mu\text{sec}$ )	280.750	
		Area Dose	( $\mu\text{C}/\text{cm}^2$ )	228.740	
		Dwell: Color 5 (255 170 000)	( $\mu\text{sec}$ )	370.470	
		Area Dose	( $\mu\text{C}/\text{cm}^2$ )	303.143	
		Dwell: Color 6 (255 255 000)	( $\mu\text{sec}$ )	485.500	
		Area Dose	( $\mu\text{C}/\text{cm}^2$ )	400.000	

Figure A.1. Run file *Sample 3* showing the parameters for writing a sample with varying doses.

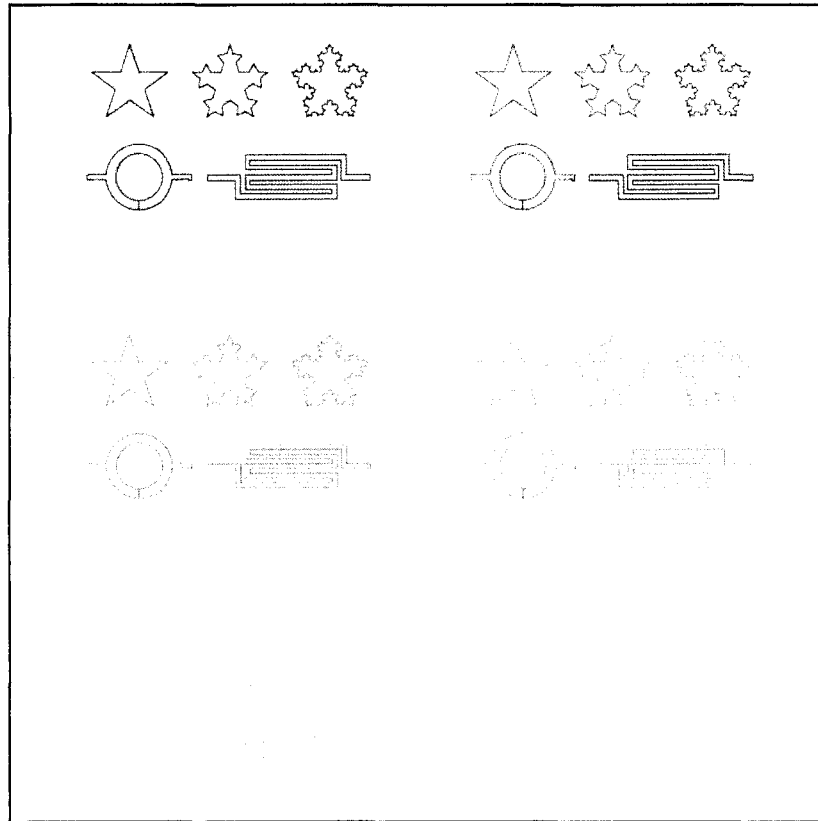


**Figure A.2.** Design CAD pattern representing an array of shapes for *Sample 3*. The different colors indicate different doses of electrons.

In Figure A.1, there are 2 entities to process, however, the first one is a comment describing the purpose of the run file and the pattern. The second entity is the actual pattern to be written which is shown in Figure A.2. The different colors in both the run file and the CAD file represent different doses of electrons. These may be adjusted according to the operator's needs. Patterns that are over-exposed will be rounded while patterns that are underexposed will have residual PMMA present.

### A.3 Initial Writing Step

The initial electron beam writing step will involve using a pre-designed pattern representing a grid of numbers and featuring four larger alignment marks in the four corners of the pattern. This run file should be labeled as Refgrid3 (short for Reference Grid). The pattern referenced in the Refgrid3 run file is composed of numbers from 1 to 100, each within brackets. The number of entities is 1. This initial writing step is required for future efforts to make contacts to individual nanotubes and nanowires. Depending on the beam current, the pattern will take 10 to 13 minutes to be written. Figure A.3 shows the CAD file representing the reference grid pattern.

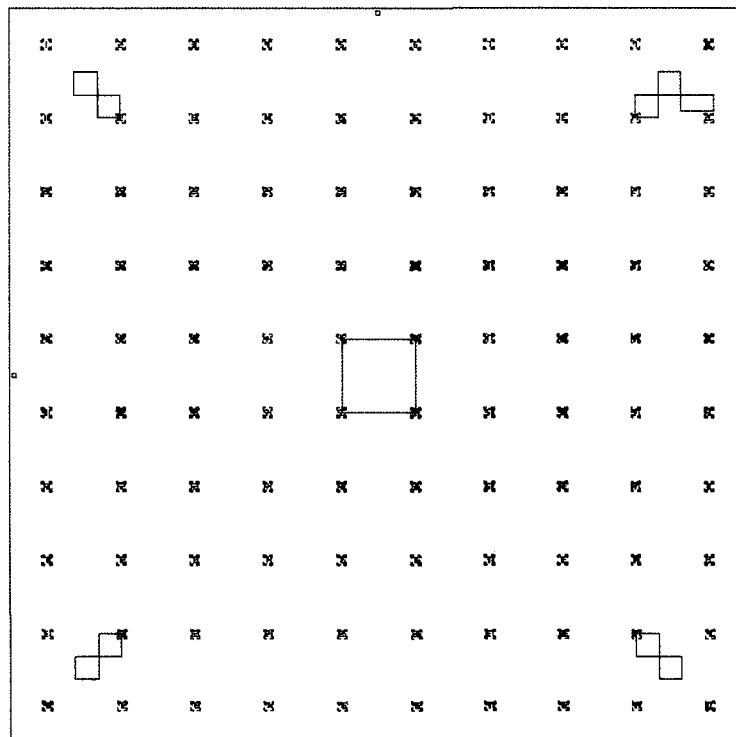


**Figure A.3.** The reference grid pattern as it appears in the CAD program.

As seen in the figure, the reference grid features the numbers 1 to 100 in brackets. Additionally, there are large features in each of the four corners. These represent alignment marks that will be used for the actual contacting of the nanotubes.

#### **A.4 Defining Nanowire Position**

The positions of the nanotubes have been recorded and are now ready to be incorporated into the CAD file to be written. This CAD file is referred to as the JEOL Starter File. It consists of the reference grid pattern in addition to larger contact pads outside the pattern. These features are 100 X 300  $\mu\text{m}$ . Copies of the JEOL Starter File should be made for future use. These should be named something familiar to the user as a reference for new patterns such as “Copy 1”, “Copy 2”, etc. The pattern chosen should be referenced as the one being used so that it will not be used again. After finding a new JEOL Starter File to use, the positions of the nanotubes can be incorporated into the Starter File.

On the computer with the NPGS software, an icon exists for Igor. Igor should be opened and under the “Macros” icon, the macro “Write Nanowire” should be chosen. The first step will be to choose the tiff file that contains the nanowire and the bracketed reference numbers. The next step will be to click on the “Open File” icon in the macro. This file will be the JEOL Starter File previously chosen for writing on. The next step is to click on the “Get XY” icon. The reference numbers in the lower left bracket are used for X and Y. The number to the right is X, and the number to the left is Y. These

numbers may be entered manually, or by consecutive clicks on the arrows representing the X and Y position.

Subsequent to locating the X and Y positions, the icon “Set Origin” should be clicked. The origin is located in the lower left bracket of the X and Y marker. The mouse should be clicked at exactly the corner of that bracket. The next step is to click on the “Define Scale” icon. Once this is done, the mouse should be clicked on exactly the lower left bracket corner of the upper right-bracketed number. The next step is to click on the “Write Wire” icon. Click the mouse once at one end of the wire and then again at the other end of the wire to define the position of the wire in the reference grid. After writing the position of the wire, the “Close File” icon should be clicked. The macro should now be closed and then reopened to write a second nanowire following the same procedure as before and using the same JEOL Starter File but a different tiff file.

After all of the nanowire positions have been written, close Igor and open the NPGS software. Find the JEOL Starter file previously used and open it. Within the reference grid, several lines should be visible. These represent the positions of the nanowires that were just defined using Igor. Now that the positions of the nanowires are known, contacts may be drawn representing the placement of the electrodes over the nanowires. (See section on Drawing Contacts to Nanotubes).

## A.5 Drawing Contacts to Nanotubes

It is necessary to find the JEOL Starter Patten used to define the positions of the nanotubes. This file consists of the same reference pattern initially written as well as larger contacts for making connections to the nanotubes located within the reference grid. A “clean” JEOL Starter File is required every time nanotubes will be contacted. If a previously used JEOL Starter File is used, the positions of tubes inserted into that file will still remain. Figure A.4 shows the JEOL Starter File.

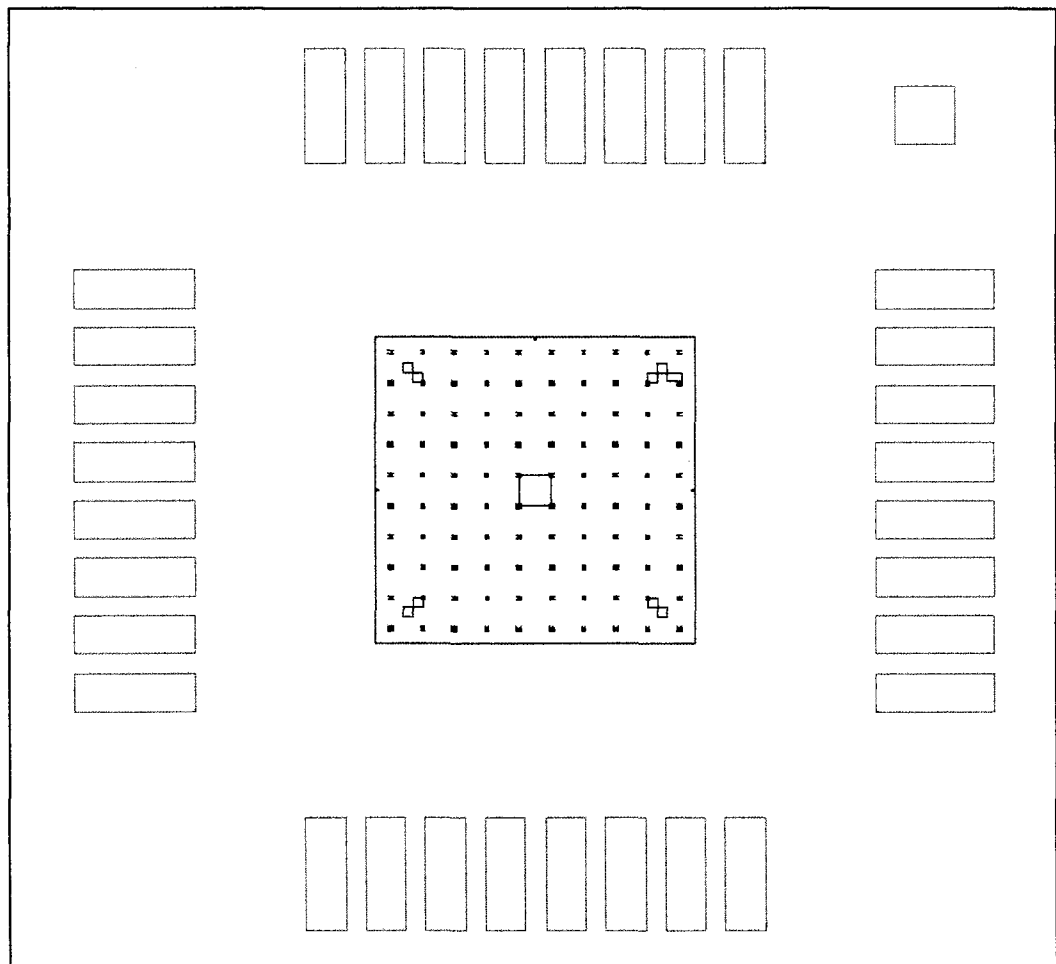


**Figure A.4.** The CAD pattern called JEOL Starter File. It consists of the same reference grid as the first one written in addition to larger patterns representing contacts that can be bridged to the nanotubes.

Once this is highlighted, click on the Design CAD icon, and the CAD program will then be displayed. The first step required after opening the JEOL Starter File is to touch the “L” on the keyboard. This will open a screen representing the different layers in a pattern. The numbers with an asterisk are the layers that will be written; the active layers. At this point, only layer 3 will have an asterisk. Click on layer 3 and then click on the “Separate” icon. This will put all of the different writing elements in different layers. There should be 3 writing elements. The first one will be the reference grid. The second one will be the large contact pads. The third one will be the nanowires that have been written. Before drawing the contacts, these layers should be moved to layers above the number 100. Layers above the number 100 will not be written. They are typically moved to layers 101, 102, and 103, respectively. The contacts may now be written. Make a note of the layer that is about to be written in for future reference. Layer 1 is typically used for the inner contacts. It is easiest to zoom in on the nanowire that is to be written on, and then proceed with drawing the desired contacts. As mentioned previously, it is wise to check for errors in the pattern as it is written. This is accomplished by exiting Design CAD after saving the file under NPGS – Save, and proceeding to the run file editor. After creating a run file, the pattern as written may be checked for errors. Go to the Process Run File icon – Error Test.

After completing all of the inner contacts, it is necessary to move to layer 2 and begin writing the intermediate contacts to the larger contact pads. A different color is

usually chosen for clarity. The intermediate contacts are usually written to every other one of the 100 X 300  $\mu\text{m}$  pads. This is done to avoid any shorting that may occur with the current measurement set-up. If this pattern is periodically checked for errors, it is important to verify that layer 2 is the active layer upon reentering the CAD program. It will default to layer 1 after reopening the program. The unused contact pads are deleted to avoid unnecessary writing time. The layer that the 100 X 300  $\mu\text{m}$  pads was previously moved to may now be moved back. They may be moved to layer 2 since the magnification for both layers is the same; typically 25. Figure A.5 is an example of a completed CAD file with contacts to the individual nanotubes.

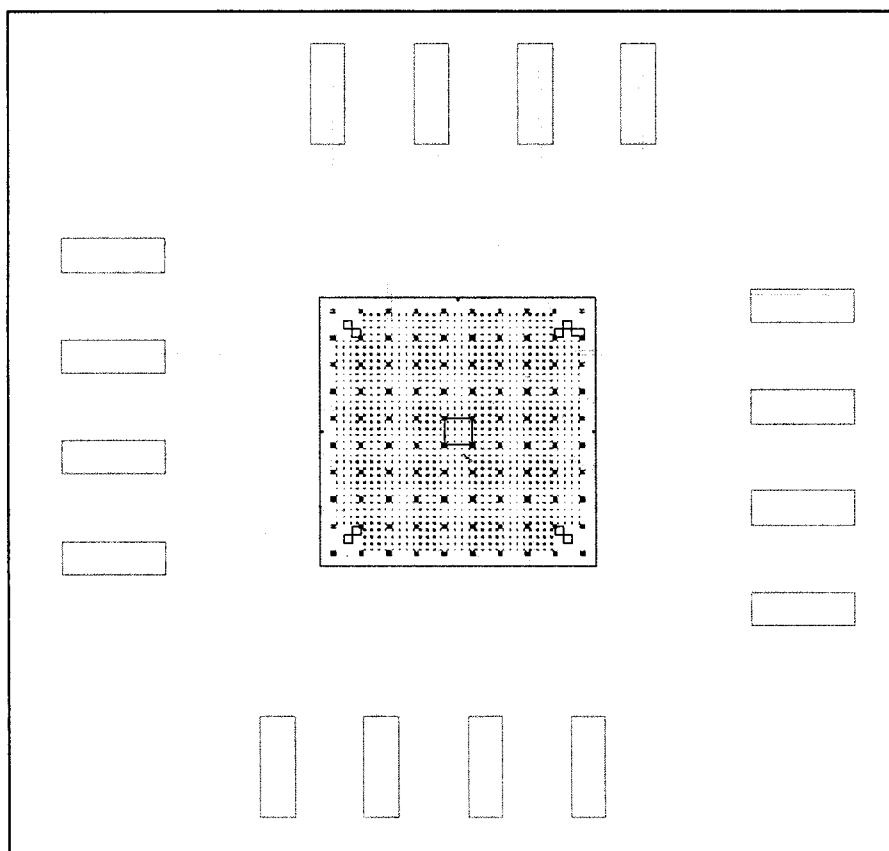


**Figure A.5.** Example of a completed CAD pattern representing the filled polygons used to design electrodes which are addressing the individual nanotubes.

Note in the figure that not all of the original 32 contact pads have been used. This is done to save time during e-beam writing. The inner contacts have a different color than the outer contacts, indicating different layers. This does not mean, however, that different colors cannot be used for one layer. The orange and yellow contacts coming in from the green contact pads are in the same layer.

## **A.6 Run File Editor For Contacting Nanotubes**

When the entire pattern for contacting nanotubes is complete, a run file will need to be created for executing the electron beam writing. The run file contains parameters such as layers and entities. The number of entities will be 2 for e-beam writing on nanotubes. The first entity will be of the alignment type. The alignment will be manual. The alignment pattern used is designated VO2 Align. It is selected by double-clicking in the blank space under the Alignment icon and scrolling down the list of CAD files until it is found. This alignment pattern consists of four shapes representing the four alignment marks in the reference grid CAD file. Executing this pattern will open “windows” into which the electron beam will shine. While aligning, the pattern will be exposed to the electron beam, but it will also allow the user to see the alignment marks and to overlay the digital alignment features with the real alignment marks on the pattern. By clicking on the alignment pattern chosen, the right part of the screen will change. This contains the default information for the microscope parameters. Although the beam current is not 10 pA, this parameter does not need to be changed. The magnification should be changed to 100. In addition, the line spacing parameter needs to be changed to 202.94

nm. This is necessary to avoid an error message previous to writing and is likely due to a bug in the software.

The second entity will be the pattern that is being written. This is the pattern that has been created and specifically designed for contacting nanotubes on a sample. This pattern will also have different layers. Different layers are necessary when multiple magnifications are used to write a pattern. When writing the contacts within the reference grid, a magnification of 100 is used and the beam current representative of a spot size 6 is also used (typically 46-48 pA). When writing the intermediate contacts and the contact pads, a magnification of 25 is used and a beam current representative of a spot size of 12 should be used. This beam current is typically 3500 – 4000 pA. A higher beam current is used to decrease the writing time. Also, when the magnification changes from layer 1 to layer 2, the Pause Before Writing command should be initiated. This is a scroll down feature in the Normal Writing box. When all of the necessary parameters in the Run File Editor have been entered, electron beam writing may proceed. Figures A.6 and A.7 show the CAD program *VO2 Align* and a completed run file containing the alignment entity and the pattern to be written, respectively.

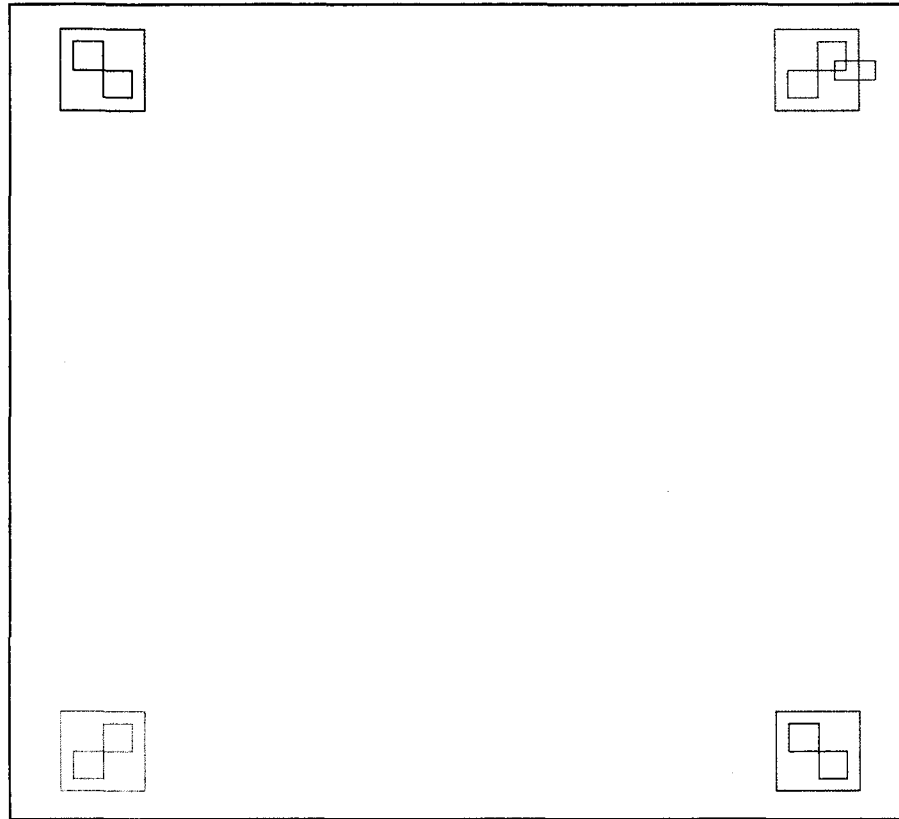


**Figure A.6.** CAD file *VO2 Align*. This file represents windows overlaying the alignment marks that will open to expose the pattern that is to be written on.

Project Chandler		NPGS Runfile: MoS2B100607.rfb		page 1 of 2	
Number of entities to process	2	Non-Stop Writing Mode		No	
Allow Advanced Modes	Yes				
Enable Global Rotation Correction <span style="float: right;">No</span>					
<hr/>					
1. Entity Type	Alignment	Layer 1		Window	
Alignment Mode	Manual	Origin Offset (x,y)	(4m,4m)	0	
Pattern Name	ccalign	Magnification		100	
Number of times to repeat pattern	1	Center-to-Center Distance	(mm)	205.99	
XY Move to Pattern Center	0,0	Line Spacing	(mm)	205.99	
		Configuration Parameter		1	
		Measured Beam Current	(pA)	10.0	
		Dwell: Color 1 (255 255 255)	Counts	20	
		Layer 2		Window	
		Origin Offset (x,y)	(4m,4m)	0	
		Magnification		100	
		Center-to-Center Distance	(mm)	205.99	
		Line Spacing	(mm)	205.99	
		Configuration Parameter		1	
		Measured Beam Current	(pA)	10.0	
		Dwell: Color 2 (128 000 000)	Counts	20	
		Layer 3		Window	
		Origin Offset (x,y)	(4m,4m)	0	
		Magnification		100	
		Center-to-Center Distance	(mm)	205.99	
		Line Spacing	(mm)	205.99	
		Configuration Parameter		1	
		Measured Beam Current	(pA)	10.0	
		Dwell: Color 3 (000 128 000)	Counts	20	
		Layer 4		Window	
		Origin Offset (x,y)	(4m,4m)	0	
		Magnification		100	
		Center-to-Center Distance	(mm)	205.99	
		Line Spacing	(mm)	205.99	
		Configuration Parameter		1	
		Measured Beam Current	(pA)	10.0	
		Dwell: Color 4 (000 000 128)	Counts	20	
<hr/>					
2. Entity Type	Pattern	Layer 1		Norms Writing	
Pattern Name	mos2bwrite:CC6C7	Origin Offset (x,y)	(4m,4m)	0	
Number of times to repeat pattern	1	Magnification		100	
XY Move to Pattern Center	0,0	Center-to-Center Distance	(mm)	13.75	
		Line Spacing	(mm)	41.20	
		Configuration Parameter		1	
		Measured Beam Current	(pA)	46.0	
		Dwell: Color 1 (255 255 000)	(usec)	35.768	
		Area Dose	(pC/cm <sup>2</sup> )	298.937	
		Layer 2		Pause First	
		Origin Offset (x,y)	(4m,4m)	0	
		Magnification		25	
		Center-to-Center Distance	(mm)	54.93	
		Line Spacing	(mm)	54.93	
		Configuration Parameter		1	

**Figure A.7.** An example of a completed run file containing the alignment and pattern entities.

Figure A.6 shows the *VO2 Align* CAD file. It consists of boxes representing windows that will open over the alignment marks when the file is used. When aligning a sample, the user is allowed to move outlines of the alignment patterns exactly over the location of the alignment marks. In Figure A.7, a completed run file containing the *VO2 Align* entity is shown. Note that there are 4 windows corresponding to the 4 boxes in the CAD file. Once the parameters for one of these windows is chosen, the software will copy these parameters for each of the subsequent windows. The second entity is the pattern to be written. In this pattern, there are two layers. The magnification and beam current between layers changes, therefore, before writing the second layer, the software will “Pause First”. This allows the user to change the magnification and beam current manually on the SEM before continuing.

## **A.7 Electron Beam Writing**

The following section assumes the user to be familiar with normal SEM operation and microscope alignment procedures. Affix the Si chip to the sample holder that contains the Farraday cup. Make a small scratch in the PMMA with a razor blade for reference in the SEM. Do not cover the Farraday cup with the sample. Place the sample in the SEM chamber. Use an aperture value of 4 instead of 3. There are two coaxial cables taped together on the right side of the SEM. Remove the cable that is connected and replace it with the other cable that leads to the picoammeter. There is a small control box on the SEM called PCD Beam Blanker. Touch the “Blank” button under “Plate Position”. This will move the beam blanker into the path of the electron beam. Set the

accelerating voltage of the SEM to 30 kV. Turn on the picoammeter and after it does a self-check, touch the “ZCHECK” button. Open the gun valve on the SEM. If no image appears, verify that the beam is on via the PCD Beam Blanker box. If it displays “Blanking On”, press the “Beam On” button under “Beam Status”.

Align the microscope as usual, however when aligning the gun, you may use the Farraday cup. Move the beam over the Farraday cup and increase the magnification. The screen will be completely dark, but the progress of aligning the gun may be monitored by the reading on the picoammeter. Align the gun by maximizing the amount of current displayed for each of the probe currents. Unless a probe current above 3500 is required, it is not necessary to align the gun in the “Large” probe current range. After the gun is aligned, it may be necessary to go back and re-align the gun after aligning the Objective Lens Aperture. For best results, the user should be able to focus on features at a magnification of 100,000.

After the alignment is complete, move toward the sample and find the scratch previously made in the PMMA. Focus on the sample and the scratch. While focusing, do not use the X and Y stigmator knobs. It is necessary to focus on the sample for the sharpest features. If writing a reference grid, go to the top of the scratch and blank the electron beam by pressing “Blank” under “Beam Status” on the PCD Beam Blanker box and move into the sample some arbitrary distance. The magnification should be at 100. If writing the contacts for nanotubes, move into the sample until the bottom alignment marks are visible at the top of the screen. Ensure that the microscope magnification is at

100. Once the alignment marks are visible, adjust the rotation of the sample if necessary to have the top of the alignment marks parallel with the tool bar at the top of the screen. It may also be necessary to move the sample in the X direction such that the left alignment mark is just below the reading of the microscope beam current. At this point, blank the beam by pressing “Blank” under “Beam Status” on the PCD Beam Blanker box. The dimensions of the initial reference grid pattern are  $800 \mu\text{m}^2$ . The sample will have to be moved (-)725 or (-)730  $\mu\text{m}$  to be appropriately centered.

Give control of the SEM to the NPGS computer by moving the toggle switch to NPGS from SEM. This switch is located on the SEM table on the right hand side. From the NPGS menu, select the run file to be written and click on “Process Run File”. If the reference grid is being written, the computer will display the pattern and begin timing the writing. The progress may be verified by looking at the picoammeter display. As the pattern is being written, the display should read some current. If the run file includes the CAD pattern in which the wires were contacted, the display will look like four windows. Ideally, the alignment marks will be visible through these windows. There are digital squares or overlays in the display representing the shapes of the alignment marks. These need to be moved by clicking and holding on the overlay of interest and dragging over the alignment marks. After all alignment overlays have been adjusted satisfactorily, press enter on the keyboard. A prompt will ask if the rotation matrix should be saved and recalculated. Press Y or enter. After the alignment, the software will ask if the alignment is to be repeated. This is entirely up to the user, but if it is satisfactory, press N and the

computer will proceed with the next entity. The display will then show a pattern representing the pattern drawn in Design CAD. Depending on the details of the pattern, this writing process may take up to 40 minutes. When the next layer is to be written, there will be a pause in the writing allowing for changes in the beam current and magnification. Once those parameters are adjusted the pattern may be continued to completion.

When the writing is finished, move the stage back to the exchange position before turning the beam back on via the beam blanker. Give control back to the SEM via the toggle switch previously mentioned. Return all of the settings on the SEM to their normal values. Remove the beam blanker by pressing the "Beam Out" button under the "Plate Position" on the beam blanker box. Turn off the picoammeter. Replace the coaxial cable that ties into the picoammeter with the coaxial cable that runs down into the SEM. Set the aperture back to 3. Remove the sample and proceed to the developing.

## References

1. Dai, H.; Wong, E. W.; Lieber, C. M.; *Science*, **1996**, *272*, 523-526.
2. Cui, Y.; Duan, X.; Hu, J.; Lieber, C. M.; *Journal of Physical Chemistry B*, **2000**, *104*, 5213-5216.
3. Yu, J-W.; Chung, S-W.; Heath, J. R.; *Journal of Physical Chemistry b*, **2000**, *110*, 11864-11870.
4. Harnack, O.; Pacholski, C.; Weller, H.; Yasuda, A.; Wessels, J. M.; *Nano Letters*, **2003**, *3*, 1097-1101.
5. Wang, D.; Lu, J. G.; Otten, C. J.; Buhro, W. E.; *Applied Physics Letters*, **2003**, *83*, 5280-5283.
6. Khoury, M.; Ferry, D. K.; *Journal of Vacuum Science and Technology B*, **1996**, *14*, 75-79.

## **Appendix B: Independent Research Proposal**

### **Study of Thermoelectric Properties of 1-Dimensional Nanowire Arrays**

#### **Abstract**

The feasibility of thermoelectric devices for commercial applications has been limited by their low efficiency. To compete with commercial refrigerating systems, thermoelectric materials must have a high figure of merit,  $ZT$ , related to the thermoelectric efficiency of the material. Currently, the most promising materials have a  $Z$  of about 1.<sup>1</sup> This value needs to be increased by a factor of 3 for thermoelectric materials to compete with the current refrigeration systems used. Several approaches have been taken to try and increase the figures of merit for thermoelectrics. Two of the most promising approaches are controlling the transport of phonons and electrons, and reducing the size of the materials down to the nano-regime. Although both of these approaches have been attempted with success individually, there have been no efforts to combine these approaches for an even more enhanced effect.

The goal of this proposal is to combine the two above-mentioned approaches to determine whether an enhanced  $ZT$  is achieved. Nanoimprint lithography will be used to make the templates in which the thermoelectric materials will reside on a quartz substrate. A low temperature metal organic chemical vapor deposition (MOCVD) technique will be used to deposit the materials. The resulting substrate will have the 1-D materials aligned along the plane of the substrate. This will be followed by measurement of the thermoelectric properties of the materials as an array, and will also allow for measurements on individual wires of the thermoelectric materials.

## Background and Significance

The figure of merit is defined by the following equation,

$$ZT = \frac{S^2 \sigma T}{\kappa}$$

$\kappa$

where  $S$  is the Seebeck coefficient (thermoelectric power defined by  $\Delta V/\Delta T$ ),  $\sigma$  is the electrical conductivity,  $T$  is the absolute temperature, and  $\kappa$  is the thermal conductivity comprising the lattice and electrical thermal conductivity. It seems relatively trivial to look at the above equation and to think that all that needs to be done is to increase the electrical conductivity and/or decrease the thermal conductivity. However these two properties are typically directly proportional to each other – if you increase one, you must also increase the other. Other approaches have been necessary to address this problem of increasing  $ZT$ . Two of the most promising approaches are to confine thermoelectric materials to a quantum confinement down to 1-dimension or to control the transport of phonons and electrons.

It has been theoretically predicted that restricting thermoelectric materials to 1-dimension will increase  $ZT$  in thermoelectric materials as a result of the increase in the density of states (DOS) near the Fermi level.<sup>2</sup> An array of these wires would be advantageous for the 1-D thermoelectric nanomaterial's enhanced figure of merit to be augmented. Recently, 1-D nanotube, nanobelt, and nanowire thermoelectric materials

have been synthesized by a variety of methods.<sup>3-6</sup> A relatively promising route for producing 1-D arrays of thermoelectric materials is to electrochemically deposit the materials in the pores of an anodic alumina membrane. A high number of 1-D materials can be made via this route, and the diameter can be controlled by the pore size of the alumina membrane. Some of the problems with this route include an uneven growth process, polycrystalline materials, and the challenge of measuring the properties of these arrays. Other routes have included the solvothermal synthesis of 1-D nanowires, but these methods result in agglomerated wires that are difficult to separate and measure. In addition, the process of making aligned, monodisperse materials for actual use in devices remains elusive. Recently, Heath's group deposited a small array of 5  $\mu\text{m}$  long bismuth nanowires on a substrate with subsequent deposition of four electrodes for thermoelectric property measurement.<sup>7</sup> The wires, unfortunately, were polycrystalline and no clear thermoelectric enhancement was observed.

It has also been theoretically predicted that a 2-D solid will also exhibit an increase in thermoelectric performance.<sup>8</sup> In the paper, a layered superlattice is proposed to limit thermal conductivity in the material based on the scattering of phonons at the interface. Different groups<sup>9,10</sup> have experimentally attempted this concept, and the results have been promising. Recently, Venkatasubramanian has demonstrated an extremely high room temperature figure of merit using a  $\text{Bi}_2\text{Te}_3/\text{Sb}_2\text{Te}_3$  superlattice.<sup>11</sup> The author claims that the reason for the large figure of merit can be attributed to the acoustic phonon mismatch between the two materials. Aside from the obvious

advantages of increasing the ZT, the experiment has additional attractive aspects. The authors have devised a low temperature MOCVD process. In the experiment, the organometallic precursor is cracked at a temperature of around 350 ° C while the substrate is kept at close to 220 ° C. This deposition process resulted in highly crystalline thin films. This low temperature process opens the door to other techniques that might yield 1-D wires of the same material. Specifically, nanoimprint lithography becomes a real option. In combining a low temperature MOCVD method with nanoimprint lithography, an array of 1-D thermoelectric nanowires may be realized. The obvious benefits of Venkatasubramanian's thermoelectric materials can be combined with an additional benefit of confining the material to 1-D, thereby opening the door to a very promising experiment in the advancement of thermoelectric materials.

### **Research Design and Materials**

Nanoimprint lithography has recently emerged as a powerful technique with which to create 1-D arrays of different materials.<sup>12</sup> In order to utilize the technique, a stamp is created out of a material and then impressed upon a substrate that has been spin-coated with a polymer. The stamp may be constructed out of many kinds of materials, provided the strength and durability of the material are high.<sup>13</sup> The substrate is heated to a temperature about 100°C above the polymer's glass transition temperature,  $T_g$ , so that the polymer easily flows when the stamp is impressed in it. The material is then allowed to cool and the stamp removed. The troughs resulting from the impression are removed

by an oxygen plasma or reactive ion etching (RIE), but this treatment does not remove the areas of greater thickness (Figure B.1).

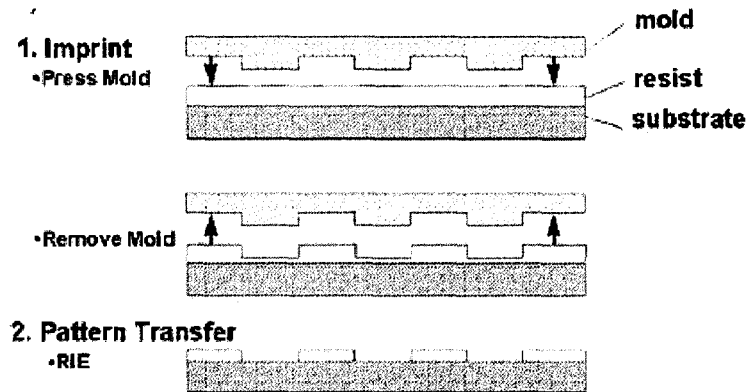


**Figure B.1.** Illustration of the process of nanoimprint lithography.<sup>13</sup>

In order to make the stamp, electron beam lithography is required. The pattern will be an array of 50 lines that are 20 nm wide separated by 5  $\mu\text{m}$  and having a length of 100  $\mu\text{m}$ . The stamp will be a Si substrate with a thin thermal oxide layer. A thin coating of polymethyl methacrylate will be spun onto it and subsequently written on with e-beam lithography. Once the pattern is developed, the thermal oxide layer will be etched with a  $\text{CF}_4$  plasma after which the residual PMMA is lifted off.

For the nanoimprint lithography to be successfully used in this experiment, a polymer with an unusually high  $T_g$  must be used. In this case, norbornyl polycarbonate (NB-polycarbonate) has been chosen because of its  $T_g$  of 230°C.<sup>14</sup> As an additional precaution against the stamp adhering to the polymer, the stamp will be coated with 1H, 1H, 2H, 2H- perfluorodecyl-trichlorosilane self-assembled monolayer.<sup>13</sup>

Once the substrate has been prepared, the thermoelectric materials will be deposited via a new, low-temperature MOCVD process.<sup>11</sup> This involves the use of a heated graphite susceptor and a thermally insulating quartz separator. The separator functions to keep the substrate from the high temperature of the susceptor and results in a highly crystalline superlattice of  $\text{Bi}_2\text{Te}_3/\text{Sb}_2\text{Te}_3$ . One of the advantages of this process is that the two materials are not alloyed, as alloyed materials with these components result in a loss of carrier mobility due to phonon scattering in the direction of current flow.<sup>15</sup>

The superlattice architecture allows acoustic phonon scattering within the van der Waals spacing between the lattices. Since this scattering is not in the direction of current flow, a decrease in lattice thermal conductivity is achieved. A thin film 20-angstrom layer of  $\text{Bi}_2\text{Te}_3$  and a 40-angstrom layer of  $\text{Sb}_2\text{Te}_3$  has been shown to yield a ZT of 2.4 at 300 K. This superlattice period is repeated for a total sample thickness on the order of microns. In the proposed experiment, the superlattice period will be repeated for a total sample thickness of 6 nm. The organometallic precursors of trimethylbismuth and diisopropyltelluride will form the  $\text{Bi}_2\text{Te}_3$  layer. Trimethylaminoantimony and diisopropyltelluride will be the organometallic precursors for the deposition of  $\text{Sb}_2\text{Te}_3$ . Both depositions will be carried out in a modified reactor. The cracking temperature will be  $350^\circ\text{C}$ , but the deposition temperature will be around  $220^\circ\text{C}$ . This will be achieved by using a graphite susceptor onto which a quartz separator is mounted.<sup>16</sup> The quartz separator acts to insulate the substrate from the higher temperature of the susceptor

(Figure B.2). After deposition and cooling, the NB-polycarbonate will be washed off with chloroform, leaving an array of lines.

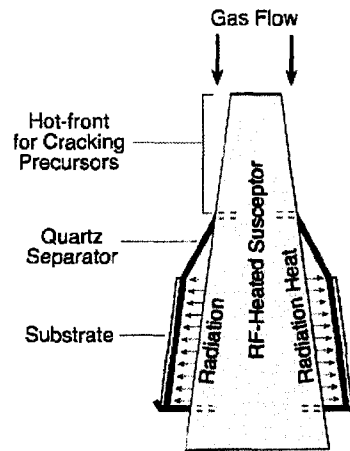


**Figure B.2.** Schematic diagram of the graphite susceptor and quartz heater.<sup>16</sup>

In order to verify the stoichiometry and crystallinity of the thermoelectric materials, XPS, EDS, and XRD will be used.

The measurement of the thermoelectric properties of this material will be carried out following an established procedure for measuring 1-D systems.<sup>7</sup> An array of electrodes will be deposited via e-beam lithography across the 1-D array of thermoelectric materials.

The outer contacts will be the current source, while the inner contacts will be voltage probes. Two heaters in the form of coiled wires will be placed at either end of the thermoelectric materials, These heaters will provide a heat gradient across the substrate as well as thermoelectric materials (Figure B.3).

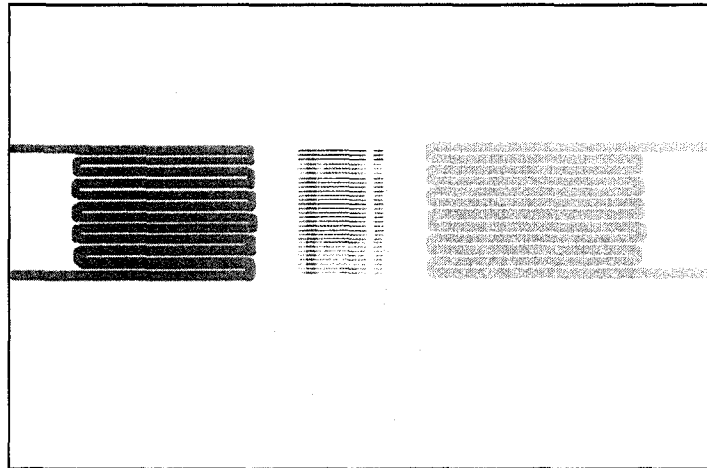


**Figure B.3.** Schematic representation of measurement device. Coiled lines (30  $\mu\text{m}$  from outer contacts) on either side represent elements for resistive heating. Red coil indicates hot side, blue coil indicates cold side. Gold lines represent contacts. Outer contacts supply current, while inner contacts measure 4-point voltage and thermoelectric voltage. Individual lines represent array of thermoelectric wires. Drawing not to scale.

In a typical experiment, one of the coils will be heated. The voltage probes will then measure the thermoelectric voltage. To obtain the temperature difference between the two inner contacts, their changes in resistance will be measured. By plotting the change in thermoelectric voltage against the change in temperature, the thermoelectric power ( $S$ ) can be determined by the slope. A four-point resistance will be measured by applying a current through the outer leads. The resulting voltage will consist of the thermoelectric voltage and the ohmic voltage. Once the current is turned off, the voltages will decay on different time scales with the thermoelectric voltage decaying at a slower rate.<sup>11</sup> From this, the intrinsic resistance of the wires can be gleaned.

In summary, this approach will combine two experimental approaches aimed at increasing the figure of merit for a thermoelectric material. The experiment will take

advantage of a very promising thermoelectric superlattice and further constrain the material to one dimension. With the added benefits of 1-D confinement, a higher figure of merit should result. In addition, the flexibility of nanoimprint lithography will allow several different experimental approaches. For example, the thermoelectric properties can be compared for wires of different lengths, thicknesses, and periodicities. This series of experiments would optimize the conditions required for a material with the highest achievable thermoelectric figure of merit to date.

## References

1. Heremans, J. P., et al., Thermoelectric Power of Bismuth Nanocomposites, *Phys. Rev. Lett.* **2002**, 88, (1), 216801.
2. Hicks, L. D., Dresselhaus, M. S., Thermoelectric Figure of Merit of a 1-Dimensional Conductor, *Phys. Rev. B.*, **1993**, 47, (24), 16631-16634.
3. Prieto, A. L., Electrodeposition of Ordered Bi<sub>2</sub>Te<sub>3</sub> Nanowire Arrays, *J. Am. Chem. Soc.*, **2001**, 123, 7160 -7161.
4. Choi, S. H., et al., Fabrication of Bismuth Nanowires With a Silver Nanocrystal Shadowmask, *J. Vac. Sci. Technol. A*, **2000**, 18, (4), 1326-1328.
5. X. B. Zhao, et al., Bismuth Telluride Nanotubes and the Effects on the Thermoelectric Properties of Nanotube-Containing Nanocomposites, *Appl. Phys. Lett.*, **2005**, 86, 06211.
6. Deng, Y. et al., Fabrication of Bismuth Telluride Nanotubes via Simple Solvothermal Synthesis, *Solid State Comm.*, **2006**, 138, 111-113.
7. Boukai, A., Xu, K., Heath, J. R., Size Dependent Transport and Thermoelectric Properties of Individual Polycrystalline Nanowires, *Adv. Mat.*, **2006**, 18, 864-869.
8. Hicks, L. D., Dresselhaus, M. S., Effect of Quantum Well Structures on the Thermoelectric Figure of Merit, *Phys. Rev. B.*, **1993**, 47, (19), 12727-12731.
9. Hicks, L. D., et al., Experimental Study of the Effect of Quantum Well Structures on the Thermoelectric Figure of Merit, *Phys. Rev. B.* **1996**, 53, (16), 10493-10496.
10. Harman, T. C., et al., *J. Electron. Mater.* **1996**, 25, 1121.
11. Venkatasubramanian, R., Thin Film Thermoelectric Devices With High Room-Temperature Figures of Merit, *Nature*, **2001**, 413, 597-602.
12. Torres, C. M. S., et al., Nanoimprint Lithography: An Alternative Nanofabrication Approach, *Mat. Sci. & Eng. C.*, **2003**, 23, 23-31.
13. Guo, L. J., Nanoimprint Lithography: Methods and Material Requirements, *Advanced Materials*, **2007**, 19, 495-513.
14. Connolly, J. J., Jones, A., Multiple Field Spin-Lattice Relaxation Study of Dissolved Poly[4,4'-bicyclo[2.2.1]heptan-2-ylidenebis(phenyl carbonate)], *Macromolecules*, **1985**, 18, 906-910.

15. Venkatasubramanian, R., et al., MOCVD of  $\text{Bi}_2\text{Te}_3$ ,  $\text{Sb}_2\text{Te}_3$  and Their Superlattice Structures for Thin-Film Thermoelectric Applications, *J. Cryst. Growth*, **1997**, 170, 817-821.
16. Venkatasubramanian, R., et al., Low-Temperature Organometallic Epitaxy and Its Application to Superlattice Structures in Thermoelectrics, *App. Phys. Lett.*, **1999**, 75, (8), 1104-1106.